

東海大学大学院 令和2年度博士論文

Study on colorimetric indicator based in
methylene blue-dyed water-soluble polymer
films for the detection of hydroxyl radicals

(メチレンブルー含有水溶性高分子フィルムを用
いたヒドロキシラジカル検知用色素インジケータ
に関する研究)

指導 岩森 暁 教授

東海大学大学院総合理工学研究科

総合理工学専攻

YENCHIT SARANYA

Contents

Chapter 1 INTRODUCTION.....	1
1-1 Research background	2
1-2 Active oxygen species and its application for the sterilization process	2
1-2-1 Definition of active oxygen species	2
1-2-2 Generation of active oxygen species by ultraviolet light	4
1-2-3 Advantages of activating active oxygen species for the sterilization process and surface modification technology	6
1-3 Applications for surface modification technology by using active oxygen species.....	7
1-3-1 An atmospheric-pressure plasma method	7
1-3-2 An ultraviolet laser irradiation method.....	8
1-4 Measurement methods for active oxygen species.....	9
1-4-1 Laser-induced fluorescence method	9
1-4-2 Electron spin resonance spectroscopy	10
1-4-3 The quartz crystal microbalance method.....	9
1-4-4 A colorimetric indicator for the detection of hydroxyl radicals in atmosphere using a methylene blue dye based on Nafion® film	11
1-5 Purpose of this study	12
1-6 Organization of this paper.....	13
Chapter 1 References	15
Chapter 2 Mechanism of Generation of Hydroxyl Radicals Across a Nonwoven Fabric Using Electron Spin Resonance.....	19
2-1 Background	20
2-2 Purpose.....	21
2-3 Experimental apparatus and experimental methods.....	22
2-3-1 Exposure to active oxygen species	22
2-3-2 Active oxygen species detection and quantification by electron spin resonance	25
2-4 Results.....	28
2-4-1 Determination of the presence of active oxygen species inside the test box by the spin-trapping method	28
2-5 Discussion.....	32

2-6	Summary	36
	Chapter 2 References	37
Chapter 3 A Colorimetric Indicators Based on Methylene Blue–Dyed Water-Soluble Polymers Uniform Thin Films for the Detection of Hydroxyl Radicals		
		39
3-1	Background	40
3-2	Purpose.....	41
3-3	Experimental apparatus and experimental methods.....	41
3-3-1	The molecular structures of methylene blue, pullulan, and sodium alginate	41
3-3-2	Exposure to active oxygen species	43
3-3-3	Preparation of a hydroxyl radical indicator using a pullulan-mixed methylene blue dye thin film.....	43
3-3-4	Preparation of a hydroxyl radical indicator using a sodium alginate–mixed methylene blue dye thin film.....	44
3-3-5	Preparation of MB and water-soluble polymers solution upon AOS exposure in high-humidity conditions for carbon-13 NMR analysis.....	44
3-3-6	Preparation of a hydroxyl radical indicator using a pullulan-mixed methylene blue dye thin film for comparing with ESR.....	45
3-3-7	Preparation of ozone exposure in different environmental conditions of active oxygen species exposure.....	46
3-4	Results.....	47
3-4-1	Decolorization of MB-dyed water-soluble polymer thin films due to AOS exposure different environmental conditions	47
3-4-2	Results of the ¹³ C-NMR analysis of the decolorization of MB-dyed pullulan thin films upon AOS exposure in high-humidity conditions.....	50
3-4-3	Results of the ¹³ C-NMR analysis of the decolorization of MB-dyed sodium alginate thin films upon AOS exposure in high-humidity conditions	52
3-4-4	Changes in the extent of bleaching determined by the distance from the nonwoven fabric	53
3-4-5	Results of AOS exposure when the test box is sealed by three layers of nonwoven fabric	54
3-4-6	Hydroxyl radical generation using ozone and water	55
3-5	Discussion	57
3-6	Summary	58
	Chapter 3 References	59

Chapter 4 Affinity of Methylene Blue Dye and Water-Soluble Polymers for Stabilization upon Active Oxygen Species Exposure.....	63
4-1 Background.....	64
4-2 Purpose.....	65
4-3 Experimental apparatus and experimental methods.....	65
4-3-1 The molecular structures of MB, pullulan, SA, and glucose.....	65
4-3-2 Exposure to AOS.....	66
4-3-3 Thin-layer chromatography analysis.....	66
4-3-4 Proton nuclear magnetic resonance (¹ H-NMR) analysis.....	67
4-3-5 Preparation of MB and pullulan solution upon AOS exposure in high-humidity conditions for carbon-13 nuclear magnetic resonance analysis.....	68
4-3-6 Microplate reader analysis.....	68
4-3-7 Fourier-transform infrared (FT-IR) analysis.....	69
4-3-8 Raman spectroscopy.....	70
4-4 Results.....	72
4-4-1 Determination of the affinity between MB, pullulan, and SA of OH* indicator by TLC analysis.....	72
4-4-2 Results of the ¹ H-NMR analysis of pullulan in a mixture of MB and pullulan.....	74
4-4-3 Results of the ¹ H-NMR analysis of interaction between MB and pullulan compared with glucose.....	75
4-4-4 Results of the ¹ H-NMR analysis of interaction between MB and SA compared with glucose.....	77
4-4-5 Results of the ¹³ C-NMR analysis of the MB-dyed pullulan thin films upon AOS exposure in high-humidity conditions.....	80
4-4-6 Determination of the affinity between the MB and pullulan of the OH* indicator by microplate reader analysis.....	81
4-4-7 Determination of the affinity between the MB and SA of the OH* indicator by microplate reader analysis.....	83
4-4-8 Determination of the affinity between the MB and pullulan of the OH* indicator by FT-IR analysis.....	85
4-4-9 Determination of the affinity between the MB and SA of the OH* indicator by FT-IR analysis.....	89
4-4-10 Determination of the molecular structure of the MB, pullulan, and SA of the OH* indicator by Raman spectroscopy.....	93
4-5 Discussion.....	98

4-6	Summary	98
	Chapter 4 References	100
	Chapter 5 CONCLUSIONS	103
	ACKNOWLEDGEMENT	107

Chapter 1
INTRODUCTION

1-1 Research background

In recent years, ethylene oxide gas (EOG) sterilizers, formalin disinfectors, and hydrogen peroxide low-temperature plasma sterilizers have been used to sterilize plastic products that are not suitable for high-pressure steam sterilization (autoclaving). However, concerns remain about the toxicity of the chemicals used, their persistence, and their effects on the environment. As an alternative, a new sterilization technique using “excited oxygen species” (or “active oxygen species” [AOS]) that are generated by irradiating oxygen gas with ultraviolet (UV) rays has already been reported⁽¹⁻¹⁾. Active oxygen is obtained by oxygen gas discharge or radiation reaction. Oxygen atoms [$O(^3P)$], excited oxygen molecules (1O_2), and ozone (O_3) are known to be the species produced by this approach⁽¹⁻²⁾.

1-2 Active oxygen species and their application for sterilization

1-2-1. Definition of active oxygen species

The term AOS refers to oxygen-based species that are characterized by high oxidizing power and are generated by irradiating oxygen molecules with a specific wavelength of UV radiation. Such species include ozone (O_3), excited singlet oxygen (1O_2), hydroxyl radical (OH^*), and excited singlet oxygen atoms [$O(^1D)$]. Among the types of AOS, 1O_2 and OH^* have high oxidizing power⁽¹⁻³⁾.

Table 1-1 shows the definition of AOS. Table 1-2 summarizes the reaction rate constants of AOS^{(1-4), (1-5)} and triplet oxygen molecules (3O_2), with the ground-state oxygen molecule rate constant being $10^{-30} \text{ L mol}^{-1} \text{ s}^{-1}$. Ground-state oxygen atom [$O(^3P)$], hydroxyl radical (OH^*), and excited singlet oxygen molecule [$O_2(^1\Delta_g)$] have reaction rate constants that are higher than those of the other AOS. The reaction rate constants of hydroxy radicals, which have the highest oxidizing power, is on the order of 10^8 to $10^9 \text{ L mol}^{-1} \text{ s}^{-1}$ ^{(1-4), (1-5)}.

Table 1-1. Definition of AOS ^{(1-4), (1-5)}

$O(^3P)$	Ground-state oxygen atom
$O(^1D)$	Excited singlet oxygen atom
$O_2(^1\Delta_g)$	Excited singlet oxygen molecule
O_3	Ozone
HO_2	Hydroperoxide
H_2O_2	Hydrogen peroxide
OH^*	Hydroxy radical
RO^*	Alkoxy radical
ROO^*	Peroxy radical

Table 1-2. The reaction rate constants of AOS ^{(1-4), (1-5)}

Reaction rate constants of AOS						
Oxygen species	OH^*	$O_2(^1\Delta_g)$	$O(^3P)$	HO_2	O_3	3O_2
Rate constant	10^8-10^9	10^6-10^7	10^5-10^6	10^2-10^3	10^2-10^3	10^{-30}

L/mol/s

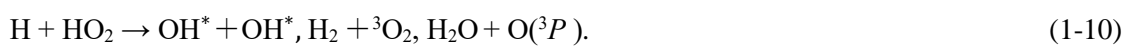
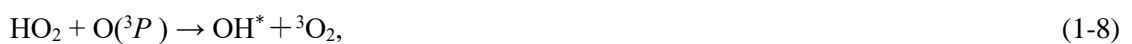
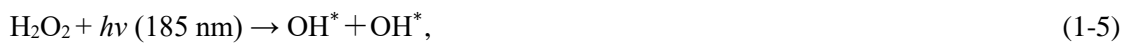
1-2-2. Generation of active oxygen species by ultraviolet light

This section describes the reaction model under the irradiation of an UV lamp. An UV lamp emits UV radiation at wavelengths of 185 and 254 nm. The reactions are conducted upon exposure to UV light with a wavelength of 185 nm; this causes a ground-state oxygen molecule ($^3\text{O}_2$) to decompose into two ground-state oxygen atoms [$\text{O}(^3\text{P})$]. Thereafter, O_3 is generated when $\text{O}(^3\text{P})$ binds with another $^3\text{O}_2$ molecule. An $\text{O}(^1\text{D})$ and an excited singlet oxygen molecule ($^1\text{O}_2$) are then generated when O_3 is decomposed via irradiation by UV light with a wavelength of 254 nm ⁽¹⁻⁶⁾⁻⁽¹⁻¹²⁾.

The generation of AOS by UV radiation emitted from a low-pressure mercury lamp at wavelengths of 185 and 254 nm is presented as follows, and $\text{O}(^3\text{P})$, O_3 , $\text{O}(^1\text{D})$, $\text{O}_2(^1\Delta_g)$, OH^* , and H are generated ⁽¹⁻¹³⁾:



Furthermore, AOS react with the UV radiation and with each other to produce hydroxy radical (OH^*).



The OH* radicals are formed when O₃ is decomposed and binds with hydrogen atoms. Furthermore, OH* radicals are generated by exposing H₂O to UV light at a wavelength of 185 nm⁽¹⁻⁶⁾. OH* radicals are also generated by exposing H₂O₂ to UV light at wavelengths of 185 and 245 nm. Thereafter, HO₂ is generated when a H atom binds with another ³O₂ molecule. OH* and ³O₂ are then generated when HO₂ binds with another O(³P) atom or when H binds with another O₃ molecule⁽¹⁻¹³⁾.

Atmospheric humidity is also an important factor influencing the type of AOS generated by irradiation with UV light. Under low-humidity conditions (relative humidity [RH] ≤ 20%), O(¹D) and O₃ are generated. Under high-humidity conditions (RH ≥ 90%), OH*, which is the most aggressive oxidant, is generated instead⁽¹⁻⁶⁾. The kinetics of the generation of these AOS has already been described^{(1-6), (1-8) -(1-10), (1-14)}.

1-2-3. Advantages of activating active oxygen species for the sterilization process and surface modification technology

AOS can be generated in the atmosphere via the combination of oxygen and UV light. The use of AOS in sterilization processes has already been reported. My colleagues and I also reported a sterilization method in which AOS are generated under UV irradiation ⁽¹⁻¹⁵⁾. The following advantages can be expected for sterilization processes and surface modification technology by activating AOS:

(1) AOS are highly oxidizing oxygen-based species; therefore, exposure to them leads to the inactivation of microorganisms ⁽¹⁻¹⁶⁾. AOS can be applied to sterilization processes and surface modifications.

(2) AOS are exceptionally safe and have no residual toxicant effects, in contrast to sterilization using EOG ⁽¹⁻¹⁷⁾⁻⁽¹⁻¹⁹⁾. They can be used for medical material sterilization, surface modifications, and consumer product manufacturing such as medical devices and food container materials.

(3) AOS are inexpensive (low initial and operating costs) ^{(1-3), (1-20)}. The only raw materials required for sterilization and surface modification by AOS technology are oxygen and UV. By using AOS technology, the costs incurred in the sterilization process decrease, thus increasing profits.

(4) AOS can be produced in a low-temperature (<60 °C) environment compared with high-pressure steam sterilization conducted in autoclaves (AC: 121 °C for 20 min) ⁽¹⁻¹⁷⁾⁻⁽¹⁻¹⁹⁾. Therefore, they can be applied to sterilization processes and the surface modification of materials with low heat resistance ^{(1-21), (1-22)}.

(5) AOS can be generated even in ambient conditions (low vacuum) without needing to install a high-vacuum chamber or high-vacuum pump. The maintenance is also easy ^{(1-21), (1-22)}.

Given these advantages, activated AOS for sterilization processes and the surface modification technology of materials can be anticipated to become a novel, highly versatile sterilization technology if an accurate indicator for detecting them can be developed.

1-3 Applications of active oxygen species for surface modification technology

AOS have strong oxidative ability. Therefore, they can be used for surface modification technology, which has been indispensable for improving the functions of polymers and has been applied in various industries. To improve the functionality of industrial equipment, such as electronic products, there is a need for greater complexity and diversity in terms of the structural materials used. Therefore, regarding the adhesion and boundary contact strength of different materials, there is a high demand for surface cleaning and modification. Currently, plasma treatment, laser irradiation, vacuum coating, etc. are significant approaches for surface modification.

1-3-1. An atmospheric-pressure plasma method ⁽¹⁻²³⁾

Atmospheric-pressure (AP) plasma can be operated in an AP environment for use in actual manufacturing environments and can be applied for surface modification and cleaning equipment via dielectric barrier discharge ⁽¹⁻²⁴⁾. AP plasma technology was applied using dielectric-barrier discharge, in which the dielectric part covers the electrodes and acts as a barrier (protecting against insulation) ⁽¹⁻²⁵⁾. Glow discharge is generated by keeping the gas-gap distance to less than 15 mm, using rare gases such as helium or argon as dilute gas, and applying a high-frequency, stable atmospheric pressure. In AP plasma, some of the helium or argon atoms are excited by a high-frequency power input to metastable radicals ⁽¹⁻²⁶⁾. Furthermore, He⁺ and Ar⁺, which ions, also increase the plasma reaction to generate reactive particles that encourage plasma reaction and surface modification. AP plasma processing can be applied to in-line industrial production processes with high productivity and improved quality production by using simple and low-cost equipment because it does not require a vacuum process; this allows compact equipment size ⁽¹⁻²³⁾.

1-3-2. An ultraviolet laser irradiation method ⁽¹⁻²³⁾

An UV laser irradiation method has been shown to be particularly useful for etching, patterning, and surface modification by interactions of high-intensity UV excimer lasers with solid-state polymers. The UV-laser pulse, ArF and KrF excimer lasers, and Nd:YAG laser were irradiated onto the interface between the polymer film and the aqueous solution of modifiers. As a result, the chemical bond (the abrasion phenomenon) in the polymer film was cleaved directly without a photosensitizer. Water, mineral solution, and amines were used as examples for modifying the polymer film via UV-laser irradiation in the media ⁽¹⁻²⁷⁾⁻⁽¹⁻³⁰⁾. The solution of the modifiers, which were reactive monomers and some polymers, were sandwiched between a quartz glass slide and a polymer film and were exposed to the UV laser for the chemical modification of the polymer surface. The functional pattern depended on the type of modifier, additional functions, and manipulated irradiation. The water contact angle of the polymer surface improved according to the hydrophilicity of the modifiers ⁽¹⁻²³⁾.

1-4 Methods for measuring active oxygen species

To establish this technology for use with AOS, it is necessary to determine the presence of AOS and provide an indicator of the sterilization process. Moreover, there is a strong need for technology that can detect reactive AOS. However, the available methods for measuring AOS in the atmosphere require specialized and expensive equipment. Furthermore, the presence or absence of AOS cannot be assessed immediately via such methods.

1-4-1. Laser-induced fluorescence method ^{(1-22), (1-31)–(1-32), (1-34)}

The laser-induced fluorescence (LIF) method is a method for measuring the generation density (calculated from a theoretical formula) of radicals in the atmosphere, such as atomic oxygen. Considering that the laser beam is focused in two-photon absorption LIF (TALIF) to obtain high power density, the strong radiation dissociates O₂ molecules and produces atomic oxygen ⁽¹⁻³³⁾. A photomultiplier tube detects the fluorescence from atomic oxygen, which is emitted when these electrons transition to a lower level, via an interference filter to a lens that collects the fluorescence. Therefore, the LIF measurement system can measure the generation density of radicals ⁽¹⁻³¹⁾. However, it requires specialized and expensive equipment, similar to an optical laser system.

1-4-2. Electron spin resonance spectroscopy

Electron spin resonance (ESR) spectroscopy is a method for detecting radicals with short lifetimes, such as $O(^1D)$ and OH^* . To identify reactive species qualitatively, the spin-trapping electron paramagnetic resonance (EPR) method can be employed. Here, a spin-trapping EPR technique based on the method described by Utsumi et al. (1994) was employed. EPR spectra were recorded at 295 K with a Bruker EMX spectrometer. The trap reagent, namely, DMPO (100 mM), was initially added into a solution containing goethite, with the solution being continuously stirred using a magnetic bar for the uniform mixing of the aqueous goethite suspended solution. A total of 15 μ l of the aliquot samples were taken at various time intervals and transferred into a capillary tube for EPR analysis. The EPR measurement was not affected by the solid suspension. A 100 kHz modulation frequency, 8.0 mT scan range, 180 s time, 5 mW microwave power, and 0.1 mT modulation amplitude were employed for the analysis. Furthermore, the radical concentration was calculated by comparing the signal intensity with that of a standard solution of diphenyl-2-picrylhydrazyl^{(1-34)–(1-36)}. As such, ESR spectroscopy also requires expensive equipment.

1-4-3. The quartz crystal microbalance method^{(1-22), (1-37)–(1-38)}

The quartz crystal microbalance (QCM) method measures the mass change on the electrode on the basis of the reaction with AOS, which can be detected as a frequency change when voltage is applied. Therefore, the amount of AOS can be monitored. Moreover, the QCM method can be applied to industrial gas analysis and AOS measurement by forming a thin film material that reacts with AOS on the quartz crystal electrode. An example of this is AOS monitoring using a QCM with a thin silver film as the detection layer; this approach measures the Ag_2O formed on the surface by reacting with the active oxygen of a silver electrode formed on a quartz oscillator^{(1-39)–(1-40)}. However, this QCM method has a drawback: the sensing values become saturated during the measurement owing to the oxidized deterioration of the silver surface. However, when performing measurements on a silver surface using this QCM method for a long time, the sensing values become saturated owing to oxidative degradation.

1-4-4 A colorimetric indicator for the detection of hydroxyl radicals in the atmosphere using a methylene blue dye based Nafion® film ⁽¹⁻⁴¹⁾

The methylene blue (MB)-based Nafion® film indicator can be used for detecting hydroxyl radicals (OH^{*}) in the atmosphere. This film contains stabilized MB with an aqueous Nafion solution, which is considered to have good affinity for organic substances. This thin film could be easily used as an indicator. The AOS were exposed under low- and high-humidity conditions to the MB-based Nafion film. The pigment on the thin film after AOS exposure in a high-humidity environment was markedly discolored and became transparent. However, the decolorization of the film after exposure to ozone and AOS under low-humidity conditions was hardly observed. Therefore, the decolorization of the film due to AOS exposure is related to the degradation reaction of MB molecules caused by hydroxyl radicals ⁽¹⁻⁴¹⁾. However, the film thickness can be uneven, and quantitative evaluation cannot be performed.

1-5 Purpose of this study

In this study, my colleagues and I aimed to investigate the sterilization process and surface modification technology by using AOS technology. The following procedures were examined as measures to achieve these goals.

First, to establish AOS technology for a sterilization method, my colleagues and I studied the presence of AOS inside the nonwoven fabric that makes up the sterilization bag by monitoring using the spin-trapping agents of ESR. It has already been reported that UV light cannot penetrate the mentioned sterilization bag compared with AOS. However, it is not known whether AOS are uniformly sterilized in nonwoven fabric.

To develop new sterilization technology involving the use of AOS for industrial processes, my colleagues and I aimed to create new uniform thin films with an AOS indicator by using MB-dyed water-soluble polymers, pullulan, and sodium alginate, which are water-soluble polymers with film-forming ability, to determine the presence of AOS. My colleagues and I aimed to evaluate uniform thin film indicators on the basis of MB-dyed water-soluble polymers to elucidate the decolorization mechanism upon exposure to OH^* . Furthermore, my colleagues and I used an indicator for detecting AOS, namely, MB-based pullulan thin film, which was installed in a nonwoven fabric that makes up the so-called sterilization bag for confirmation with the ESR method.

My colleagues and I then analyzed the uniform thin film indicator to elucidate the chemical affinity of MB/pullulan and MB/sodium alginate, as well as the decolorization mechanism generated under high-humidity conditions. The stability of MB-dyed water-soluble polymers was investigated by comparing the uniform thin film indicators of MB and water-soluble polymers with glucose as a monomer of pullulan and sodium alginate. It was considered that the affinity between MB and water-soluble polymers may contribute to the stability against AOS, excluding OH^* .

The findings obtained from the above examination procedures are summarized in this paper, and the possibility of applying the investigated process using AOS for sterilization processes and surface modification technology is examined.

1-6 Organization of this paper

This paper consists of the following chapters:

Chapter 1 is an introduction and describes the sterilization technology that is anticipated to become prevalent in industrial process with AOS as an example. The definition and mechanism of AOS generation are also described, and the advantages obtained by applying them to sterilization processes are summarized. Thereafter, the method of measuring AOS, and the purpose of this study are described.

As described in Chapter 2, the use of a spin-trapping agent for application to the sterilization process using AOS was employed to confirm the presence of AOS inside the nonwoven fabric constituting the sterilization bag. Considering that it is unlikely that the short-lifetime AOS generated outside the sterilization bag will be released into this bag, the lifetime of the AOS was evaluated using an aluminum test box with three internal stages. To check whether AOS were present in the test box, the AOS spin trap was arranged in three stages in a test box that has an opening covered with a sterile bag. Thereafter, the AOS diffusion rate, particularly the existence of hydroxyl radicals, was investigated by ESR. OH^* spread on all the stages in the test box. The interior of the test box is a three-layer nonwoven fabric as a “seal” to completely block out UV. The OH^* present in the test box sealed with the nonwoven fabric was generated by the ozone outside the test box owing to UV irradiation penetrating the nonwoven fabric and reacting with the water in the nonwoven fabric or by the ozone and water generated in the nonwoven fabric. It was assumed that OH^* was generated in the test box owing to the ozonolysis of water molecules.

In Chapter 3, my colleagues and I describe the development of a new uniform AOS indicator thin film produced using MB-dyed pullulan and MB-dyed sodium alginate, which are water-soluble polymers with film-forming properties. This indicator thin film can be used to visually determine the presence or absence of AOS in a short time. By using a uniform thin film indicator composed of a mixture of MB and water-soluble polymers, my colleagues and I developed a technology that reacts only to OH^* generated under high humidity among AOS and decolorizes it. It was found that MB was decomposed only when OH^* was irradiated among AOS, and decolorization occurred.

In Chapter 4, OH* detection characteristics were examined using thin films in which MB was mixed with water-soluble polymers, namely, pullulan and sodium alginate. The stability of MB was investigated by comparing the uniform thin film indicator of MB and water-soluble polymers with glucose as a monomer instead of sodium alginate. The results confirmed the interaction between MB and pullulan. Given that MB molecules are protected by pullulan, consider that AOS other than OH* cannot analyze MB. Furthermore, MB and sodium alginate formed an ionic bond, as evidenced by a shift in the peak corresponding to the benzene ring of MB in the mixture of MB and sodium alginate. It was concluded that the interaction between MB and pullulan, as well as the binding between MB and sodium alginate, may contribute to the stability to AOS excluding OH*.

Chapter 5 summarizes the results obtained in Chapters 2–4.

References

- (1-1) K. Yoshino, H. Matsumoto, T. Iwasaki, S. Kinoshita, K. Noda and S. Iwamori, Study on sterilization system using reactive oxygen species, *Journal of the Vacuum Society of Japan*, Vol. 54 (2011), pp. 467-473 (in Japanese).
- (1-2) H. Sugimoto: *Application and Foundation of Ozone*, (Korin, Tokyo, 1996) p. 20 [in Japanese].
- (1-3) K. Yoshino, H. Matsumoto, T. Iwasaki, S. Kinoshita, K. Noda, K. Oya, and S. Iwamori, Investigation of a Sterilization System Using Active Oxygen Species Generated by Ultraviolet Irradiation, *Biocontrol Science*, Vol. 20, No.1 (2015), pp. 11-18.
- (1-4) M. Kwiatkowski, P. Terebun, and T. Murakami, RF-Powered Atmospheric-Pressure Plasma Jet in Surface Treatment of High-Impact Polystyrene, *IEEE TRANSACTIONS ON PLASMA SCIENCE*, Vol. 44, No. 3 (2016), pp. 314-320.
- (1-5) 杉光英俊, オゾンの基礎と応用, 光琳, (2004).
- (1-6) K. Oya, R. Watanabe, Y. Soga, Y. Ikeda, T. Nakamura, and S. Iwamori, Effect of humidity conditions on active oxygen species generated under ultraviolet light irradiation and etching characteristics of fluorocarbon polymer, *Journal of Photochemistry and Photobiology A: Chemistry*, Vol. 298 (2015), pp. 33-39.
- (1-7) D. L. Baulch et al., Evaluated Kinetic Data for Combustion Modeling: Supplement II, *Journal of Physical and Chemical, Reference Data*. Vol. 34 (2005), pp. 757-1397.
- (1-8) R. Atkinson, D. L. Baulch, R. A. Cox, J. N. Crowley, R. F. Hampson, R. G. Hynes, M. E. Jenkin, M. J. Rossi, and J. Troe, Evaluated kinetic and photochemical data for atmospheric chemistry: Volume I — gas phase reactions of Ox, HOx, NOx and SOx species, *Atmospheric Chemistry and Physics*, Vol. 4 (2004), pp. 1461-1738.
- (1-9) L. T. Molina and M. J. Molina, Absolute absorption cross sections of ozone in the 185- to 350-nm wavelength range, *J. Geophysical Research*, Vol. 91 (1986), pp. 14501-14508.
- (1-10) D. S. Stafford and M. J. Kushner, O₂ (¹D) production in He/O₂ mixtures in flowing low pressure plasmas, *Journal of Applied Physics*, Vol. 96 (2004), pp. 2451-2465.

- (1-11) J. A. Manion, R. E. Huie, R. D. Levin, D. R. Burgess Jr., V. L. Orkin, W., Tsang, W. S. McGivern, J. W. Hudgens, V. D. Knyazev, D. B. Atkinson, E., Chai, A. M. Tereza, C-Y. Lin, T. C. Allison, W. G. Mallard, F., Westley, J. T. Herron, R. F. Hampson, D. H. Frizzell, NIST Chemical Kinetics Database (National Institute of Standards and Technology, Gaithersburg, U.S., 2008) NIST Standard Reference Database 17, Version 7.0 (Web Version), Release 1.4.3, Data version, 2008.12.
- (1-12) R. Atkinson, D. L. Baulch, R. A. Cox, R. F. Hampson, J. A. Kerr, and J. Troe, Evaluated Kinetic and Photochemical Data for Atmospheric Chemistry: Supplement IV. IUPAC Subcommittee on Gas Kinetic Data Evaluation for Atmospheric Chemistry, *Journal of Physical and Chemical Reference Data*, Vol. 21 (1992), pp. 1125.
- (1-13) R. Ono, Y. Nakagawa, Y. Tokumitsu, H. Matsumoto, and T. Oda, Effect of humidity on the production of ozone and other radicals by low-pressure mercury lamps, *Journal of Photochemistry and Photobiology A: Chemistry*, Vol. 274 (2014), pp. 13-19.
- (1-14) K. Yoshihara, Y. Takatori, K. Miyazaki, and Y. Kajii, Ultraviolet light-induced water-droplet formation from wet ambient air, *Proceedings of the Japan Academy, Series B*, Vol. 83 (2007), pp. 320-325.
- (1-15) K. Yoshino, H. Matsumoto, T. Iwasaki, S. Kinoshita, K. Noda, and S. Iwamori, 紫外線励起酸素を用いた滅菌システムにおける酸素注入条件の検, *Journal of the Vacuum Society of Japan*, Vol. 55 (2012), pp. 389-394 [in Japanese]
- (1-16) K. Hosoya, K. Takahashi, K. Oya, and S. Iwamori, Simultaneous process of surface modification and sterilization for polystyrene dish, *Vacuum*, Vol. 148 (2018), pp. 69-77.
- (1-17) T. Sasaki, A. Nakamura, K. Mise, *The Method of Sterilization and Killing of Microorganisms*, 1st ed., Japanese Standards Association, Tokyo, (1998), pp. 63–70 (Chapter 3).
- (1-18) T. Sasaki, ISO standards on sterilization of health care products, (Japanese standards association, Tokyo, 77-104 (2011), pp. 223-271 (in Japanese).
- (1-19) S. Seymour, S. Block, *Disinfection, Sterilization, and Preservation*, 5th ed., Lippincott Williams & Wilkins, Philadelphia, (2001), pp. 765-793 (Chapter 39).

- (1-20) K. Yoshino, H. Matsumoto, T. Iwasaki, S. Kinoshita, K. Noda, K. Oya, S. Iwamori, Investigation of a sterilization system using active oxygen species generated by ultraviolet irradiation, *Biocontrol Science*, Vol. 54 (2015), pp. 467-473.
- (1-21) K. Hosoya, 紫外線励起活性酸素による高分子材料の表面改質に関する研究, 博士学位論文 (2018) (in Japanese).
- (1-22) 吉野 潔, 活性酸素による微生物の滅菌効果の検証と滅菌プロセスに関する研究, 博士学位論文 (2014) (in Japanese).
- (1-23) S. Iwamori (ed.) Polymer surface modification and polymer coating by dry process technologies, *Research signpost* (2005), pp. 19-63.
- (1-24) Y. Sawada, K. Yamazaki, Y. Inoue and M. Kogoma, Proc. 8th microelectronics symp. (Japan Institute of Electronics Packaging, Ohmiya, (1998) pp 213-216.
- (1-25) B. Eliasson and U. Kogelschatz, *Nonequilibrium Processes in Partially Ionized Gases*, M. Capitelli and J. N. Bardsley (Ed.), Plenum Press, New York, 401 (1990).
- (1-26) S. Okazaki and M. Kogoma, Proc. Inst. Electrostatics Jpn., Vol. 15 (1991), pp. 222. [in Japanese]
- (1-27) M. Murahara and M. Okoshi, *J. Adhesion Sci. Technol.*, Vol. 9 (1995), pp. 1593.
- (1-28) M. Okoshi and M. Murahara, *Appl. Phys. Lett.*, Vol. 72 (1998), pp. 2616.
- (1-29) H. Niino and A. Yabe, *Phys. Lett.*, Vol. 63, No. 25, 1993, pp. 3527.
- (1-30) P. Laurens, B. Sadras, F. Decobert, F. Arefi and J. Amouroux, *Appl. Surf. Sci.*, Vol. 93 (1999), pp. 138-139.
- (1-31) R. Ono, Y. Yamashita, K. Takezawa and T. Oda, Behaviour of atomic oxygen in a pulsed dielectric barrier discharge measured by laser-induced fluorescence, *Journal of Physics D: Applied Physics*, Vol.38, No.16 (2005), pp. 2812-2816.
- (1-32) 山部長兵衛, OH ラジカル類の生成と応用技術, *NTS* (2008), pp.90-93.

- (1-33) T. Oda, Y. Yamashita, K. Takezawa, and R. Ono, Oxygen atom behavior in the nonthermal plasma, *Thin Solid Films*, Vol. 506-507 (2006), pp. 669-673.
- (1-34) S. K. Han, T. M. Hwang, Y. Yoon, and J. W. Kang, Evidence of singlet oxygen and hydroxyl radical formation in aqueous goethite suspension using spin-trapping electron paramagnetic resonance (EPR), *Chemosphere*, Vol. 84 (2011), pp. 1095-1101.
- (1-35) G. Liu, J. Zhao, and H. Hidaka, ESR spin-trapping detection of radical intermediates in the TiO₂-assisted photo-oxidation of sulforhodamine B under visible irradiation, *Journal of Photochemistry and Photobiology A: Chemistry*, Vol. 133 (2000), pp. 83-88.
- (1-36) H. Utsumi, M. Hakodam, S. Shimbara, H. Nagaoka, Y. S. Chung, and A. Hamada, Active oxygen species generated during chlorination and ozonation, *Water Sci. Technol.*, Vol. 30 (1994), pp. 91-99.
- (1-37) 松本裕之, 金沢大学自然科学研究科, 博士学位論文, pp.6-9 (2010)
- (1-38) 松本裕之, *Iwasaki 技報*, 第 19 号 pp.22-26 (2008)
- (1-39) H. Matsumoto, M. Matsuoka, K. Noda, Development of an active oxygen detector using a quartz crystal microbalance with a carbon/silver layer, *Chem. Lett.* 38 (2009) 216e217.
- (1-40) H. Matsumoto, M. Matsuoka, K. Yoshino, T. Iwasaki, S. Kinoshita, K. Noda, S. Iwamori, Investigation of silver oxidation behavior under active oxygen processing utilizing the quartz crystal microbalance method, *Chem. Lett.* 38 (2009) 1146e1147.
- (1-41) S. Iwamori, N. Nishiyama and K. Oya, A colorimetric indicator for detection of hydroxyl radicals in atmosphere using a methylene blue dye based on nafion film, *Polymer Degradation and Stability*, Vol. 123 (2016), pp. 131-136.

Chapter 2

Mechanism of Generation of Hydroxyl Radicals Across a Nonwoven Fabric Using Electron Spin Resonance

2-1 Background

As the diversification of medical devices and materials advances, there is a need to develop highly versatile sterilizers that can be used on devices with complex shapes and/or made with various materials. The present study focuses on sterilizers that rely on the properties of active oxygen species (AOS) produced following the irradiation of atmospheric air with ultraviolet (UV) light. To select the AOS-based sterilization technique that fits a given purpose, the identities of the specific AOS generated should be determined, and a suitable indicator of the said sterilization process should be developed or made available ^{(2-1), (2-2)-(2-3)}. In this context, a technology for detecting AOS is indispensable. However, the lifetimes of these species are generally very short [$O(^1D)$: 1.1×10^{-9} s; 1O_2 : 1.7×10^{-3} s], except for ozone, which has a lifetime that extends to several hours ^{(2-4), (2-5)}.

The AOS detection technique that is used in this study is a spin-trapping method based on electron spin resonance (ESR) spectroscopy. In this approach, a spin-trapping agent is dissolved in a liquid solvent. This agent reacts with unstable, short-lifetime radicals that are present in the solution and converts them to stable, long-lifetime radicals, thus enabling researchers to determine the structure and amount of radical species that are originally present.

In fact, the structure and amount of radicals captured by the spin trap and converted into long-lifetime radical species can be determined using an ESR spectrometer. ESR spectroscopic data can be utilized to measure the magnetic energy of species that have unpaired electrons (paramagnetic species) and to infer their microstructures ⁽²⁻⁶⁾. However, problems exist such as the inability to perform judgment on the spot and the need for large-scale equipment. Therefore, there is a need for an approach that can detect and measure AOS that can be more simply utilized than just a technology for detecting AOS.

2-2 Purpose

To investigate the process of sterilization by AOS, spin-trapping agents are installed in a nonwoven fabric that makes up the so-called sterilization bag. Compared with AOS, UV light cannot penetrate the mentioned sterilization bag. However, it is not known whether AOS are uniformly sterilized in the nonwoven fabric. Therefore, in this study, the presence of AOS inside the nonwoven fabric that makes up the sterilization bag was monitored using an MB-based thin film and spin-trapping agents.

Thus, an aluminum test box was used. This box has an interior that is divided into three chambers (stages) for the evaluation of the lifetime of AOS. It is considered that the AOS cannot reach all along the long-distance stage into nonwoven fabric. Furthermore, the upper section of the box was sealed with nonwoven fabric. Spin-trapping agents were placed in the three stages inside the box, and AOS diffusion and the presence of OH^* were investigated by monitoring the degree of thin-film decolorization observed in the different stages of the aluminum box ⁽²⁻⁷⁾.

2-3 Experimental apparatus and experimental methods

2-3-1 Exposure to active oxygen species

Active Dry[®] (Iwasaki Electric) was used as an AOS generator. This instrument was equipped with two 6 W UV lamps and one 4 W UV lamp (total wattage of 16 W). These UV lamps produce AOS at the same time by emitting UV radiation at wavelengths of 185 and 253.7 nm. Notably, the type of AOS generated by the lamps depends on the humidity. Therefore, in this study, AOS generation was conducted in conditions with controlled humidity. Exposure to AOS was achieved at a starting temperature of 30 °C under low-humidity conditions (relative humidity [RH] \leq 20%) and under high-humidity conditions (RH $>$ 90%). Furthermore, spin-trapping agents installed in the nonwoven fabric (Tyvek[™]) were used to seal the aluminum test box (see Fig. 2-1 and the description below). Compared with gas, UV light could hardly permeate into the nonwoven fabric. By using this approach, it was possible to investigate only the activity of AOS in the absence of any interference by UV light.

A cubic aluminum box (test box) with sides of 100 mm in length was designed. The interior of the test box was subdivided into three chambers (stages) to enable researchers to investigate the manner in which the effectiveness of bleaching is affected by the distance from the nonwoven fabric seal. Specifically, the distance from the nonwoven fabric placed at the top of the test box was 50 mm for the upper stage, 100 mm for the middle stage, and 150 mm for the lower stage. Spin-trapping agents were placed on each stage, and the lid of the test box was covered with nonwoven fabric. The test box (schematically depicted in Fig. 2-1) was installed in Active Dry[®] and was exposed to AOS generated in high-humidity conditions ⁽²⁻⁷⁾.

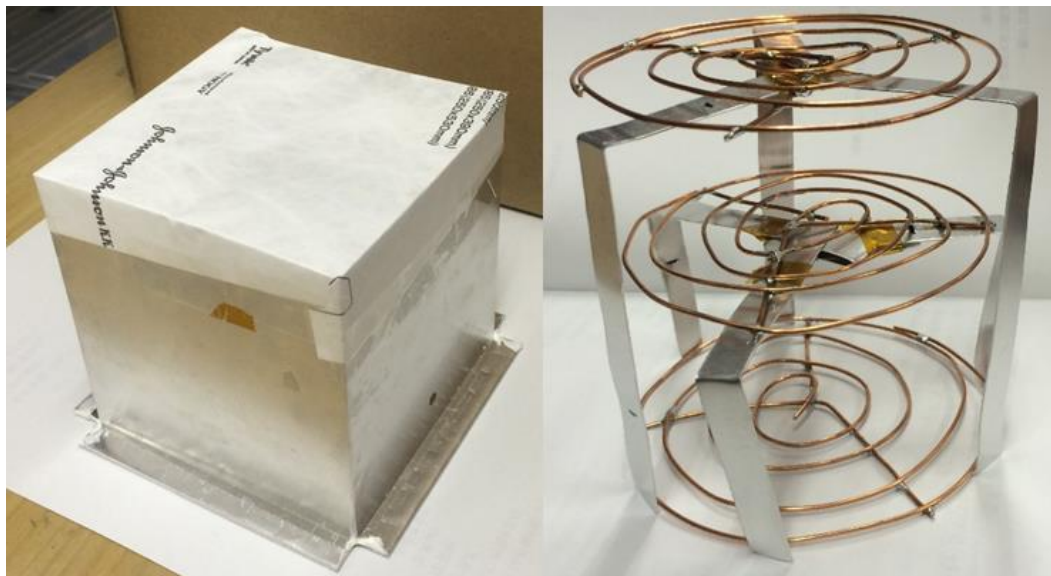
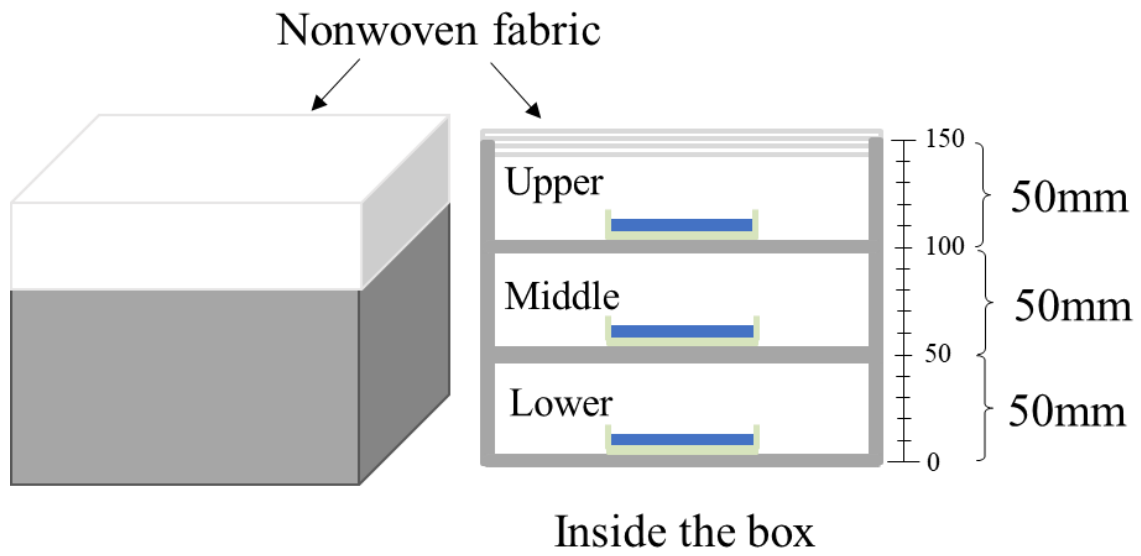


Fig. 2-1. Views of the exterior and interior of the test box ⁽²⁻⁷⁾.

A small amount of UV light is known to be transmitted by a single layer of nonwoven fabric. Fig. 2-2 shows the UV light transmittance of a layer of nonwoven fabric at 190 and 254 nm, as measured in this study. The values for the UV light transmittance at 190 and 254 nm were 0.008% and 0.023%, respectively. Therefore, it is conceivable that the AOS present in a test box “sealed” by a single layer of nonwoven fabric are generated both outside the box after permeating the nonwoven fabric ⁽²⁻¹⁾ and, to a small extent, inside the box by the UV light transmitted across the nonwoven fabric. To avoid this scenario, my colleagues and I covered the lid of the test box with three superimposed layers of nonwoven fabric, and the active oxygen exposure was performed with the complete blocking of UV light ⁽²⁻⁷⁾.

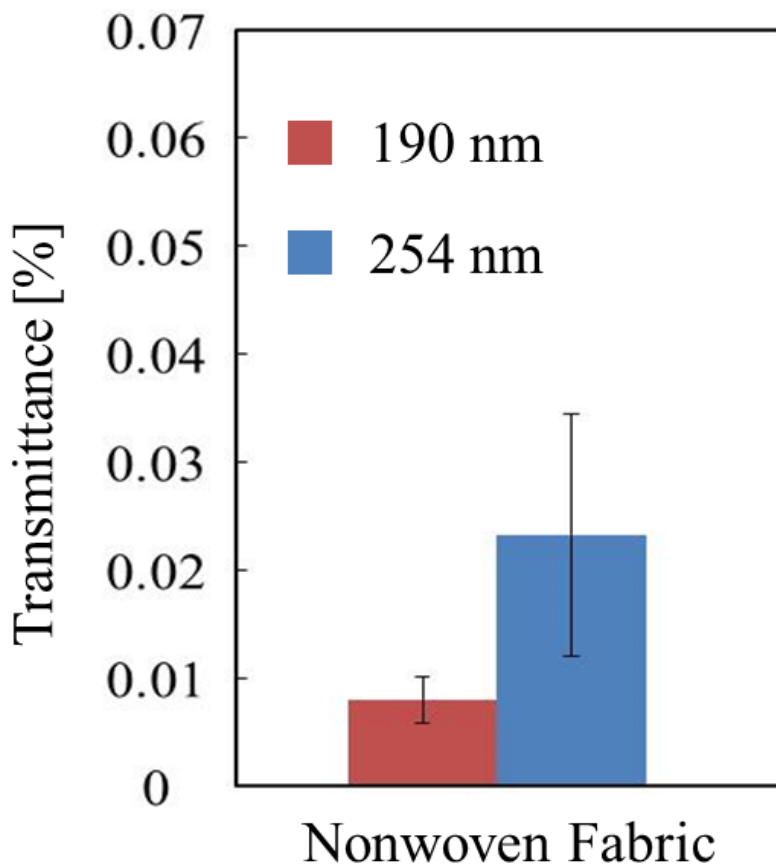


Fig. 2-2. UV light transmittance of the nonwoven fabric at 190 and 254 nm ⁽²⁻⁷⁾.

2-3-2 Active oxygen species detection and quantification by electron spin resonance

The spin-trapping agents 2,2,6,6-tetramethyl-4-piperidinol (TEMP; Sigma–Aldrich Co., LLC, USA) and 2-(5,5-dimethyl-2-oxo-2λ5-[1,3,2]dioxaphosphinan-2-yl)-2-methyl-3,4-dihydro-2H-pyrrole 1-oxide (CYPMPO; Kokko Pharmaceutical Industry Co., Ltd.) were used to detect and measure the amounts of $^1\text{O}_2$ and OH^* , respectively ^{(2-8), (2-9)}. Thus, ESR spectroscopy measurements were performed on AOS-exposed 1 mM TEMP solutions and 40 mM CYPMPO solutions. Fig. 2-3 shows the reaction schemes for CYPMPO and TEMP ⁽²⁻⁶⁾.

The generated $\text{O}(^1\text{D})$ species were detected via their reaction with a spin-trapping agent, namely, TEMP, thus resulting in stable molecules of 4-hydroxy-2,2,6,6-tetramethyl-piperidin-1-oxyl (TEMPOL) (Fig. 2-3). The UV lamps were used to irradiate a 1 mM TEMP solution for 30 min under high-humidity conditions. The concentration of the produced TEMPOL was detected using an ESR apparatus (JES-FA200, Jeol Ltd., Japan). A calibration curve was prepared using a TEMPOL solution ⁽²⁻⁶⁾.

The generated OH^* was also detected by the spin-trapping method. OH^* reacts with CYPMPO to produce stable molecules that are normally referred to as CYPMPO-OH (Fig. 2-3). The CYPMPO was dissolved in N,N-dimethylformamide, and the final concentration of the solution was 40 mM. The solution was placed into the AOS system for 5 min at high humidity. The generated CYPMPO-OH molecules were also detected using ESR ⁽²⁻⁶⁾⁻⁽²⁻⁷⁾.

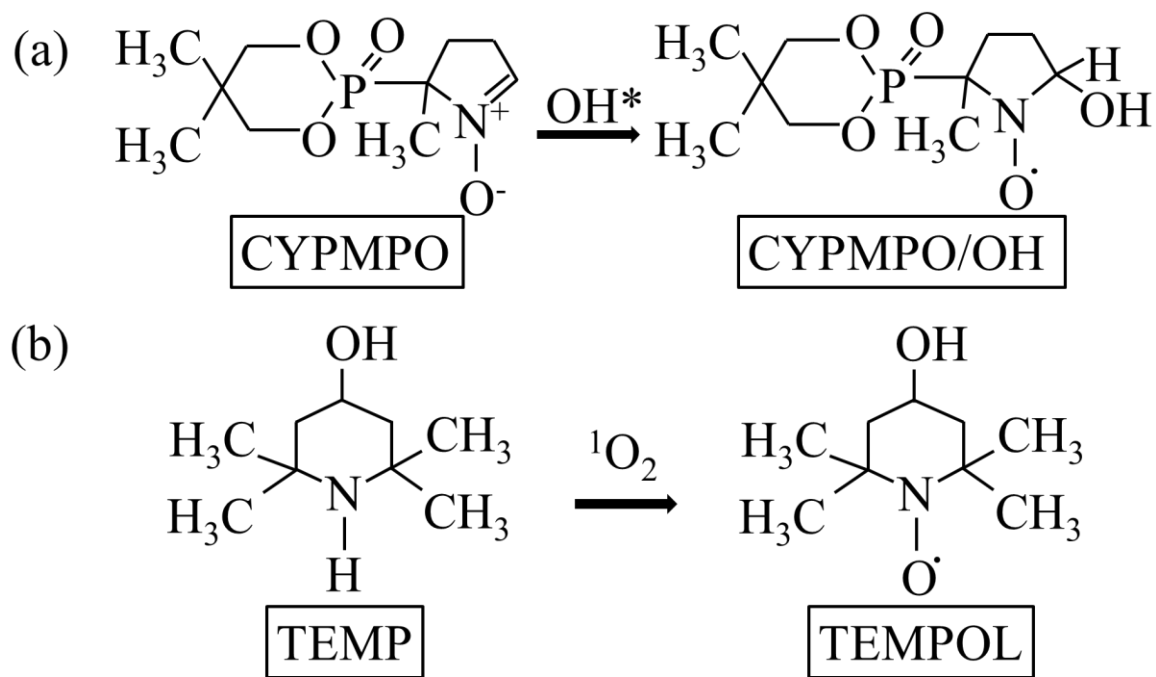


Fig. 2-3. Reaction schemes for (a) CYPMPO and (b) TEMP⁽²⁻⁷⁾.

Considering that AOS are highly reactive, they are quickly inactivated. Therefore, it is necessary to determine whether AOS have moved across the nonwoven fabric into the test box and reached down into the lower stage of the box, i.e., the stage that is most distant from the lid of the container. My colleagues and I investigated the presence of AOS inside the test box by using the spin-trapping method. In particular, dishes containing the solutions of the spin-trapping agents TEMP and CYPMPO were placed on each stage of the test box, which was covered with a triple layer of nonwoven fabric, and AOS exposure was performed in a high-humidity environment.

After the solutions of the spin-trapping agents were exposed to AOS, their ESR spectra were measured (JES-FA 200; JEOL RESONANCE Co., Ltd.), and the conditions detailed in Table 2-1 were implemented ⁽²⁻⁷⁾.

Table 2-1. ESR measurement conditions

Microfrequency	9.0 GHz
Magnetic field range	314.5–329.5 mT
Modulation frequency	100 kHz
Time	4 min
Mn	600
Time const.	0.03 s
Mod. width	0.2×1 mT
Amplitude	1.00×100

2-4 Results

2-4-1 Determination of the presence of active oxygen species inside the test box by the spin-trapping method

Fig. 2-4 (a) shows the ESR spectrum of a 1 mM solution of TEMP following its reaction with $^1\text{O}_2$. The measured value was obtained using the difference between the minimum and maximum values of the central peak. Fig. 2-4 (b) reports the ESR spectrum of a 40 mM CYPMPO solution following its reaction with OH^* . The measured value was also determined as the difference between the minimum and maximum values observed for the fourth or fifth peak from the left ⁽²⁻⁷⁾.

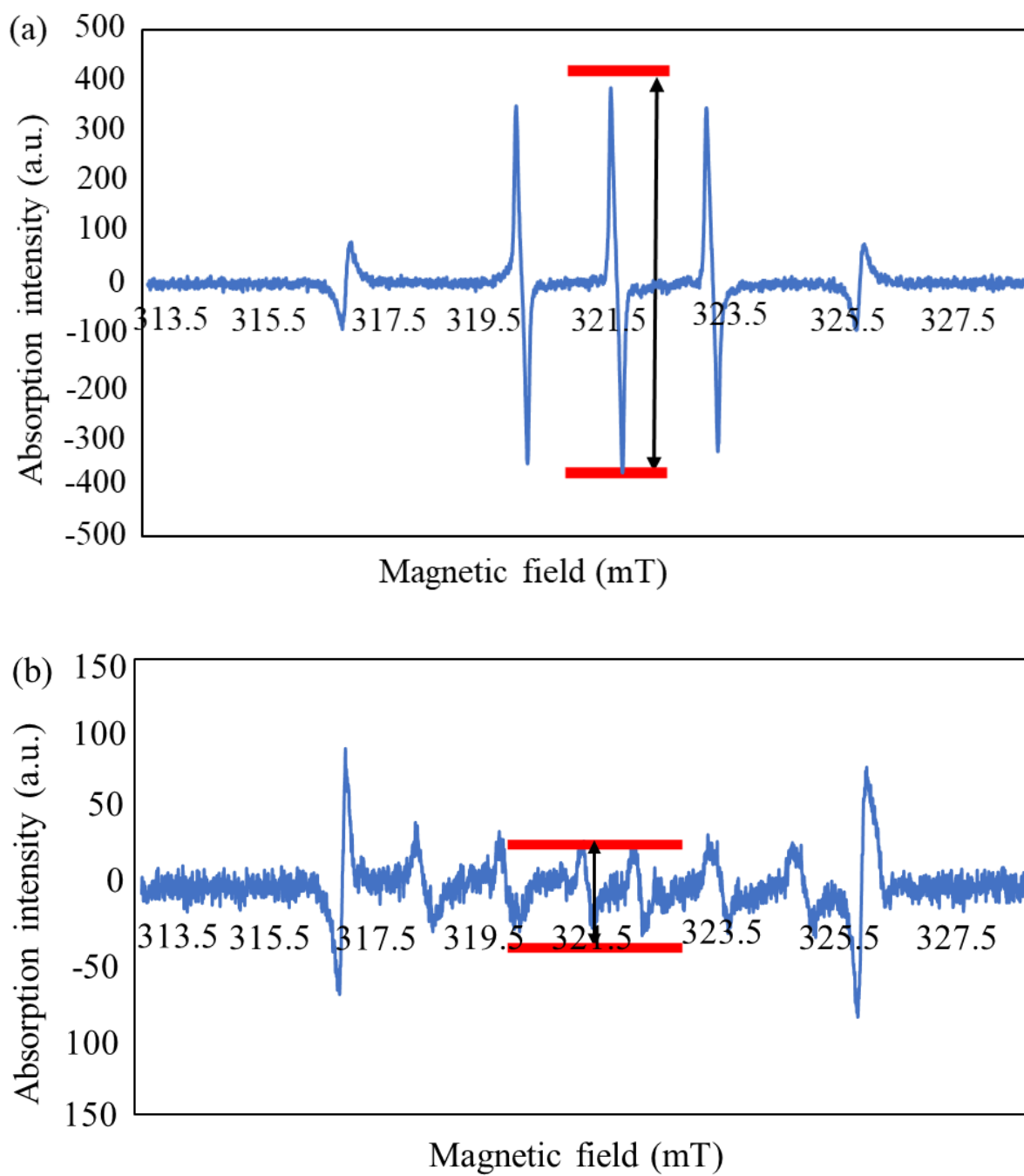


Fig. 2-4. ESR spectra of (a) a 1 mM TEMP solution after reacting with $^1\text{O}_2$ and (b) a 40 mM CYPMPO solution after reacting with OH^* ⁽²⁻⁷⁾.

Fig. 2-5 shows the absorption intensities of the solutions of the spin-trapping agents (1 mM TEMP and 40 mM CYPMPO) exposed to AOS in each stage. As the figure shows, the presence of AOS could be confirmed even in the lowest stage, which is the chamber furthest away from the UV light source. The peaks in the ESR spectrum associated with the presence of TEMPOL in a relevant solution of the spin-trapping agent suggest that TEMP reacted with $^1\text{O}_2$ (see Fig. 2-3) in all three stages. Similarly, the peaks in the ESR spectrum associated with the presence of CYPMPO/OH in the relevant solution of spin-trapping agent suggest that CYPMPO reacted with OH^* in all stages. Therefore, the evidence indicates that OH^* is also present in the lower stage despite its short lifetime ⁽²⁻⁷⁾.

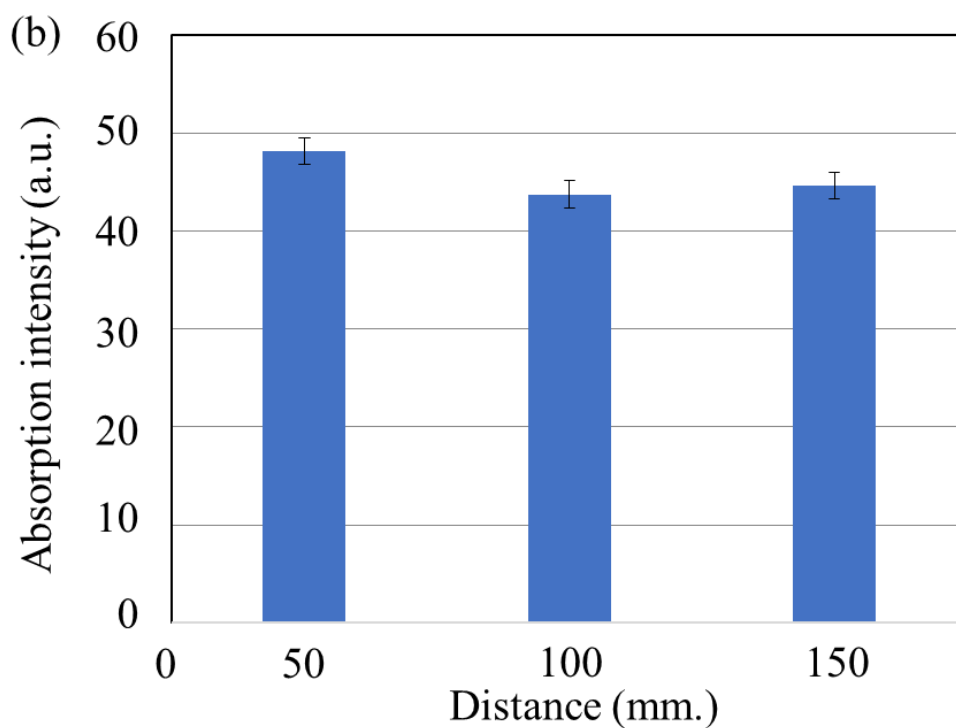
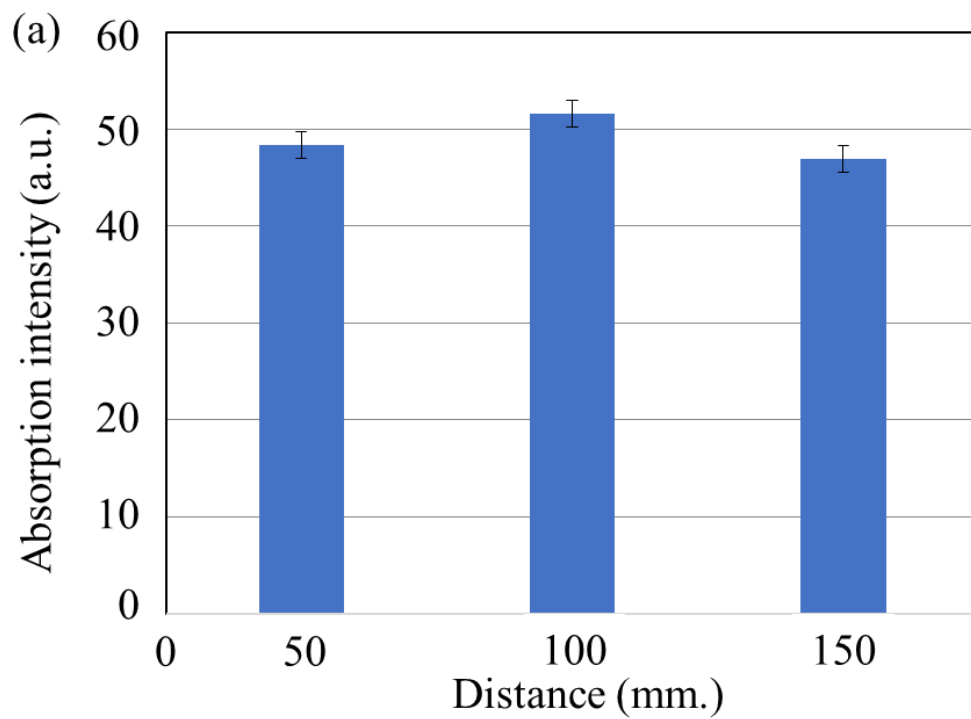
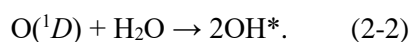
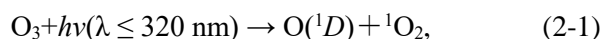


Fig. 2-5. Absorption intensity of the solution of spin-trapping agent (a) TEMP (1 mM) and (b) CYPMPO (40 mM) exposed to AOS in each stage of the test box: 50 (upper stage), 100 (middle stage), and 150 mm (lower stage) ⁽²⁻⁷⁾.

2-5 Discussion

According to the data reported in Fig. 2-5 (b), the absorption intensity of the solution of spin-trapping agent CYPMPO (40 mM) exposed to AOS in each stage of the test box placed in the upper stage was enhanced compared with the solution placed in the lower and middle stages. These results may be due to the lifetime of OH*. Given that the lifetime of OH* is short ⁽²⁻¹⁾ (i.e., approximately 70 ns), it is expected that OH* does not reach the lower stage, even if it passes through the nonwoven fabric. Furthermore, as shown in the intensity of the ESR peak associated with CYPMPO/OH, evidence confirmed that OH* groups are present as far down as the lower stage of the test box. The intensity of the ESR peak associated with CYPMPO/OH was observed even when the test box was sealed by the UV light-blocking triple layer of nonwoven fabric; thus, my colleagues and I believe that it is unlikely that any OH* is generated by UV light inside the test box. However, the lifetime of OH* is too short for it to reach the lower stage of the box. On the other hand, a long-lasting AOS such as ozone, which has lifetime of several hours ^{(2-1), (2-5)}, can move across the nonwoven fabric. This compound is known to react with ions (Equation 2-3).

The decomposition reaction of O₃ in the presence of UV light in high-humidity conditions is described as follows ⁽²⁻¹⁰⁾:



These equations indicate that OH* is generated in the presence of UV light and wet ozone outside the test box.

An OH* production model based on the reactivity between ozone and water inside the test box is considered. Given that OH* has a short lifetime, it is difficult for this species to reach the lower stage of the test box after going across the nonwoven fabric. Although the lifetime of AOS for ozone extends to several hours, the lifetime of these species is generally short [O(¹D): 1.1 × 10⁻⁹ s; ¹O₂: 1.7 × 10⁻³ s]. OH* formation as a consequence of the reactivity between ozone and water has already been reported ^{(2-11), (2-12)}. The autolysis reaction of ozone in water is described as follows ⁽²⁻¹³⁾:



The above shows that rather than the fact that OH^* is generated because of the UV light through the nonwoven fabric. The OH^* generated outside the nonwoven fabric permeates into the nonwoven fabric or some type of active oxygen such as ozone penetrates through the nonwoven fabric. Therefore, a chemical reaction with the water molecules in the nonwoven fabric occurred. OH^* was generated by the chemical reaction with the water molecules in the nonwoven fabric occurred. OH^* was generated by the chemical reaction with water via the autolysis of ozone inside the test box (Equation 2-3) ⁽²⁻¹³⁾, and this supports the possibility of reaching the lower stage (Fig. 2-6) ⁽²⁻⁷⁾.

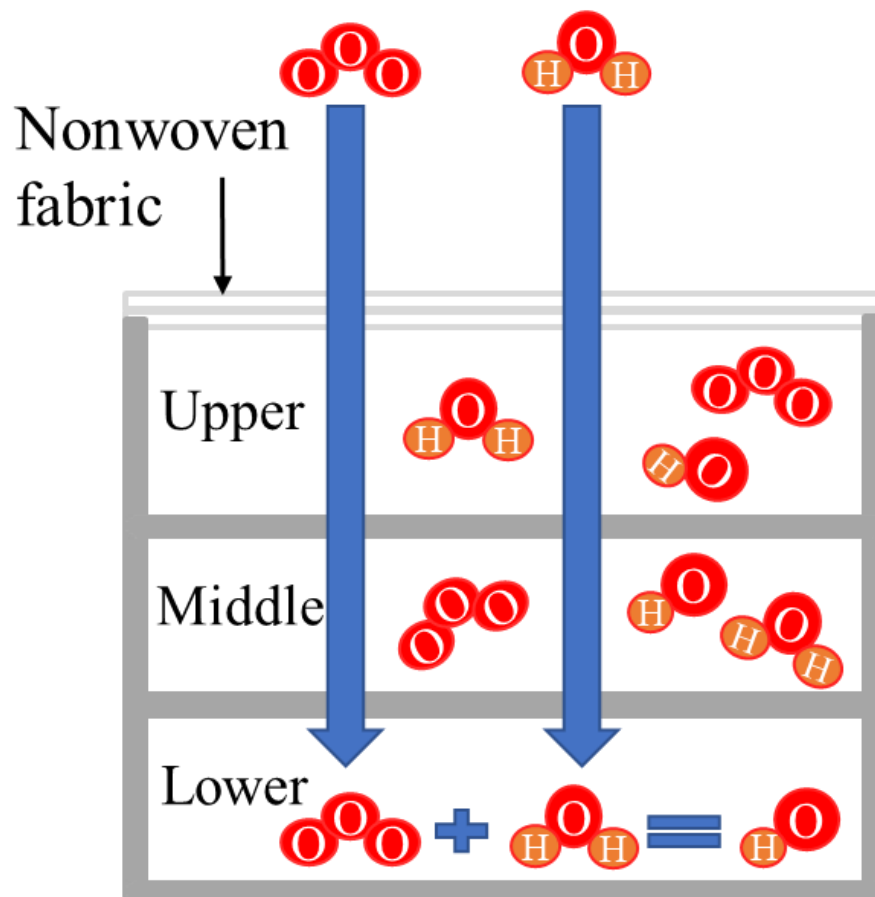


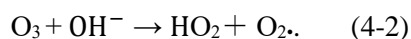
Fig. 2-6. Reactivity of O_3 with H_2O ⁽²⁻⁷⁾.

Ono et al. ⁽²⁻¹⁴⁾ reported on the effect of humidity on the density of AOS in a cylindrical reaction chamber equipped with UV lamps. Humid air was introduced, and the temperature (T) was maintained at 25 °C. The effect of humidity on the density of various radicals was examined. The levels of RH under the low- and high-humidity conditions in the present study were 20% and 90% RH, respectively. In their work on O₃ density in a chamber, Ono et al. ⁽²⁻¹⁴⁾ installed UV lamps with radiation powers of 1.9 and 12.2 W at 185 and 254 nm, respectively. These radiation powers are approximately the same as those of the UV lamps used in the present study. As already discussed, the O₃ densities generated under the low- and high-humidity conditions were predicted to be approximately 120 and 40 ppm, respectively ⁽²⁻⁶⁾. However, Ono et al. ⁽²⁻¹⁴⁾ controlled the O₃ density between 100 and 1000 ppm and predicted the O₃ density to be 275 and 104 ppm in the low- and high-humidity conditions, respectively. The chamber volume in the present study is 13,200 cm³, which is greater than that used in Ono's study (1508 cm³). The difference in the O₃ density between Ono's study and the present study is attributable to this difference in chamber size. However, when my colleagues and I evaluate the AOS concentrations on the basis of previously reported simulation results ⁽²⁻¹⁴⁾, the O₃ density ratios (i.e., the O₃ density under the low- and high-humidity conditions) in Ono's study and in the current study are 3.0 and 2.6, respectively.

The results show that the concentrations of the O₃, excited singlet oxygen [O₂(¹aΔg)], hydroperoxyl (HO₂), OH*, and oxygen atoms (O) are 6.88×10^{15} , 4×10^{13} , 2.4×10^{12} , 2×10^{11} , and 3.4×10^{10} cm⁻³, which represent 98.58%, 0.57%, 0.034%, 0.0029%, and 0.0005% of the total AOS density under the low-humidity conditions, respectively. The densities are 2.6×10^{15} , 3.1×10^{13} , 2.2×10^{12} , 6×10^{11} , and 1.2×10^{10} cm⁻³, which represent 97.57%, 1.16%, 0.083%, 0.023%, and 0.0005% of the total AOS density under the high-humidity conditions, respectively ⁽²⁻¹⁴⁾. These results indicate that the O₃ concentration is the highest among these radicals under both the low- and high-humidity conditions. OH* and HO₂ are produced under high-humidity conditions; however, the reaction rate constants for HO₂ and OH* are 10^2 – 10^3 L mol⁻¹ s⁻¹ and 10^8 – 10^9 L⁻¹ mol⁻¹ s⁻¹, respectively ⁽²⁻¹⁵⁾. My colleagues and I considered that the OH* plays an important role in the oxidation reaction under both humidity conditions.

My colleagues and I have already discussed the model of OH* production by O₃ and water inside the nonwoven fabric ⁽²⁻⁷⁾. Furthermore, an OH* formation reaction by O₃ and water has already been reported. Equation 2-3 shows the autolysis reaction of the O₃ under water ⁽²⁻¹³⁾.

The O₃ under water is easily decomposed. The decomposition reaction starts with the production of H₂O₂ via the reaction of O₃ and hydroxide ion, which is a dissociation component of water:



HO₂⁻ is a dissociation component of H₂O₂, which decomposes O₃ and generates products such as OH radicals. Therefore, O₃ is decomposed into oxygen molecules, and OH* radicals are generated in the process. However, the OH* radicals at the surface and/or in the indicator react quickly and disappear; thus, they do not accumulate.

2-6 Summary

For sterilization with AOS, it is necessary to use a nonwoven fabric. However, it is difficult to know whether the AOS have been uniformly sterilized spatially in the nonwoven fabric. Therefore, spin-trapping agents were placed on these three stages inside the box, and the AOS diffusion and presence of OH^* were investigated by monitoring the intensity of the ESR peak associated with the CYPMPO/OH observed in the different stages of the aluminum box. The peaks in the ESR spectrum with the presence of CYPMPO/OH, which is the product of the reaction CYPMPO between OH^* , were investigated in all stages to probe the mechanism by which OH^* diffuses across the various stages in the test box. The interior of the test box was rendered UV light impermeable by using three layers of nonwoven fabric as a “seal.” My colleagues and I found that only a small amount of OH^* was generated via UV light irradiation inside the test box sealed by a single layer of nonwoven fabric even if this seal did not fully prevent UV light from entering the test box. My colleagues and I conclude that the OH^* present inside the test box sealed with nonwoven fabric was mostly generated either outside the test box via UV light irradiation or inside the box via ozone decomposition due to the reaction of this species with water.

References

- (2-1) K. Yoshino, H. Matsumoto, T. Iwasaki, S. Kinoshita, K. Noda, K. Oya, and S. Iwamori, Investigation of a Sterilization System Using Active Oxygen Species Generated by Ultraviolet Irradiation, *Biocontrol Science*, Vol. 20, No.1 (2015), pp. 11-18.
- (2-2) 杉光英俊, オゾンの基礎と応用, 光琳, (1996), pp. 20-29.
- (2-3) 日本化学会編, 活性酸素種の化学, 季刊化学総説, No. 7 (1990), pp. 6-17.
- (2-4) K. Yoshino and S. Iwamori, Measurement of excited singlet oxygen molecule in a vacuum sterilization system, using electric spin resonance (ESR) with a water-soluble polymer thin film, *Journal of Photochemistry and Photobiology A: Chemistry*, Vol. 328 (2016), pp. 148-153.
- (2-5) M. C. DeRosa and R. J. Crutchley, Photosensitized singlet oxygen and its applications, *Coordination Chemistry Reviews*, 233/234 (2002), pp. 351-371.
- (2-6) K. Oya, R. Watanabe, Y. Soga, Y. Ikeda, T. Nakamura, and S. Iwamori, Effect of humidity conditions on active oxygen species generated under ultraviolet light irradiation and etching characteristics of fluorocarbon polymer, *Journal of Photochemistry and Photobiology A: Chemistry*, Vol. 298 (2015), pp. 33-39.
- (2-7) S. Yenchit, Y. Tadokoro, and S. Iwamori, Measuring Active Oxygen Species Across a Nonwoven Fabric Using a Pullulan-mixed Methylene Blue Thin Film and Electron Spin Resonance, *IEEJ Transactions on Sensors and Micromachines*, Vol. 139, No. 3 (2019), pp. 54-60.
- (2-8) Y. Lion, M. Delmelle, and A. van de Vorst, New method of detecting singlet oxygen production, *Nature*, Vol. 263 (1976), pp. 442-443.
- (2-9) M. Lee, Biomedical Application of Electron spin Resonance (ESR) Spectroscopy, *Yakugaku Zasshi*, Vol. 128, No. 5 (2008), pp. 753-763.
- (2-10) X. Wang, L. Liu, W. Fang, and X. Chen, Theoretical insight towards the photo-dissociation dynamics of O_3-H_2O complex: Deep understanding the source of atmospheric hydroxyl radical, *Chemical Physics Letters*, Vol. 608 (2014), pp. 95-101.
- (2-11) 吉田隆, OH ラジカル類の生成と応用技術, NTS, (2008), p. 228.

- (2-12) A. Kurokawa, Surface-Treatment Methods Using Ozone, Journal of the Vacuum Society of Japan, Vol. 56, No. 8 (2013), pp. 307-314.
- (2-13) 「オゾンと OH ラジカル (その 2) 」, 関西オゾン技術研究会技術ノート, No. 2 (2012).
- (2-14) R. Ono, Y. Nakagawa, Y. Tokumitsu, H. Matsumoto, and T. Oda, Effect of humidity on the production of ozone and other radicals by low-pressure mercury lamps, Journal of Photochemistry and Photobiology A: Chemistry, Vol. 274 (2014), pp. 13-19.
- (2-15) H. Sugimitsu, Application and Foundation of Ozone (Korin, Tokyo, 1996), p. 20 [in Japanese].

Chapter 3

A Colorimetric Indicator Based on Methylene Blue–Dyed Water-Soluble Polymer Uniform Thin Films for the Detection of Hydroxyl Radicals

3-1 Background

Owing to their remarkably strong oxidative ability, the active oxygen species (AOS) generated in the atmosphere can be applied in various industrial processes. It is well known that excited singlet oxygen atoms [$O(^1D)$], ozone (O_3), and OH^* are valuable in the field of surface modification. AOS can also be generated by ultraviolet (UV) lamps with wavelengths of 185 and 254 nm⁽³⁻¹⁾. Although numerous different AOS with long lifetimes or high oxidization abilities, such as $O(^1D)$, O_3 , OH^* , and hydrogen peroxide (H_2O_2), are known, $O(^1D)$ and OH^* are of particular interest⁽³⁻²⁰⁾. In our previous work, my colleagues and I noted that the OH^* concentration increased under high-humidity conditions⁽³⁻²⁾. To establish this technology for use with AOS, determining the presence of AOS and providing an indicator for the sterilization process are necessary; moreover, technology for detecting reactive AOS is highly necessary. However, the methods for measuring AOS in the atmosphere require specialized and expensive equipment. My colleagues and I previously reported that methylene blue (MB) can be decomposed by O_3 ^{(3-3)–(3-6)}. MB is a convenient indicator for the detection of AOS because the dye decomposes and decolorizes following exposure to AOS⁽³⁻⁷⁾. Therefore, my colleagues and I set out to develop a sensor that can be used to visually determine whether AOS is present in solution by way of the decolorization of MB. Notably, O_3 has lower oxidative ability than other AOS. To detect AOS with higher oxidative ability, it is necessary to stabilize MB by mixing it with water-soluble polymers, pullulan, and sodium alginate, which have high affinity for the dye, to form MB/pullulan and MB/sodium alginate composite films. My colleagues and I succeeded in developing an indicator that reacts only with OH^* , which is the AOS with the highest oxidizing power. Furthermore, my colleagues and I applied MB-dyed pullulan thin films to the aluminum test box sealed with nonwoven fabric. Pullulan and sodium alginate are natural and water-soluble polysaccharides that exhibit excellent film-forming ability.

Humidity affects the type of generated AOS. $O(^1D)$ and O_3 are typically produced under low-humidity conditions, whereas the oxidative species “ OH^* ” is mostly generated under high-humidity conditions. On the basis of this observation, the decolorization mechanism of the composite film is been investigated, and it was found that decolorization occurred only at high humidity; this is presumably caused by the presence of OH^* species⁽³⁻²⁾. MB degradation due to the reaction with OH^* has already

been reported ^{(3-8)–(3-10)}. Moreover, the specific decolorization mechanism of MB-dyed Nafion[®] films has been reported ⁽³⁻⁷⁾. However, the described indicator film was not a uniform thin film.

3-2 Purpose

It was clarified that MB mixed with a water-soluble polymer to form a thin film did not react with AOS, except hydroxyl radicals. However, the mechanism behind this was unknown. Therefore, to elucidate the decolorization mechanism upon exposure to OH* and apply it to industrial processes, my colleagues and I aimed to create a uniform thin film indicator based on MB and water-soluble polymers, namely, pullulan and sodium alginate. Furthermore, the decolorization mechanism was investigated by comparing the nuclear magnetic resonance (NMR) spectra of MB mixed with water-soluble polymers before and after exposure to AOS ^{(3-11)–(3-13)}.

3-3 Experimental apparatus and experimental methods

3-3-1 The molecular structures of MB, pullulan, and sodium alginate ^{(3-12), (3-13)}

Fig. 3-1 presents the molecular structures of the MB dye, pullulan, and sodium alginate. MB is a redox dye used as a colorimetric oxygen indicator ^{(3-4), (3-5)}. MB was previously used to investigate the photochemical stability of biopolymers ⁽³⁻¹⁴⁾. As a consequence of its stability, the decomposition of MB is known to be particularly used in conventional wastewater treatment methods ⁽³⁻¹⁵⁾. On the other hand, pullulan is a polysaccharide polymer consisting of maltotriose units with excellent film-forming abilities. The three glucose units in maltotriose are connected by an α -1,4 glycosidic bond, whereas the consecutive maltotriose moieties are connected to each other by an α -1,6 glycosidic bond ⁽³⁻¹⁶⁾. Pullulan also contains numerous OH groups, which are considered to form interactions with MB at N+/S+. Sodium alginate (C₆H₇O₆Na) is a linear polysaccharide that is derivative of alginic acid. Alginates are linear binary copolymers comprising homopolymeric regions of β -D-mannuronic acids (M) and α -L-guluronic acids (G), residues connected via (1,4)-glycoside linkages in regions of M-, G-, and MG-sequential block structures (Fig. 3-1 [c]) ^{(3-17), (3-18)}. Sodium alginate is a cell-wall component of marine brown algae and contains approximately 30%–60% alginic acid. The conversion of alginic acid to

sodium alginate confers solubility in water, and this process facilitates its extraction⁽³⁻¹⁹⁾. Furthermore, sodium alginate contains OH and COONa, which are also considered to interact with MB at N+/S+.

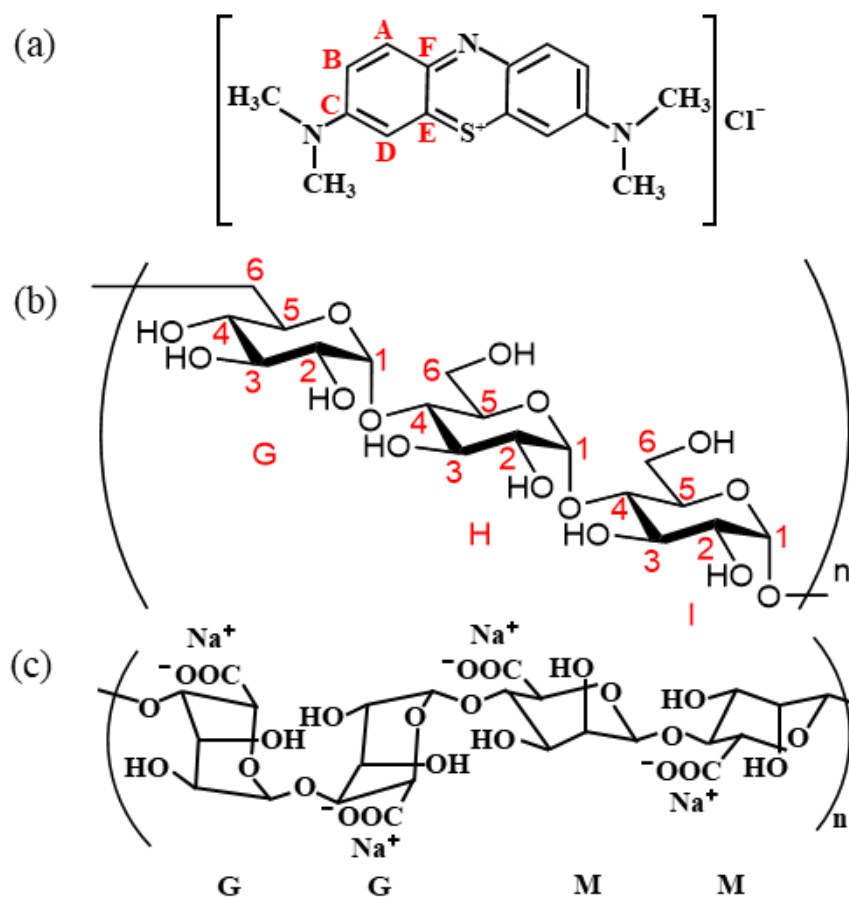


Fig. 3-1. The molecular structures of (a) MB, (b) pullulan, and (c) sodium alginate. The letters and numbers marked in red indicate the positions of protons and carbon atoms in the ¹³C- NMR spectra⁽³⁻

12), (3-13).

3-3-2 Exposure to active oxygen species

My colleagues and I used Active Dry® (Iwasaki Electric Co., Ltd., Tokyo, Japan) to generate AOS. Three UV lamps were installed in the chamber, with two having a power of 6 W and one having a power of 4 W. The utilized UV lamps emitted UV radiation at 185 and 253.7 nm to generate AOS⁽³⁻¹⁾. Given that humidity affects the type of AOS generated, the MB-dyed pullulan films in the present study were exposed to AOS in different humidity conditions. To achieve high-humidity conditions (humidity > 90%), warm air was produced by pumping boiled water at a temperature of 30 °C, and Active Dry® was used. Furthermore, to achieve low-humidity conditions (humidity < 20%), dry air was pumped through silica gel (large granules containing a blue indicator), which was maintained at 30 °C without passing through boiled water and was connected to Active Dry®⁽³⁻²⁾. Experiments up to 50 RH% were attempted on the low-humidity side, but no decolorization occurred. On the high-humidity side, the behavior clearly appeared at 90 RH% or more even though decolorization occurred from 70 RH%. To clarify the decolorization mechanism, the evaluation was performed by focusing on the low-humidity side (20 RH%) and the high-humidity side (90 RH%). Although the phenomenon of decolorization may change depending on the applied temperature, my colleagues and I aimed to analyze the phenomenon at 30 °C near room temperature.

3-3-3 Preparation of a hydroxyl radical indicator using a pullulan-mixed methylene blue dye thin film

The OH* indicator “MB-dyed pullulan” was prepared as follows. A Petri dish of ϕ 40 mm \times 13.5 mm containing 1,300 μ L of water was prepared, and 700 μ L of 100 g/L pullulan (model number PU 101, Hayashibara) solution and 400 μ L of 0.6 g/L MB (model number 1 B-429, WALDECK) solution were added and mixed. Thereafter, the Petri dish was placed in an incubator set at 40 °C for 15 h. The thicknesses of the thin film that formed after 15 h were 0.4 ± 0.02 mm and 0.5 ± 0.02 mm in the middle and edge, respectively⁽³⁻¹³⁾.

3-3-4 Preparation of a hydroxyl radical indicator using a sodium alginate–mixed methylene blue dye thin film

The OH* indicator “MB-dyed sodium alginate” was prepared as follows. A Petri dish of ϕ 40 mm \times 13.5 mm containing 1,300 μ L of water was prepared, and 700 μ L of 20 g/L sodium alginate solution and 400 μ L of 0.6 g/L MB solution were added and mixed. Thereafter, the Petri dish was placed in an incubator set at 40 °C for 15 h. The thickness of the thin film that was formed after 15 h was 7.6 ± 0.02 μ m in the middle and edge⁽³⁻¹²⁾.

3-3-5 Preparation of MB and water-soluble polymer solution upon AOS exposure in high-humidity conditions for carbon-13 NMR analysis

The decolorization of the MB using a thin film indicator based on MB and water-soluble polymers indicated that the chemical structure of MB molecules changed; this change could be confirmed using proton NMR (¹H-NMR) and carbon-13 NMR (¹³C-NMR) spectra^{(3-21)–(3-24)}. The carbon signals of the benzene ring and methyl group of MB disappeared, and this was caused by the AOS generated under high-humidity conditions.

The AOS generated under high-humidity conditions induced the decolorization of the MB-dyed water-soluble polymer film; this was investigated by comparing the ¹³C-NMR spectra before and after the exposure of the solution of the MB and water-soluble polymers to the AOS generated under high-humidity conditions. Under high-humidity conditions, the mixture after the AOS exposure of a mixture of MB/pullulan was prepared by mixing 60 μ l of 100 g l⁻¹ pullulan with 200 μ l of 0.6 g l⁻¹ aqueous MB solution (total volume = 260 μ l), and a mixture of MB/sodium alginate was prepared by mixing 300 μ l of 10 mM sodium alginate with 300 μ l of 25 mM MB (total volume = 600 μ l). To elucidate the mechanism of decolorization of the MB-dyed water-soluble polymer film caused by OH*, ¹³C-NMR analyses were performed utilizing a Bruker® AVANCE III 500 MHz Ultra Shield spectrometer. Deuterium oxide was used as the solvent to distinguish from hydrogen in the MB, pullulan, and sodium alginate. A large amount of the MB sample was required for the NMR analysis. The solutions were spread on a glass substrate and dried to form a thin film. To acquire a large amount of sample and to

eliminate the effects of UV light on the decolorization reaction, 20 glass substrates of a mixture of MB/pullulan solution and 3 glass substrates of a mixture of MB/sodium alginate solution were placed in a sterilization bag comprising a plastic film and a nonwoven fabric (Johnson and Johnson K.K.). UV light could not penetrate the sterilization bag; however, AOS could permeate the bag⁽³⁻¹⁾. The samples were used for the NMR analyses. Each thin film was subjected to AOS exposure until it was completely decolorized after 7 h under high-humidity conditions. Subsequently, each thin film-coated glass substrate was placed in 15 ml of D₂O, and the thin film was dissolved using an ultrasonic cleaner. To increase the concentration of the solution mixture for ¹H-NMR and ¹³C-NMR analyses, the resulting solution was heated and evaporated until the volume of 10 ml was reached^{(3-12), (3-13)}. For the ¹³C-NMR analysis, a highly concentrated solution was prepared using the FD-1[®] freeze-dryer.

3-3-6 Preparation of a hydroxyl radical indicator using a pullulan-mixed methylene blue dye thin film for comparing with ESR

A uniform thin film can be formed by mixing pullulan (model number PU 101, Hayashibara) with an aqueous MB solution (model number 1 B-429, WALDECK)⁽³⁻²⁵⁾. In the current study, the homogeneous thin film was prepared by mixing together 525 μ L of 0.12 g/L aqueous MB solution, 600 μ L of 100 g/L aqueous pullulan solution, and 1275 μ L of pure water. The resulting 2400 μ L mixture was then poured into a \varnothing 40 mm \times 13.5 mm polystyrene Petri dish. The dish was in turn placed in an incubator (AS ONE Corporation), where it was allowed to dry at 40 °C for 15 h. The thicknesses of the thin film were 0.4 ± 0.02 mm and 0.5 ± 0.02 mm in the middle and at its edge, respectively. The pullulan-mixed MB dye thin film indicator was installed in the nonwoven fabric used to seal the aluminum test box at all stages. Furthermore, to obtain correlation with AOS diffusion in the nonwoven fabric, a pullulan-mixed MB thin film was also placed together with the ESR spectrum by using spin-trapping agents, and AOS exposure experiments, which generated in high-humidity conditions by Active Dry[®], were conducted⁽³⁻¹¹⁾.

The transmittance of the thin film exposed to AOS was measured using an UV-visible spectrophotometer (UV-2450, Shimadzu Corporation). The thin film was fixed to the light transmission

section of the spectrophotometer, and the measurement was performed within the 300–800 nm wavelength range. The transmittance of the thin film was evaluated at 670 nm, which is the maximum absorption wavelength.

3-3-7 Preparation of ozone exposure in the different environmental conditions of active oxygen species exposure

My colleagues and I used an ozonizer (YGR-203N, REI-SEA), which is an equipment that generates ozone, to generate ozone in this study. Experiments were conducted with “dry ozone,” wherein the amount of water present was made as low as possible by using silica gel, and with “wet ozone,” wherein a high concentration of moisture was introduced from a bottle of boiling water. In these experiments, the ozonizer was connected to an oxygen tank with an O₂ flow rate of 1 L/s (see Fig. 3-2) (3-11).

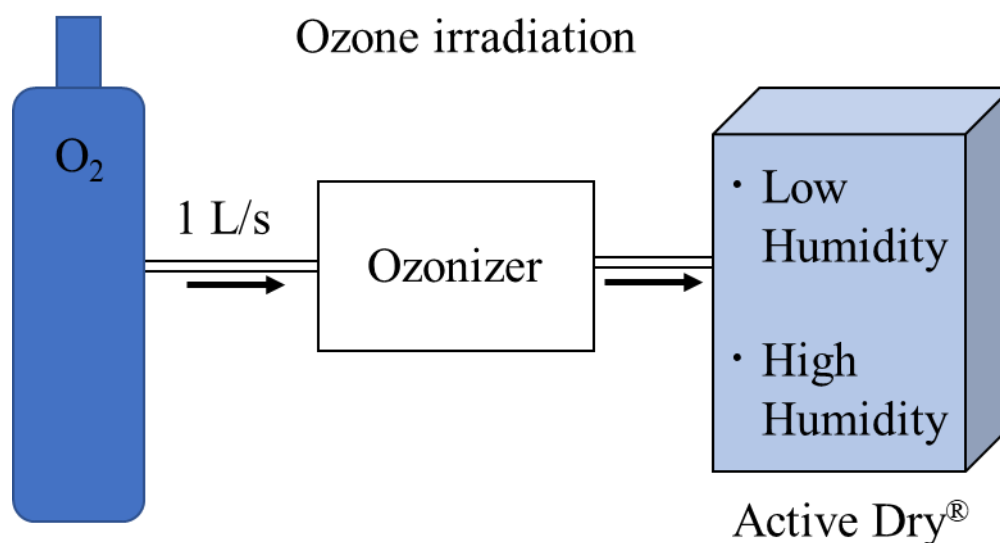


Fig. 3-2. Setup for investigating ozone exposure in different environmental conditions (3-11).

3-4 Results

3-4-1 Decolorization of the MB-dyed water-soluble polymer thin films due to AOS exposure under different environmental conditions

Figures 3-3 and 3-5 show the thin films of MB-dyed pullulan and sodium alginate and the decolorization of the films deposited on the glass substrates after AOS exposure, respectively. It is evident that the MB-dyed pullulan film and sodium alginate film lost coloration upon exposure to AOS under high-humidity conditions, which was maintained at >90%. Furthermore, the shape of the MB-dyed pullulan thin film after the AOS exposure under high-humidity conditions drastically changed. In the presence of water vapor, the weight of the thin film slightly increased (approximately 9 mg) after AOS exposure in high-humidity conditions. On the other hand, the film was hardly decolorized upon exposure to AOS under low-humidity conditions. It is widely known that AOS such as HO_2 and OH^* are generated under high-humidity conditions with UV light. OH^* is of particular interest with regard to stability and oxidative ability in the atmosphere⁽³⁻²⁾. The superoxide anions and OH^* are the major reactive species produced during photocatalytic reactions⁽³⁻²⁶⁾. Furthermore, the amount of generated OH^* depends on the humidity⁽³⁻¹⁾, and it is considered that the OH^* may affect the decolorization of the film under high-humidity conditions^{(3-2), (3-12), (3-13)}.

Figures 3-4 and 3-6 show the decolorization transmittance spectra of the MB-dyed pullulan thin films and the MB-dyed sodium alginate thin film, respectively, due to AOS exposure for 1 h under low- and high-humidity and untreated conditions. The decolorization signal of the thin film after AOS exposure for 1 h under high-humidity conditions at a wavelength of 600–700 nm was dramatically increased compared with that of the untreated signal and AOS exposure for 1 h under low-humidity conditions⁽³⁻¹²⁾.

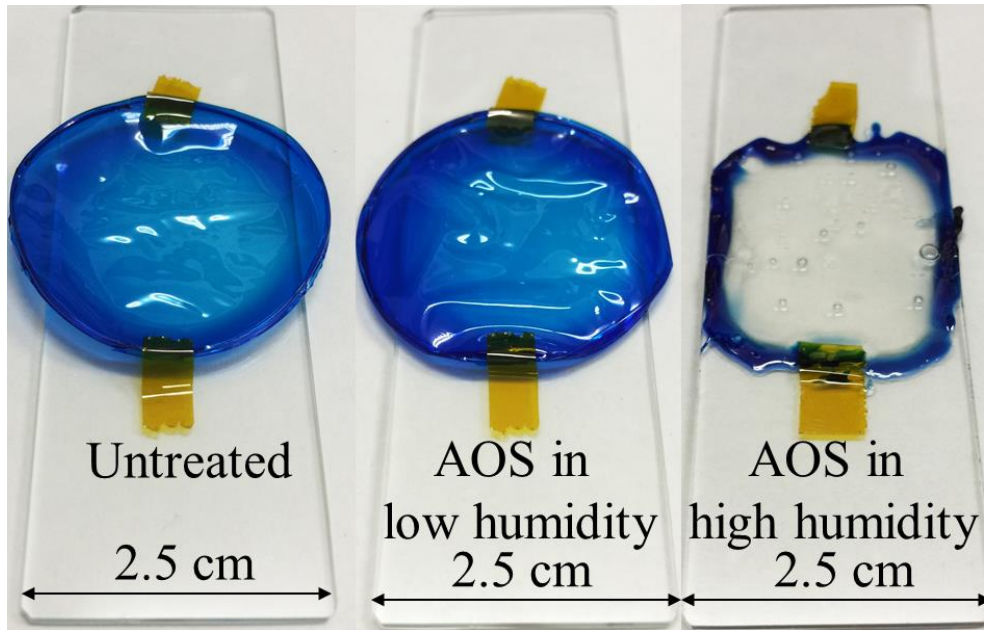


Fig. 3-3. Decolorization of MB-dyed pullulan thin films set on glass substrates after exposure to AOS under low- or high-humidity conditions ⁽³⁻¹³⁾.

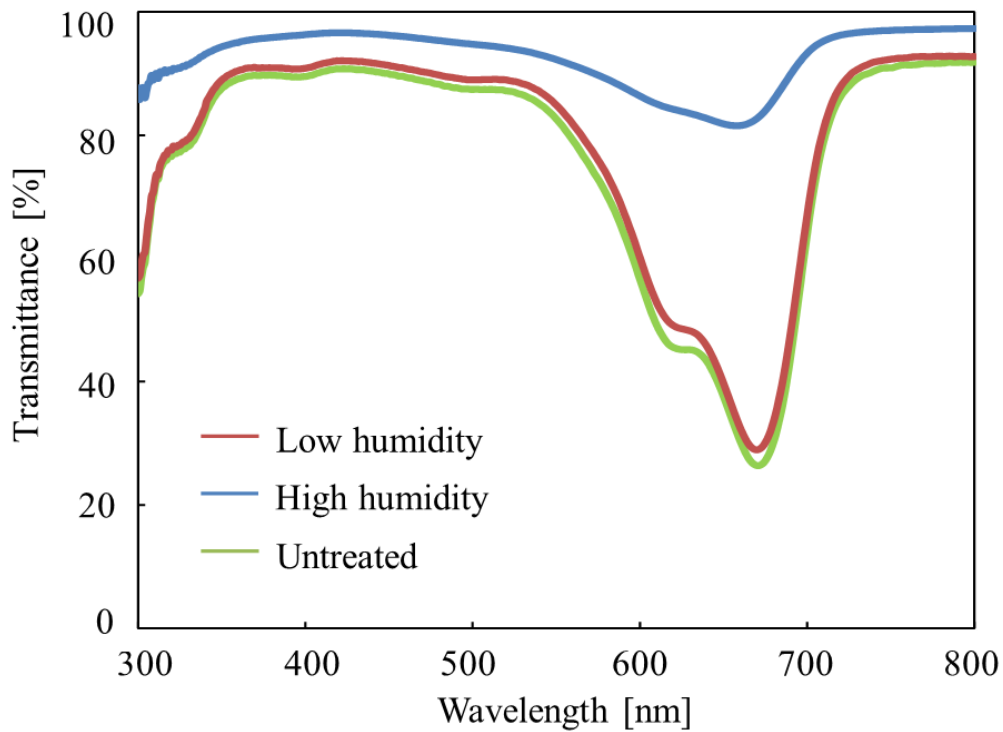


Fig. 3-4. Transmittance of the decolorization of MB-dyed pullulan thin films due to AOS exposure for 1 h under low- and high-humidity conditions and untreated conditions.

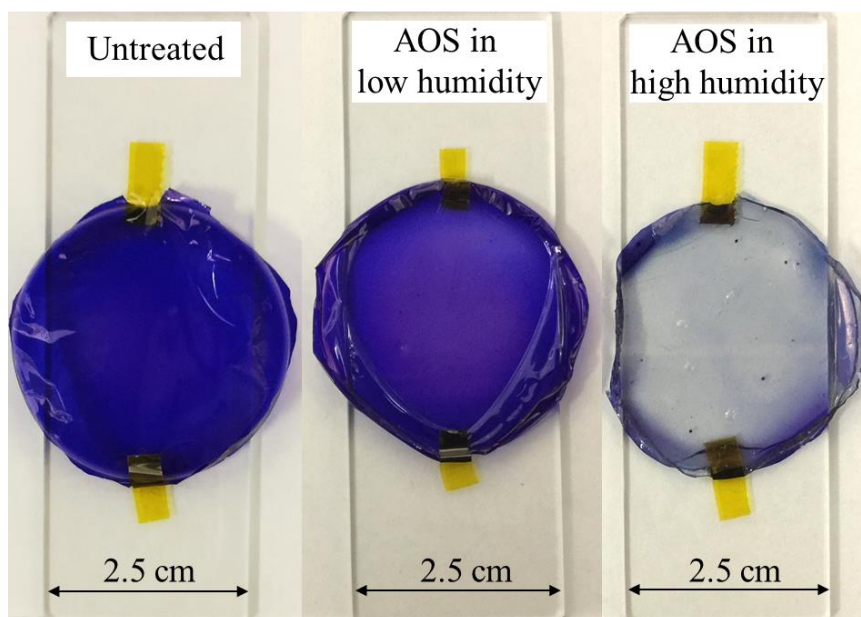


Fig. 3-5. Decolorization of MB-dyed sodium alginate thin films set on glass substrates due to AOS exposure for 1 h under low- and high-humidity conditions ⁽³⁻¹²⁾.

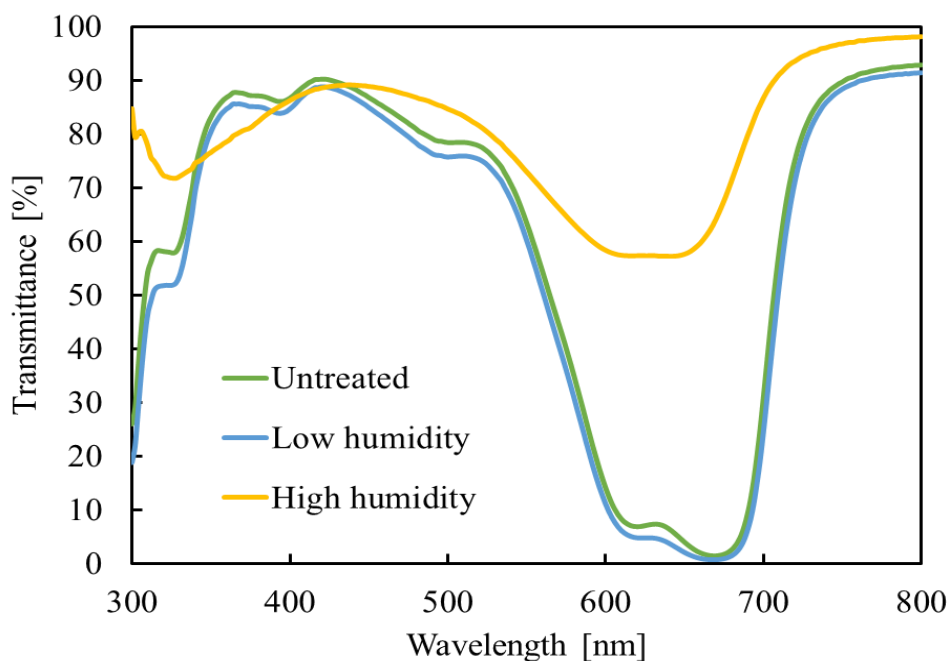


Fig. 3-6. Transmittance of decolorization of MB-dyed sodium alginate thin films due to AOS exposure for 1 h under low- and high-humidity conditions and untreated conditions ⁽³⁻¹²⁾.

3-4-2 Results of the ^{13}C -NMR analysis of the decolorization of MB-dyed pullulan thin films upon AOS exposure in high-humidity conditions

Figure 3-7 illustrates the ^{13}C -NMR spectra of the mixtures of MB and pullulan before and after OH^* exposure under high-humidity conditions. This figure shows that the peaks observed at approximately 100.2, 99.7, 77.8, 77.4, and 71.3 ppm correspond to pullulan (Fig. 3-7 (a))⁽³⁻²⁷⁾. As shown by the ^{13}C -NMR spectra of the interior carbon atom, spectral lines can be observed at 101.2, 100.7, 78.8, 78.4, and 72.3 ppm⁽³⁻²⁸⁾. Moreover, the six peaks between 105 and 155 ppm corresponding to the carbon atoms of the benzene ring disappeared upon AOS exposure under high-humidity conditions (Fig. 3-7 [b]). The spectra of a mixture of MB and pullulan before and after OH^* exposure under high-humidity conditions exhibit characteristic peaks at approximately 63–60 ppm, which can be assigned to the C_6 atoms. Furthermore, the signals corresponding to the C_1 atoms are present at approximately 100–104 ppm. The multitude of signals assigned to the $\text{C}_{2,3,5}$ atoms are located between 69 and 76 ppm^{(3-29)–(3-31)}. All peaks in the spectra of the mixture of MB and pullulan remain unchanged, with the exception of the signals corresponding to the benzene ring of MB. Therefore, the decolorization of the MB-dyed pullulan film was achieved by the OH^* exposure under high-humidity conditions⁽³⁻¹³⁾.

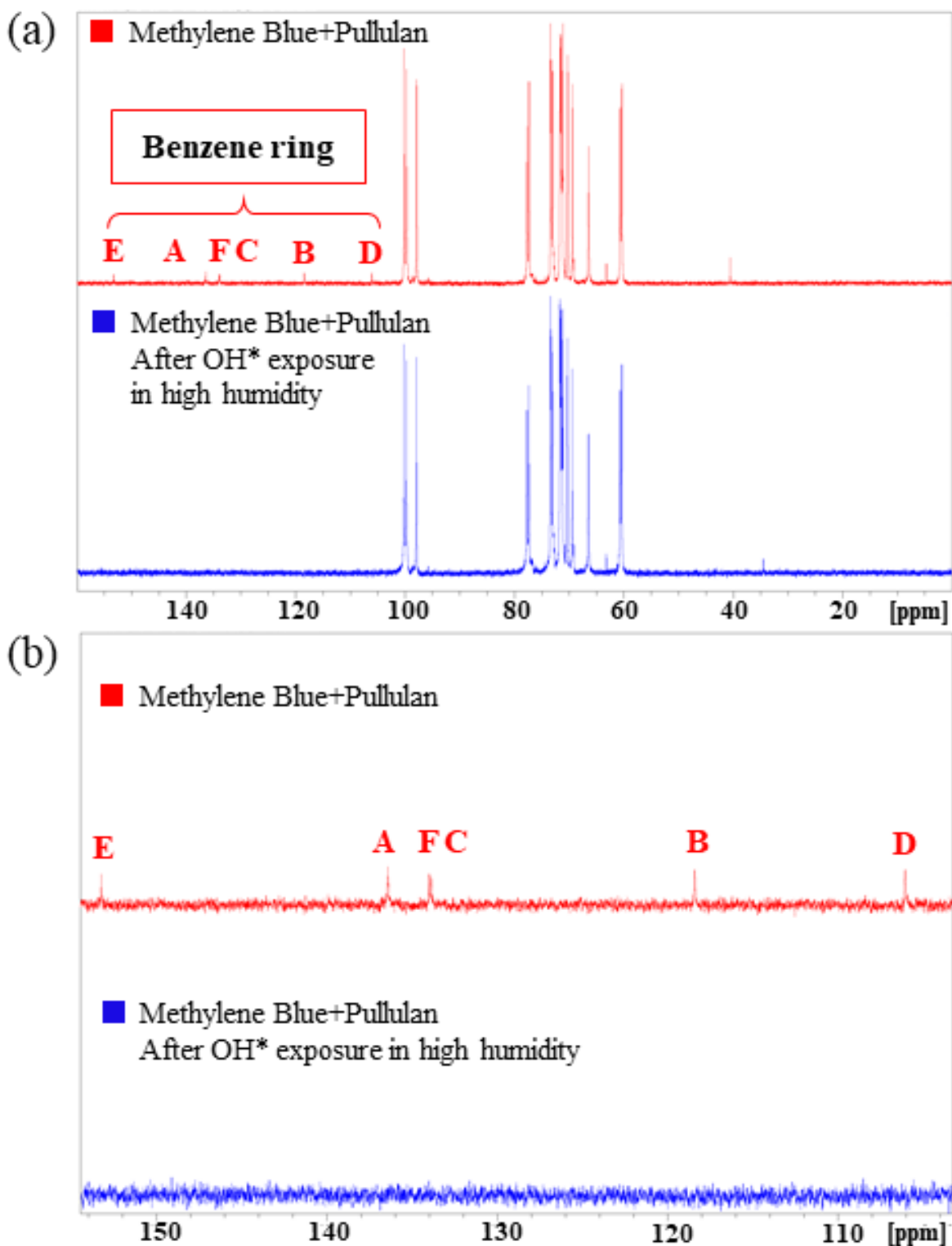


Fig. 3-7. ^{13}C -NMR spectra of the mixtures of MB and pullulan before and after OH* exposure under high-humidity conditions. (a) The entire spectrum and (b) benzene ring of MB. A, B, C, D, E, and F correspond to the carbon positions shown in Fig. 3-1 (a) ⁽³⁻¹³⁾.

3-4-3 Results of the ^{13}C -NMR analysis of the decolorization of MB-dyed sodium alginate thin films upon exposure to AOS under high-humidity conditions

Figure 3-8 shows the ^{13}C -NMR spectra of the mixtures of MB and sodium alginate before and after the AOS exposure under high-humidity conditions. The results suggest that the six peaks between 105 and 153 ppm (A, B, C, D, E, and F) corresponding to the benzene ring of MB disappeared owing to the AOS exposure under high-humidity conditions. On the basis of quantum chemical calculations, the benzene ring is known to have decomposed^{(3-32)–(3-35)}. Therefore, the decolorization of the MB-dyed sodium alginate film was achieved via AOS exposure under high-humidity conditions. This indicates that MB was decomposed by the AOS generated under the high-humidity conditions, as reported previously⁽³⁻²⁾. Furthermore, the MB degradation reaction owing to AOS has been previously reported^{(3-12), (3-36)}.

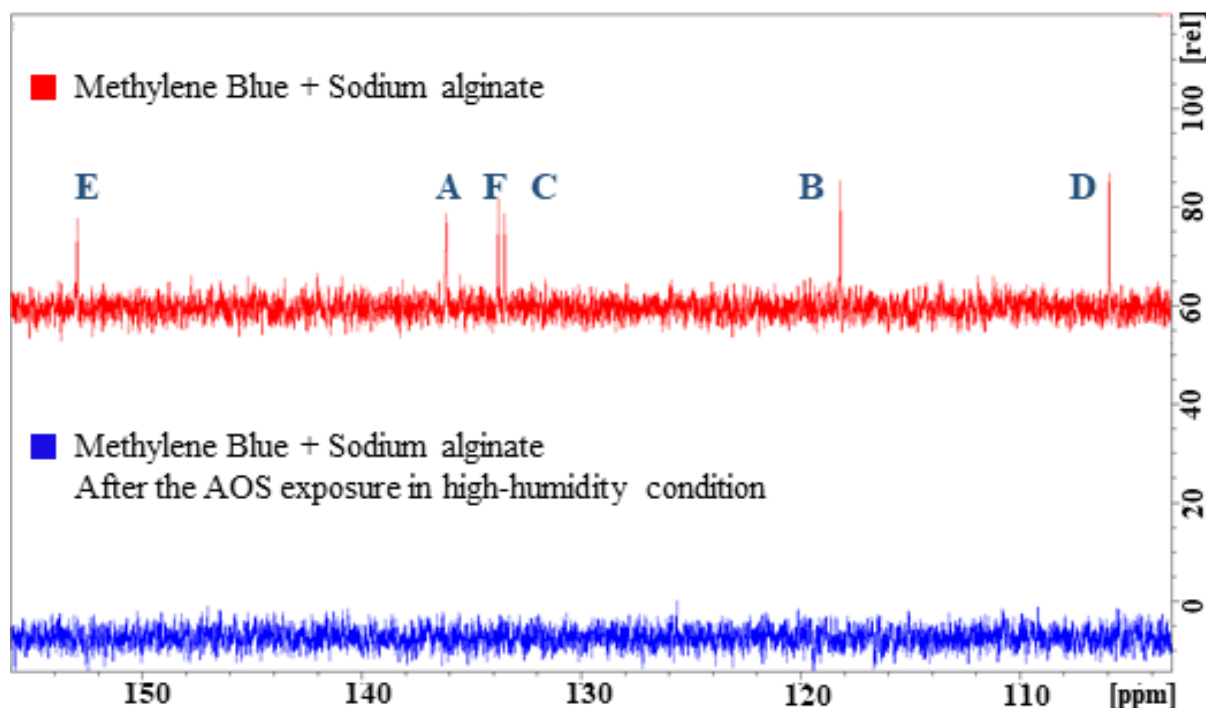


Fig. 3-8. ^{13}C -NMR spectra of the mixtures of the MB and sodium alginate before and after AOS exposure under high-humidity conditions. A, B, C, D, E, and F correspond to the carbon positions shown in Fig. 4-1 (a)⁽³⁻¹²⁾.

3-4-4 Changes in the extent of bleaching determined by the distance from the nonwoven fabric

Figure 3-9 shows the summary of the decolorization data on the pullulan-mixed MB dye thin film for each stage exposed to AOS. After a 15 min exposure, the thin film with the highest transmittance was the one that had been placed in the upper stage. The decolorization of thin films was confirmed at all stages. The evidence suggests that the tendency of the thin films to decolorize depended on the stage where each film was located. As a result, it is expected that the amount of OH^* generated decreases as the exposure time increases ⁽³⁻¹¹⁾.

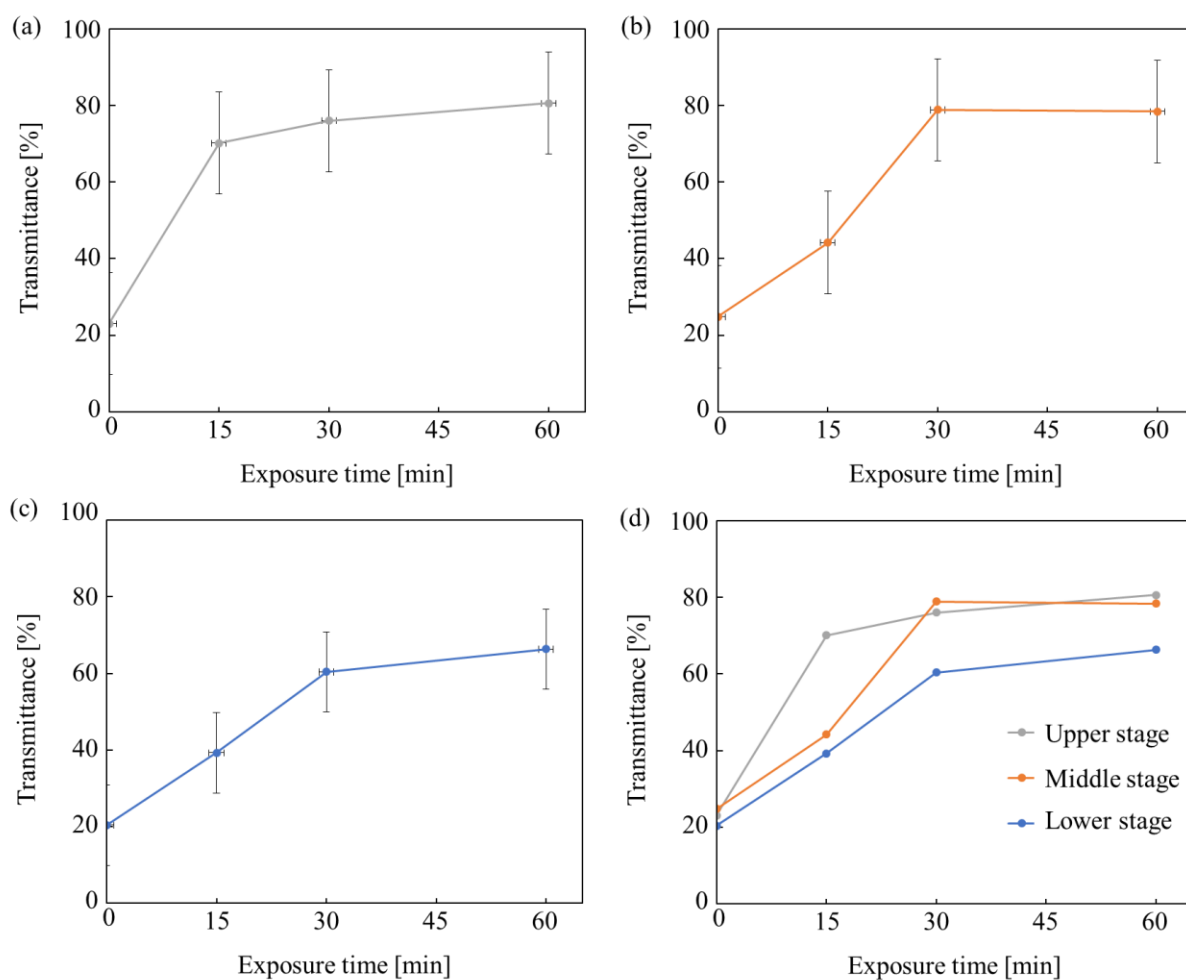


Fig. 3-9. Decolorization of the thin films located in the (a) upper stage, (b) middle stage, (c) lower stage, and (d) all stages ⁽³⁻¹¹⁾.

3-4-5 Results of AOS exposure when the test box was sealed by three layers of nonwoven fabric

Figure 3-10 shows the results of measuring the transmittance at the maximum absorption wavelength of the pullulan-mixed MB dye thin film. These results indicate that the thin film was decolorized to the same extent in all three stages. On the basis of this evidence, my colleagues and I believe that light penetrated the test box because thin film decolorization occurred even though the test box interiors were shielded from UV light by three overlapping layers of nonwoven fabric. Furthermore, given that decolorization was also observed to take place in the lower stage, the evidence indicates that even in the presence of a seal formed by three overlapping layers of nonwoven fabric, OH* was present all the way down to the lower stage of the box. The results of the ESR spectrum also suggest that a pullulan-mixed MB film can be used as an indicator of OH* presence ⁽³⁻¹¹⁾.

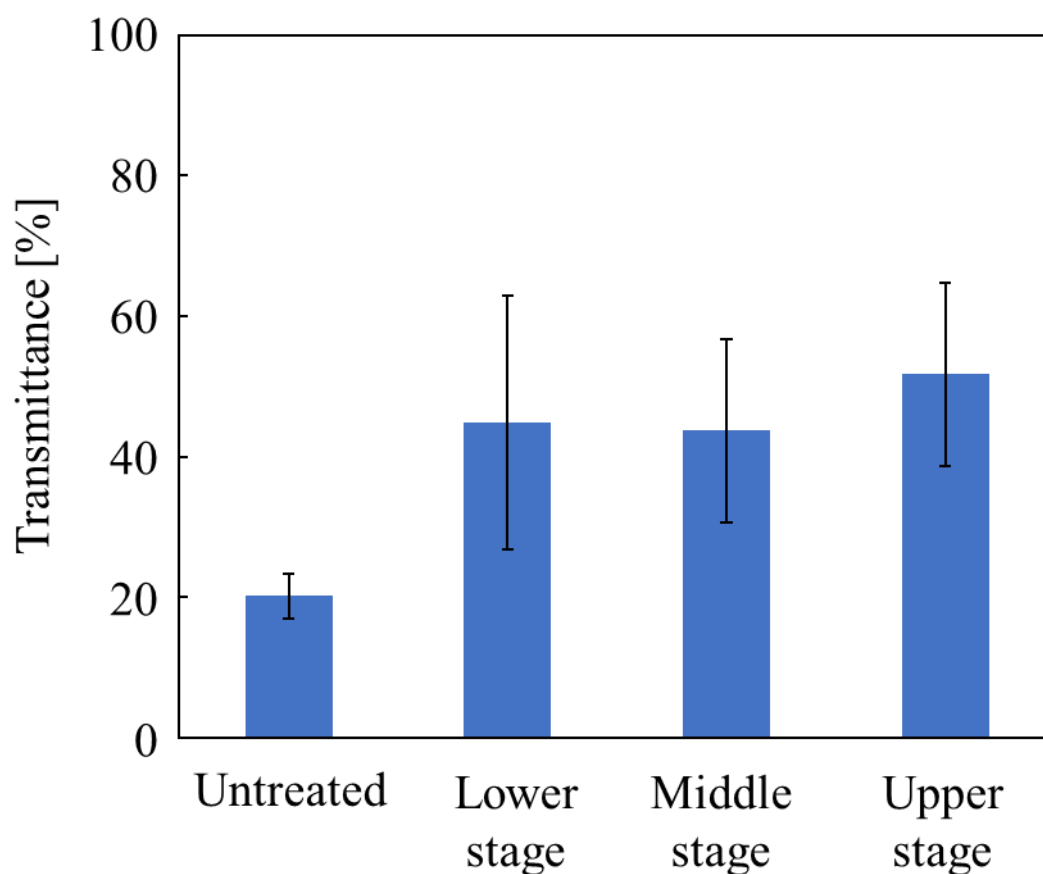


Fig. 3-10. Transmittance of a thin film exposed to AOS in a test box sealed by three overlapping layers of nonwoven fabric ⁽³⁻¹¹⁾.

3-4-6 Hydroxyl radical generation using ozone and water

As a result of thin film exposure to ozone in atmospheres characterized by different humidity conditions (Fig. 3-11), it was found that dry ozone cannot decolorize the pullulan-mixed MB thin film compared with wet ozone. This suggests that OH^* was generated inside the test box owing to ozone decomposition in the presence of water and that this mechanism of OH^* generation allowed this species to be present in the lower stage of the test box ⁽³⁻¹¹⁾.

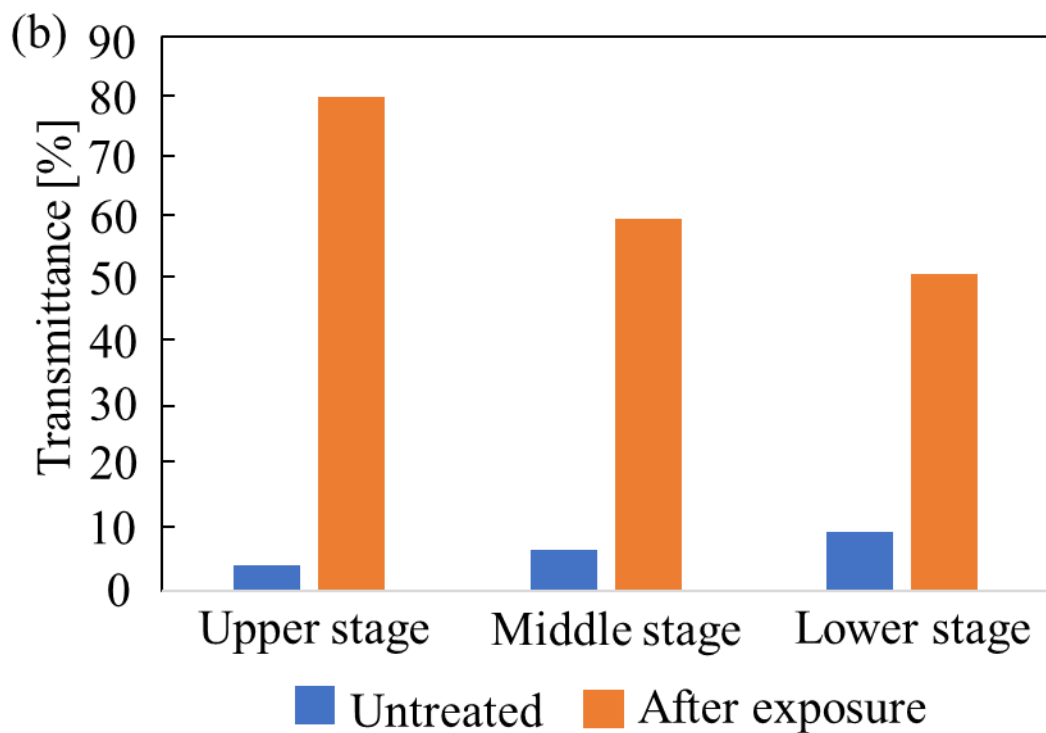
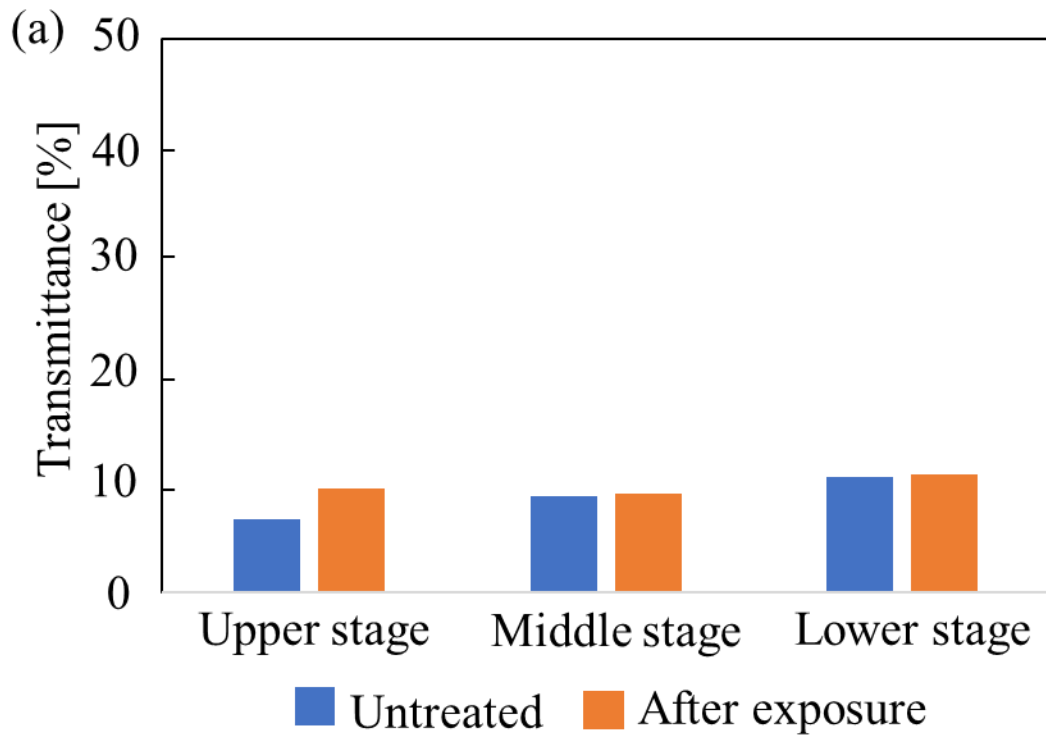


Fig. 3-11. Decolorization of the thin films located in different humidity conditions:

(a) dry ozone and (b) wet ozone ⁽³⁻¹¹⁾.

3-5 Discussion

On the basis of the data reported in Fig. 3-10, the decolorization of the pullulan-mixed MB film placed in the upper stage appeared to be enhanced compared with that of the films placed in the lower and middle stages. The results also indicate that the lifetime of OH^* is short. Therefore, the pullulan-mixed MB thin film placed in the upper stage (i.e., closest to the nonwoven fabric) was decolorized to a great extent. The obtained results show that my colleagues and I successfully confirmed the findings in Chapter 2.

As a result of thin film exposure to ozone in atmospheres characterized by different humidity conditions (Fig. 3-11), it was found that dry ozone cannot decolorize the pullulan-mixed MB thin film compared with wet ozone. This suggests that OH^* was generated inside the test box because of ozone decomposition in the presence of water and that this mechanism of OH^* generation allowed this species to be present in the lower stage of the test box.

3-6 Summary

My colleagues and I successfully developed uniform MB-dyed pullulan and sodium alginate thin films and thoroughly investigated their decolorization characteristics upon exposure to OH^* . The results showed that the peaks corresponding to the benzene carbon atoms of MB in the mixture of MB/pullulan and MB/sodium alginate in the ^{13}C -NMR spectrum disappeared after the OH^* exposure under high-humidity conditions. This indicates that film decolorization is caused by the decomposition of MB upon OH^* exposure. Moreover, the MB-dyed pullulan and sodium alginate uniform thin films selectively reacted with OH^* , which is the AOS generated under the high-humidity conditions. Thus, my colleagues and I deduced that the decolorization of the MB-dyed pullulan and sodium alginate thin films due to the AOS generated under the high-humidity conditions was related to the decomposition of MB by OH^* .

Moreover, MB-dyed pullulan thin films were placed on the three stages inside the box, and the AOS diffusion and presence of OH^* were investigated by monitoring the degree of thin film decolorization at the different stages of the aluminum box. The decolorization of a pullulan-mixed MB thin film caused by its exposure to OH^* was investigated to probe the mechanism by which OH^* diffuses across the various stages inside the test box.

References

- (3-1) K. Yoshino, H. Matsumoto, T. Iwasaki, S. Kinoshita, K. Noda, K. Oya and S. Iwamori, Investigation of a Sterilization System Using Active Oxygen Species Generated by Ultraviolet Irradiation, *Biocontrol Science*, Vol. 20, No. 1 (2015), pp. 11-18.
- (3-2) K. Oya, R. Watanabe, Y. Soga, Y. Ikeda, T. Nakamura and S. Iwamori, Effect of humidity conditions on active oxygen species generated under ultraviolet light irradiation and etching characteristics of fluorocarbon polymer, *Journal of Photochemistry and Photobiology A: Chemistry*, Vol. 298 (2015), pp. 33-39.
- (3-3) H. Kuwahata, T. Yoshizawa, and S. Kezuka, Decomposition of Methylene Blue by Ultraviolet Irradiation onto TiO₂ Thin Film in Methylene Blue Aqueous Solution, *東海大学紀要工学部*, Vol. 52, No. 2 (2012), pp. 151-156.
- (3-4) A. Mills and D. Hazafy, Nanocrystalline SnO₂-based, UVB-activated, colourimetric oxygen indicator, *Sensors and Actuators B*, Vol. 136 (2009), pp. 344-349.
- (3-5) K. Lawrie, A. Mills, and D. Hazafy, Simple inkjet-printed, UV-activated oxygen indicator, *Sensors and Actuators B: Chemical*, Vol. 176 (2013), pp. 1154-1159.
- (3-6) K. Turhan, I. Durukan, S. A. Ozturkcan, and Z. Turgut, Decolorization of textile basic dye in aqueous solution by ozone, *Dyes and Pigments*, Vol. 92 (2012), pp. 897-901.
- (3-7) S. Iwamori, N. Nishiyama and K. Oya, A colorimetric indicator for detection of hydroxyl radicals in atmosphere using a methylene blue dye based on nafion film, *Polymer Degradation and Stability*, Vol. 123 (2016), pp. 131-136.
- (3-8) C. Galindo and A. Kalt, UV-H₂O₂ oxidation of monoazo dyes in aqueous media: a kinetic study, *Dyes and Pigments*, Vol. 40 (1998), pp. 27-35.
- (3-9) G. Zhou, F. Fang, Z. Chen, Y. He, H. Sun, and H. Shi, Catalyzed oxidative degradation of methylene blue by in situ generated cobalt (II)-bicarbonate complexes with hydrogen peroxide, *Cat. Com.*, Vol. 62 (2015).
- (3-10) X. Liu, Y. Yang, X. Shi, and K. Li, Fast photocatalytic degradation of methylene blue dye using a low-power diode laser, *Journal of Hazardous Materials*, Vol. 283 (2015).

- (3-11) S. Yenchit, Y. Tadokoro and S. Iwamori, Measuring Active Oxygen Species Across a Nonwoven Fabric Using a Pullulan-mixed Methylene Blue Thin Film and Electron Spin Resonance, *IEEJ Transactions on Sensors and Micromachines*, Vol. 139, No. 3 (2019), pp. 54-60.
- (3-12) S. Yenchit, H. Yamanaka, P. Temeprasertkij, Y. Oda, O. Kanie, Y. Okamura, T. Inazu and S. Iwamori, Chemical stability of a colorimetric indicator based on sodium alginate thin film and methylene blue dye upon active oxygen species exposure, *Japanese Journal of Applied Physics*, Vol. 59, No. SD (2020), SDDF09.
- (3-13) S. Yenchit, H. Yamanaka, P. Temeprasertkij, Y. Oda, Y. Okamura, T. Inazu and S. Iwamori, A Colorimetric Indicator Based on Methylene Blue-Dyed Pullulan Thin Films for the Detection of Hydroxyl Radicals, *材料の科学と工学*, (Accepted).
- (3-14) A. Sionkowska, The influence of methylene blue on the photochemical stability of collagen, *Polymer Degradation Stability*, Vol. 67 (2000), pp. 79-83.
- (3-15) A. Ma, Y. Wei, Z. Zhou, W. Xu, F. Ren, H. Ma, and J. Wang, Preparation $\text{Bi}_2\text{S}_3\text{-TiO}_2$ heterojunction/polymer fiber composites and its photocatalytic degradation of methylene blue under Xe lamp irradiation, *Polymer Degradation Stability*, Vol. 97 (2012), pp. 125-131.
- (3-16) B. H. A. Rehm, Caister Academic Press., 230 (2009).
- (3-17) A. M. Stephen (ed.) *Food Polysaccharides and their Applications* (Marcel Dekker, New York, 1995), pp. 245.
- (3-18) N. K. Sachan, S. Pushkar, A. Jha, and A. Bhattacharya, Sodium alginate: the wonder polymer for controlled drug delivery, *Journal of pharmacy research*, Vol. 2 (2009), Issue 8, pp. 1191-1199.
- (3-19) L. A. Loureiro dos Santos, *Reference Module in Materials Science and Materials Engineering* (Elsevier, Amsterdam, 2017).
- (3-20) D. L. Baulch, C. T. Bowman, C. J. Cobos, R. A. Cox, J. A. Th Just, Kerr, M. J. Pilling, D. Stocker, J. Troe, W. Tsang, R.W. Walker and J. Warnatz, Evaluated Kinetic Data for Combustion Modeling: Supplement II, *Journal of Physical and Chemical Reference Data* 34 (2005), pp. 757-1397.

- (3-21) R. Rohs, H. Sklenar, R. Lavery, and B. Röder, Methylene Blue Binding to DNA with Alternating GC Base Sequence: A Modeling Study, *Journal of the American Chemical Society*, Vol. 122 (2000), pp. 2860-2866.
- (3-22) S. Hongxia, X. Junfeng, Z. Yazhou, X. Guangzhi, X. Lianghua, and T. Yalin, *Chin. Sci. Bull.* 15, 14 (2006).
- (3-23) J. Jähnchen, M. G. M. Purwanto, and K. Weisz, NMR studies on self-complementary oligonucleotides conjugated with methylene blue, *Biopolymer*, Vol. 79 (2005), Issue 6.
- (3-24) L. Liu, S. Fan, and Y. Li, Removal Behavior of Methylene Blue from Aqueous Solution by Tea Waste: Kinetics, Isotherms and Mechanism, *International journal of environmental research and Public Health*, Vol. 15 (2018), Issue 7, pp. 1321.
- (3-25) Y. Saranya, Y. Tadokoro, and S. Iwamori, Chemical stability of pullulan thin film employing methylene blue dye for active oxygen species, 4th Japan-Korea International Symposium on Materials Science and Technology 2017 (JKMST2017).
- (3-26) M. Okuda, T. Tsuruta and K. Katayama, Lifetime and diffusion coefficient of active oxygen species generated in TiO₂ sol solutions, *Physical Chemistry Chemical Physics*, Vol. 11 (2009), pp. 2287.
- (3-27) R. A. Reis, C. A. Tischer, P. A.J. Gorin and M. Iacomini, A new pullulan and a branched (1→3)-, (1→6)- linked β-glucan from the lichenised ascomycete *Teloschistes flavicans*, *FEMS Microbiology Letters*, Vol. 210 (2002), pp. 1-5.
- (3-28) A. J. Benesi and D. A. Brant, Trends in molecular motion for a series of glucose oligomers and the corresponding polymer pullulan as measured by carbon-13 NMR relaxation, *Macromolecules*, Vol. 18 (1985), pp. 1109-1116.
- (3-29) C. Arnosti and D.J. Repeta, Nuclear Magnetic Resonance Spectroscopy of Pullulan and Isomaltose: Complete Assignment of Chemical Shifts, *Starch-Stärke*, Vol. 47 (1995), pp. 73-75.
- (3-30) A. Spatareanu, M. Bercea, T. Budtova, V. Harabagiu, L. Sacarescu and S. Coseri, Synthesis, characterization and solution behaviour of oxidized pullulan, *Carbohydrate Polymers*, Vol. 111 (2014), pp. 63-71.

- (3-31) J.M. Pereira, M. Mahoney and K.J. Edgar, Synthesis of amphiphilic 6-carboxypullulan ethers, Carbohydrate Polymers, Vol. 100 (2014), pp. 65-73.
- (3-32) I. V. Tokmakov, G.-S. Kim, V. V. Kislov, A. M. Mebel, and M. C. Lin, The reaction of phenyl radical with molecular oxygen: a G2M study of the potential energy surface, The Journal of Physical Chemistry A, Vol. 109 (2005), pp. 6114-6127.
- (3-33) Y. Murakami, T. Oguchi, K. Hashimoto, A. Nakamura, Y. Sakai, and H. Ando, Density functional study of the phenylethyl + O₂ reaction: Kinetic analysis for the low- temperature autoignition of ethylbenzenes, International Journal of Quantum Chemistry, Vol. 112 (2012), pp. 1968-1983.
- (3-34) S. Iwamori et al. (ed.) Polyimides and Other High Temperature Polymers (CRC Press, Boca Raton, FL, 2003) Vol. 2, p. 407.
- (3-35) C. Galindo and A. Kalt, UV-H₂O₂ oxidation of monoazo dyes in aqueous media: a kinetic study, Dyes Pigments, Vol. 40 (1999), pp. 27-35.
- (3-36) S. Shahabuddin, N. M. Sarih, S. Mohamad, and J. J. Ching, SrTiO₃ Nanocube-Doped Polyaniline Nanocomposites with Enhanced Photocatalytic Degradation of Methylene Blue under Visible Light, Polymers, Vol. 8, Issue 2 (2016).

Chapter 4

Affinity of Methylene Blue Dye and
Water-Soluble Polymers for
Stabilization upon Active Oxygen
Species Exposure

4-1 Background

The active oxygen species (AOS) generated in the atmosphere can be applied to various industrial processes owing to their extremely strong oxidative ability. It is well known that $O(^1D)$, O_3 , and OH^* are valuable in surface modification. AOS can be generated using ultraviolet (UV) lamps that emit light with wavelengths of 185 and 254 nm⁽⁴⁻¹⁾. My colleagues and I have reported that methylene blue (MB) can be decomposed by O_3 . MB is a convenient indicator for detecting AOS because it decolors after exposure to AOS owing to the degradation of the dye⁽⁴⁻²⁾. By utilizing this characteristic, my colleagues and I aimed to develop a sensor that can visually determine the presence or absence of AOS via MB decolorization. O_3 has a lower oxidative ability than other AOS. According to Chapter 3, it is necessary to stabilize MB by mixing it with water-soluble polymers, which have high affinity for MB, to detect AOS with higher oxidative abilities. This approach forms MB/pullulan and MB/sodium alginate (SA) composite films. Pullulan and SA are natural and water-soluble polysaccharides with excellent film-forming ability. Humidity affects the type of AOS generated: $O(^1D)$ and O_3 are generated under low-humidity conditions, whereas an extremely highly oxidative species, such as OH^* , is generated under high-humidity conditions⁽⁴⁻³⁾. On the basis of these characteristics, the decolorization mechanism of the composite film was investigated. It was previously observed that decolorization occurs only under high-humidity conditions and is presumably caused by OH^* ⁽⁴⁻⁴⁾. Therefore, the stabilization mechanism between MB and water-soluble polymer (pullulan and SA) uniform thin film indicators for detecting OH^* was elucidated.

4-2 Purpose

My colleagues and I developed a new indicator uniform thin film based on MB-dyed water-soluble polymers, namely, pullulan and SA, which have film-forming ability. These thin films can achieve uniformity and can be quantitatively evaluated. My colleagues and I used thin films to develop indicators that can visually indicate the presence or absence of AOS on the spot. My colleagues and I aimed to analyze the uniform thin film indicators to elucidate the chemical reactions of MB/pullulan and MB/SA. The stabilization feature of MB was investigated by comparing the uniform thin film indicators of MB and water-soluble polymers with glucose as a monomer instead of pullulan. My colleagues and I cannot employ MB dye as a pristine powder or MB solution in the vacuum process, such as for the surface treatment processes used in the semiconductor industry ^{(4-5), (4-6)}.

4-3 Experimental apparatus and experimental methods

4-3-1 The molecular structures of MB, pullulan, SA, and glucose

Figure 4-1 shows the molecular structure of glucose. Glucose is a monosaccharide, which is a carbohydrate compound comprising six carbon atoms and an aldehyde functionality ^{(4-5), (4-7)}.

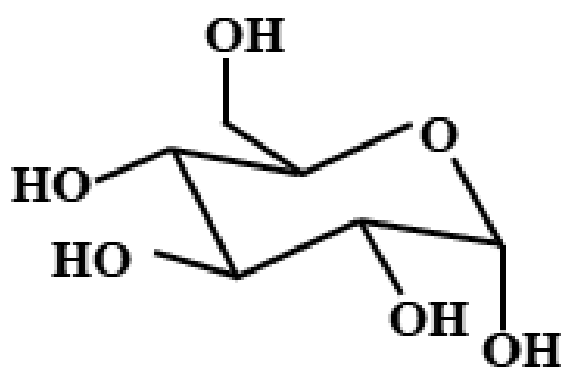


Fig. 4-1. Molecular structure of glucose. OH and O correspond to a hydroxide molecule and oxygen atom, respectively ⁽⁴⁻⁵⁾.

4-3-2 Exposure to AOS

My colleagues and I used Active Dry[®] (Iwasaki Electric Co., Ltd., Tokyo) to generate AOS. Three UV lamps were installed in an experimental chamber with dimensions of 24 cm × 25 cm × 22 cm (height × width × depth): two lamps had a power of 6 W (total 12 W), and one lamp had a power of 4 W. These UV lamps emitted UV radiation at 4 W with wavelengths of 185 and 253.7 nm and at 12 W with a wavelength of 253.7 nm, thereby facilitating AOS generation ^{(4-1), (4-3), (4-8), (4-9)}. Although several AOS are known, those with long lifetimes or high oxidization abilities, such as O(¹D), O₃, OH*, and H₂O₂, are of particular interest ^{(4-10), (4-11)–(4-18)}. Given that humidity is known to affect the type of generated AOS, the chamber temperature was maintained at 30 °C by using warm air, which was produced by pumping it through recently boiled water and Active Dry[®] to produce high-humidity conditions (90% or higher humidity). To produce low-humidity conditions (less than 20% humidity), dry air was pumped through a bottle of silica gel (large granules with blue indicator), which was maintained at 30 °C and connected to Active Dry[®] (i.e., without passing air over the boiled water) ⁽⁴⁻⁴⁾. The air pumping was ceased when AOS exposure was performed.

4-3-3 Thin-layer chromatography analysis

Thin-layer chromatography (TLC) involves the separation of two or more compounds or ions. These two phases can be solid–liquid, liquid–liquid, or gas–liquid; according to the distribution distance can be seen between two phases, one is moving, and the other is stationary ⁽⁴⁻¹⁹⁾.

The benefits of TLC include its short analysis time, simplicity, inexpensive separation technique, simple extract cleanup, and low requirement for organic solvents. Moreover, TLC analysis does not use complicated instrumentation and is easy to perform, with the possibility of using alkaloid-selective and sensitive derivatizing agents. These advantages make TLC popular from an economic perspective ⁽⁴⁻²⁰⁾.

To examine the MB-dyed pullulan and SA film, my colleagues and I performed TLC to assess the affinity between the MB/pullulan and MB/SA. TLC was performed on a glass sheet coated with a thin layer of silica gel. The developing solvents were chloroform, methanol, and water at a 4:1:0.1 ratio. For TLC analysis, 10 mM MB and 10 mM pullulan solutions were used as the MB-dyed pullulan

solution. Furthermore, 10 mM MB and 10 mM SA solutions were used as the MB-dyed SA solution. The molecular weights (M_w) of MB, pullulan, and SA are 319, 75,000, and 11,000 g mol⁻¹, respectively. Three drops of each were placed on the glass sheet: a 10 mM MB solution spot on the left, a 10 mM pullulan or SA mixed with 10 mM MB spot on the right, and a mixture of these two spots in the middle. The spots were observed under UV light to examine the behavior of the MB benzene ring in response to the degradation of MB by the UV light. My colleagues and I then performed coloration by using iodine to examine the behavior of substances that are difficult to observe under UV light. Finally, the sample was heated on a hot plate to apply a color former (anise reagent) to the glass sheet. The behavior of water-soluble polymers can be confirmed via this process ^{(4-5), (4-6)}.

4-3-4 Proton nuclear magnetic resonance analysis

The proton signals of the benzene ring and methyl group of MB were found to be shifted. These results suggest that a chemical change occurred in the MB structure. Therefore, the stabilization of MB/pullulan and MB/SA thin film indicator for the AOS was investigated using proton nuclear magnetic resonance (¹H-NMR), which was performed using a Bruker® AVANCE III 500 MHz Ultra Shield spectrometer. A mixture of MB and pullulan at a 1:1 ratio was prepared by mixing 60 µl of a 100 g l⁻¹ pullulan solution and 200 µl of a 0.6 g l⁻¹ aqueous MB solution. A mixture of MB and SA at a 1:1 ratio was prepared by mixing 300 µl of 10 mM SA with 300 µl of 25 mM MB (total volume of 600 µl). A mixture of MB and glucose at a 1:1 ratio was also prepared by mixing 300 µl of 10 mM glucose with 300 µl of 25 mM MB (total volume of 600 µl). In addition, 600 µl of 10 mM solutions of each of MB, pullulan, sodium alginate, and glucose were prepared. All of the solutions were dissolved in D₂O, which was used as the solvent to distinguish it from the hydrogen in the MB, pullulan, SA, and glucose. Subsequently, all mixtures of MB and water-soluble polymers were prepared by mixing 480 µl of D₂O, 60 µl of the water-soluble polymer solution, and 60 µl of the MB solution ^{(4-5), (4-6)}.

4-3-5 Preparation of MB and pullulan solution upon AOS exposure under high-humidity conditions for carbon-13 nuclear magnetic resonance analysis

To elucidate the affinity between the MB and pullulan of the decolorized MB-dyed pullulan film caused by OH*, carbon-13 nuclear magnetic resonance (^{13}C -NMR) analyses were performed using 60 μl of a 100 g l^{-1} pullulan solution and 200 μl of a 0.6 g l^{-1} aqueous MB solution. D_2O was used as the solvent to distinguish it from hydrogen in the MB and pullulan. A large amount of MB sample was required for the nuclear magnetic resonance (NMR) analysis. The solutions were spread on a glass substrate and dried to form a thin film. To acquire a large amount of sample, 20 glass substrates were used for the NMR analyses. Each thin film was subjected to AOS exposure until being completely decolorized under high-humidity conditions. Subsequently, each thin film-coated glass substrate was placed in 15 mL D_2O , and the thin film was dissolved using an ultrasonic cleaner. To increase the concentration of the solution mixture for ^{13}C -NMR analysis, the resulting solution was heated and evaporated until a volume of 10 mL was reached. For the ^{13}C -NMR analysis, a highly concentrated solution was prepared using the FD-1[®] freeze dryer ^{(4-5), (4-6)}.

4-3-6 Microplate reader analysis

To examine the stabilization of MB dye in the MB/pullulan and MB/SA composite films, my colleagues and I analyzed the chemical bonds between MB-dye water-soluble polymers, namely, pullulan and SA, by using a microplate reader. Pullulan is a polysaccharide that has glucose as a monomer. Sodium alginate is also a polysaccharide; thus, my colleagues and I used glucose, which is a monosaccharide with a M_w of 180 g mol^{-1} , to compare the stabilities of MB, pullulan, and SA. Microplate reader analyses were performed using a Corona Grating Microplate reader[®] SH-9000 series with 0.05 mM MB, 0.05 mM pullulan, 0.05 mM SA, and 0.05 mM aqueous glucose solutions. Mixtures of these solutions at 1:1 ratios of MB/pullulan, MB/SA, and MB/glucose were prepared. In each hole of a 96-well plate, 200 μl of these solutions was dropped for microplate reader analyses. The measurement was performed at an absorbance wavelength of 450–800 nm ^{(4-5), (4-6)}.

4-3-7 Fourier-transform infrared analysis

Fourier-transform infrared (FT-IR) analysis identifies chemical bonds in a molecule by producing an infrared absorption spectrum with an analytical FT-IR spectrometer from 400 to 4000 cm^{-1} . My colleagues and I performed FT-IR analysis to evaluate the affinity between MB and the water-soluble polymers, namely, pullulan and SA, which have high affinity for forming MB/pullulan and MB/SA composite films. FT-IR analyses were performed using a Horiba® Fourier-Transform Infrared Spectrometer FT-720 series with a mixture of MB and pullulan prepared using 0.1 g/L pullulan and 0.9 g/L MB thin film, and a mixture of MB and SA was prepared using 10 mM SA and 10 mM MB thin film. They were made into powder by using the KBr tablet method. The baseline data were measured using only potassium bromide. Furthermore, the sample of a mixture of MB/pullulan was produced by mixing a 0.9 g/L aqueous MB solution and a 0.1 g/L aqueous pullulan solution at a 1:1 ratio. The sample of a mixture of MB/SA was produced by mixing with a 10 mM aqueous MB solution and a 10 mM aqueous SA solution at ratios of 1:1, 1:2, 1:10, and 1:0.2 (Table 4-1). Thin films were then obtained using a dryer. Thereafter, the obtained thin film was peeled off, made into a powder, thoroughly stirred in a mortar that was subsequently washed with potassium bromide as many as 10 to 100 times, and compressed by pressing under reduced pressure. Infrared was transmitted, and the spectrum was obtained. MB mixtures with water-soluble polymers were analyzed using FT-IR spectra in N_2 gas and were measured in the wavelength range from 400 to 4000 nm. During the experiment, my colleagues and I used nitrogen gas to avoid the wetness in the air and connected nitrogen gas to the FT-IR machine. Moreover, along the path of the nitrogen gas tube to the FT-IR machine, my colleagues and I had to add a cylinder of silica gel to make the air dry. FT-IR spectroscopy identifies chemical bonds in a molecule by producing an infrared absorption spectrum. The spectrum provides a profile of the sample, i.e., a distinctive molecular fingerprint that can be used to screen and scan samples for many different components. Therefore, my colleagues and I can obtain the spectra of the components of MB, pullulan, and SA via FT-IR spectroscopy ^{(4-5), (4-6)}.

Table 4-1. FT-IR experimental conditions (MB and SA mixture)

Material	Ratio	Solution (μL)	Ratio	Solution (μL)	Ratio	Solution (μL)	Ratio	Solution (μL)
MB	1	150	1	150	1	60	1	300
Sodium alginate	1	150	2	300	10	600	0.2	150

4-3-8 Raman spectroscopy

Raman spectroscopy is a fundamental form of molecular spectroscopy⁽⁴⁻²¹⁾ that measures and analyses Raman scattered radiation from a sample. In Raman spectroscopy, a sample is excited by a monochromatic laser with wavelengths in the near infrared, visible, or UV region⁽⁴⁻²²⁾. A Raman spectrometer detects Raman scattered radiation from 0 to 4000 cm^{-1} . My colleagues and I performed Raman spectroscopy to analyze the molecular structure of MB, pullulan, SA, a mixture of MB and pullulan, and a mixture of MB and SA, which have high affinity for forming MB/pullulan and MB/SA composite films. Raman spectroscopy analyses were performed using a Horiba® XproRA Raman spectroscope with a 10 mM aqueous MB solution and a 10 mM aqueous pullulan solution at a 1:10 ratio (Table 4-2) and with a 10 mM aqueous MB solution and a 10 mM SA aqueous solution at a 1:10 ratio (Table 4-3). Thereafter, 260 μL of solution was dropped on a glass slide, which was placed in an incubator (40 °C) for 8 h. The baseline data were calibrated using a Si wafer. Table 4-4 shows the Raman experimental conditions. The excitation wavelength was 532 nm and the exposure time was 10 s^{(4-5), (4-6)}.




Table 4-2. Raman sample preparation conditions (MB and pullulan mixture) ⁽⁴⁻⁶⁾.

Material	Ratio	Solution (μL)
MB	1	30
Pullulan	10	300

Table 4-3. Raman sample preparation conditions (MB and SA mixture) ⁽⁴⁻⁵⁾.

Material	Ratio	Solution (μL)
MB	1	30
Sodium alginate	10	300

Table 4-4. Raman experimental conditions.

Laser	Filter	Hole	Slit	Spectrometer	Precision: 600T	Acquisition
532 nm	10%	300	100	520 cm^{-1}	Lens $\times 100$	 Laser time: 1 s
	or					 Save time: 3 s
	100%					 Cycles: 50

4-4 Results

4-4-1 Determination of the affinity between MB, pullulan, and SA of OH* indicator by TLC analysis

Figures 4-2 (a) and (b) show the TLC patterns of the MB/mixtures of MB and pullulan and the MB/mixtures of MB and SA, respectively. In the TLC experiment, the mixing ratio of MB and water-soluble polymers was 1:1 (M_w), and the changes in the distance of the spots were barely observable. The retention factor ($R_f = a/b$) is defined as the distance from the origin to the spot center (a) divided by the distance from the origin to the mobile phase front (b). However, there was a slight difference between the left side ($R_f = 0.36$) and right side ($R_f = 0.32$) for the MB/mixtures of MB and pullulan and between the left side ($R_f = 0.30$) and right side ($R_f = 0.28$) for the MB/mixtures of MB and SA. This result confirmed the repeatability. It is considered that there is weak affinity between MB/pullulan and between MB/SA ^{(4-5), (4-6)}.

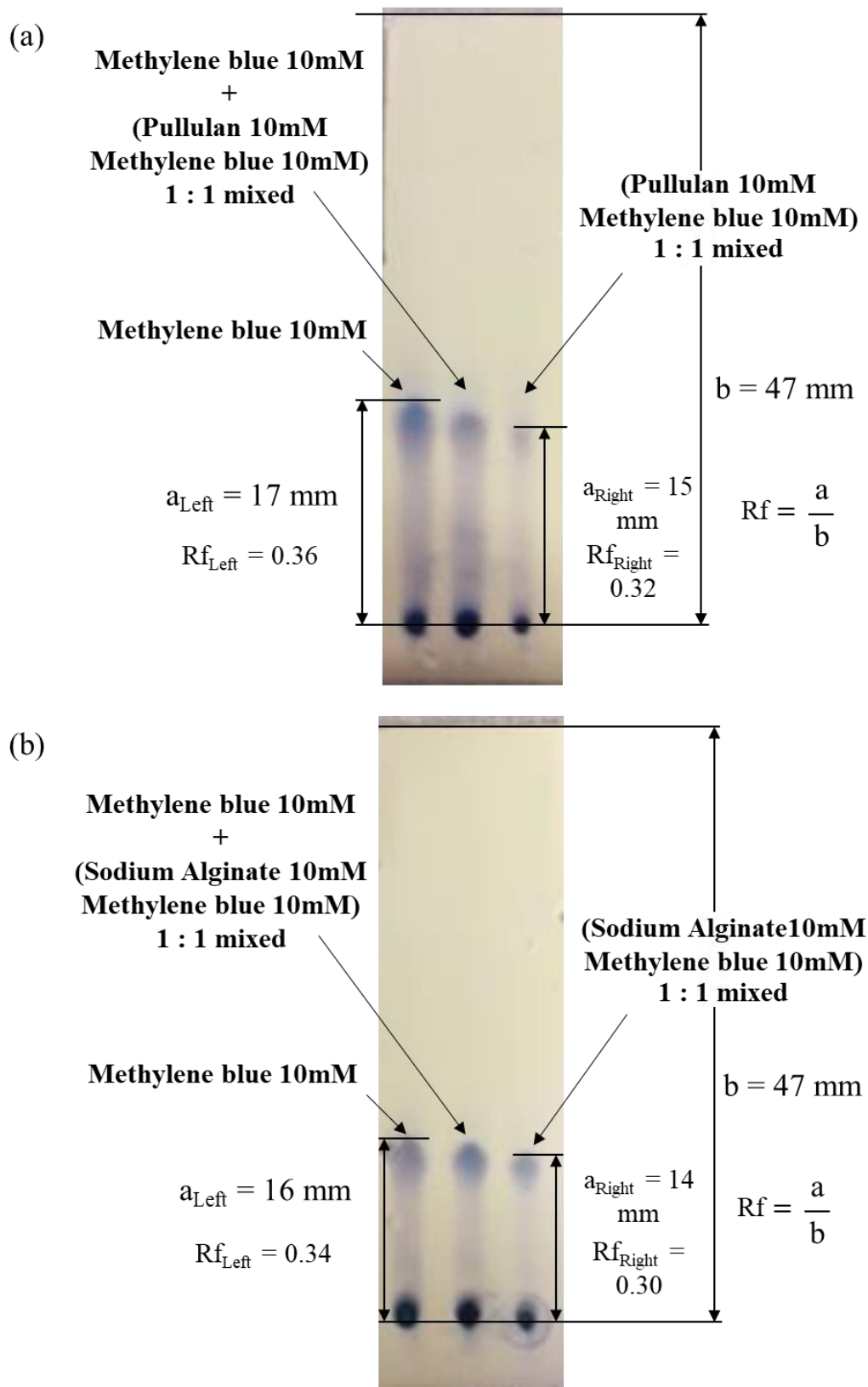


Fig. 4-2. TLC analysis of the affinity between (a) MB and pullulan and between (b) MB and SA ⁽⁴⁻⁵⁾.

Rf: retention factor, a: distance moved from the point of origin to the spot, b: distance moved by solvent from the point of origin.

4-4-2 Results of the ^1H -NMR analysis of pullulan in a mixture of MB and pullulan

Figure 4-3 shows the ^1H -NMR spectra of pullulan and a mixture of MB and pullulan. The spectra suggested that the peaks in the ^1H -NMR spectrum of the mixture of MB and pullulan were almost the same as those of pristine pullulan because the number of places that are not involved in the interaction far outnumbered the parts interacting with MB.

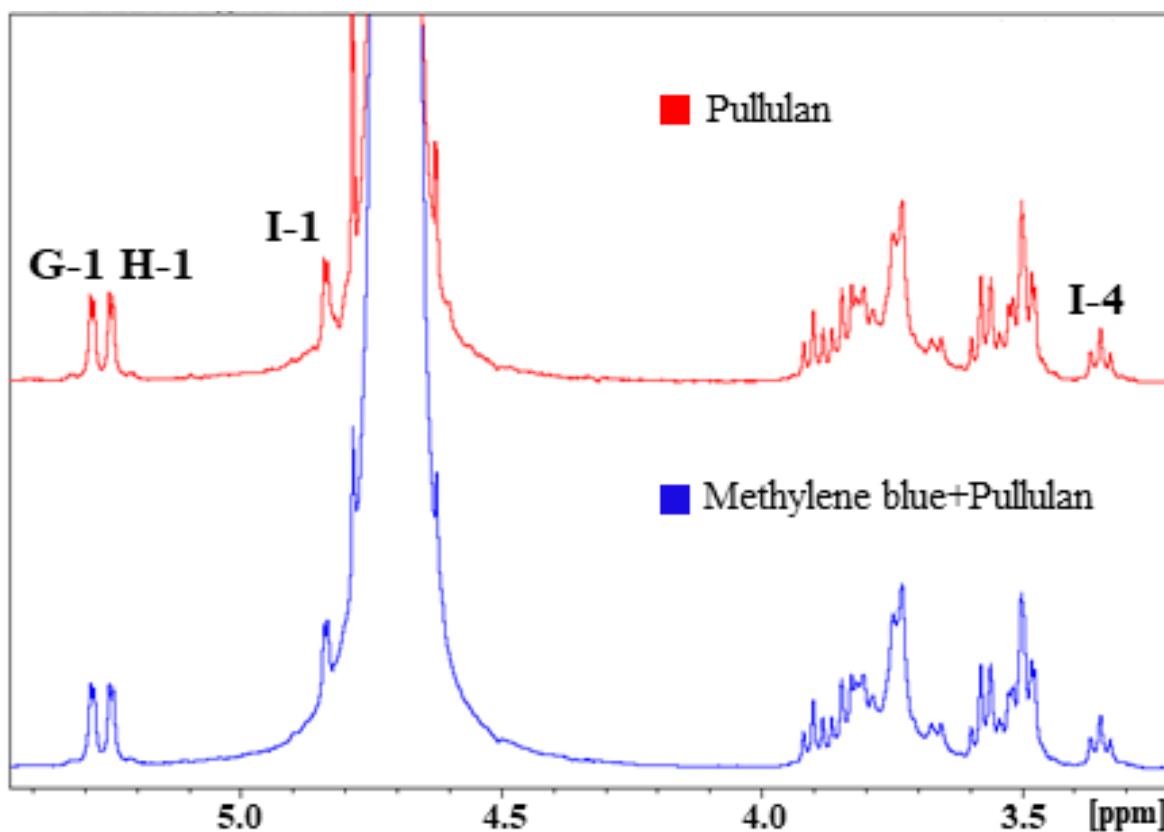


Fig. 4-3. ^1H -NMR spectra of pullulan and a mixture of MB and pullulan. G-1, H-1, I-1, and I-4 correspond to the proton positions shown in Fig. 3-1 (b).

4-4-3 Results of the ^1H -NMR analysis of interaction between MB and pullulan compared with glucose

Figure 4-4 shows the ^1H -NMR spectra of MB, the mixture of MB and pullulan, and the mixture of MB and glucose. The characteristic peaks corresponding to the benzene ring of MB in the mixture of MB and pullulan following AOS exposure under low-humidity conditions after OH^* exposure under high-humidity conditions can be observed at approximately 6.74, 6.96, and 7.27 ppm. Moreover, the distinctive aromatic signals corresponding to the protons of the benzene ring of MB in the mixture of MB and glucose can be observed at approximately 6.83, 7.04, and 7.38 ppm. Although the positions and shapes of the peaks assigned to the benzene ring of MB in the mixture of MB and glucose are nearly identical to those of pristine MB, some minor peak shifts at positions A, B, and D in Fig. 1 (a) relative to the pristine signals can be observed in each spectrum. These shifts are significantly smaller than the peak shifts observed for the spectrum of the mixture of MB and pullulan. These results suggest that there is an interaction between pullulan and MB at the N (nitrogen) or S (sulfur) position and a weaker interaction between MB and glucose. Furthermore, the signals corresponding to the protons of MB and pullulan were somewhat broad, and the shapes of the peaks changed compared with pristine MB. It is assumed that the molecular motion of MB is suppressed by the presence of the macromolecule (pullulan); therefore, the signal appears broad. These broad signals suggest that several MB molecules interact with pullulan molecules. Furthermore, considering the above, it appears that the MB peak shifted because the positions of the signals corresponding to pullulan and MB are close. Furthermore, my colleagues and I compared the molecular structures of untreated MB and the dye treated with AOS under low- or high-humidity conditions. The ^1H -NMR spectra of MB-dyed pullulan before and after AOS exposure under high-humidity conditions showed that only three peaks between 6.5 and 7.5 ppm disappeared as a result of OH^* exposure, and these peaks correspond to the hydrogen atoms of the benzene ring. On the other hand, the ^1H -NMR spectrum of MB-dyed pullulan showed that the aforementioned three peaks remained after the AOS exposure under low-humidity conditions. These observations indicate that MB was decomposed by OH^* ^{(4-2), (4-6)}.

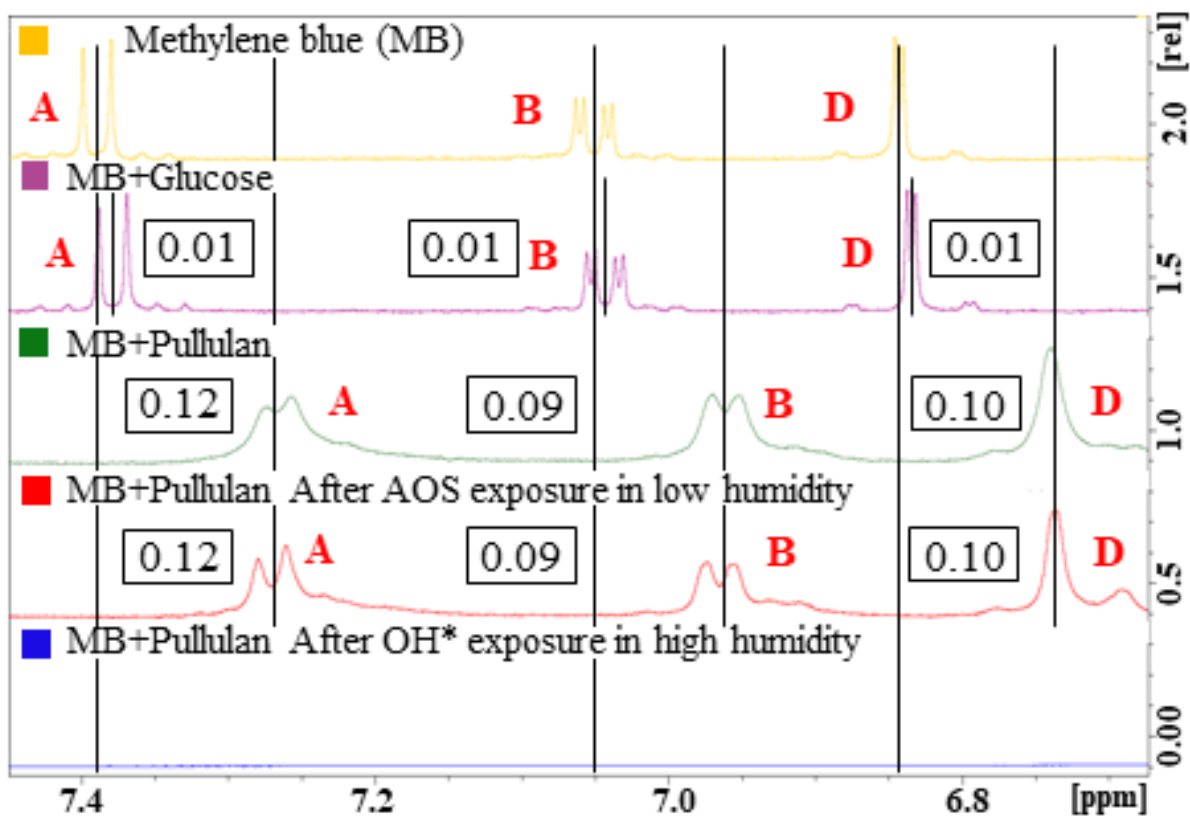


Fig. 4-4. ¹H-NMR spectra of MB, a mixture of MB and glucose, a mixture of MB and pullulan, and a mixture of MB and pullulan following the exposure to AOS under low-humidity conditions and following the exposure to OH* under high-humidity conditions. A, B, and D correspond to the proton positions shown in Fig. 3-1 (a) ⁽⁴⁻⁶⁾.

4-4-4 Results of the $^1\text{H-NMR}$ analysis of the interaction between MB and SA compared with glucose

The $^1\text{H-NMR}$ spectra of MB, SA, mixture of MB and SA, glucose, and mixture of MB and glucose. The characteristic peaks corresponding to the benzene ring of MB in the mixture of MB and SA can be observed at approximately 6.66, 6.88, and 7.14 ppm, whereas those of the mixture of MB and glucose can be observed at approximately 6.62, 6.85, and 7.10 ppm (Fig. 4-5). The methyl group (CH_3) of MB in the mixture of MB and SA can be observed at approximately 2.99 ppm, whereas that of the mixture of MB and glucose can be observed at approximately 2.98 ppm (Fig. 4-6). These are assigned to the protons in the functional groups. Although the shapes of the peaks corresponding to the benzene ring and CH_3 of MB in the mixture of MB and SA are the same as those of pristine MB, there are some peak shifts relative to the pristine signals (0.05, 0.03, 0.04, and 0.02 ppm). Therefore, the MB peak shifted because SA and MB exhibit an intermolecular interaction with one another. However, the positions and shapes of the peaks corresponding to the benzene ring and CH_3 of MB in the mixture of MB and glucose are the same as those of pristine MB; in other words, glucose and MB do not interact. These results suggest that SA and MB ionically bond with one another at the $-\text{COO}^-$ (carboxylate salt) of SA and the N^+ (nitrogen) or S^+ (sulfur) position of MB ⁽⁴⁻⁵⁾.

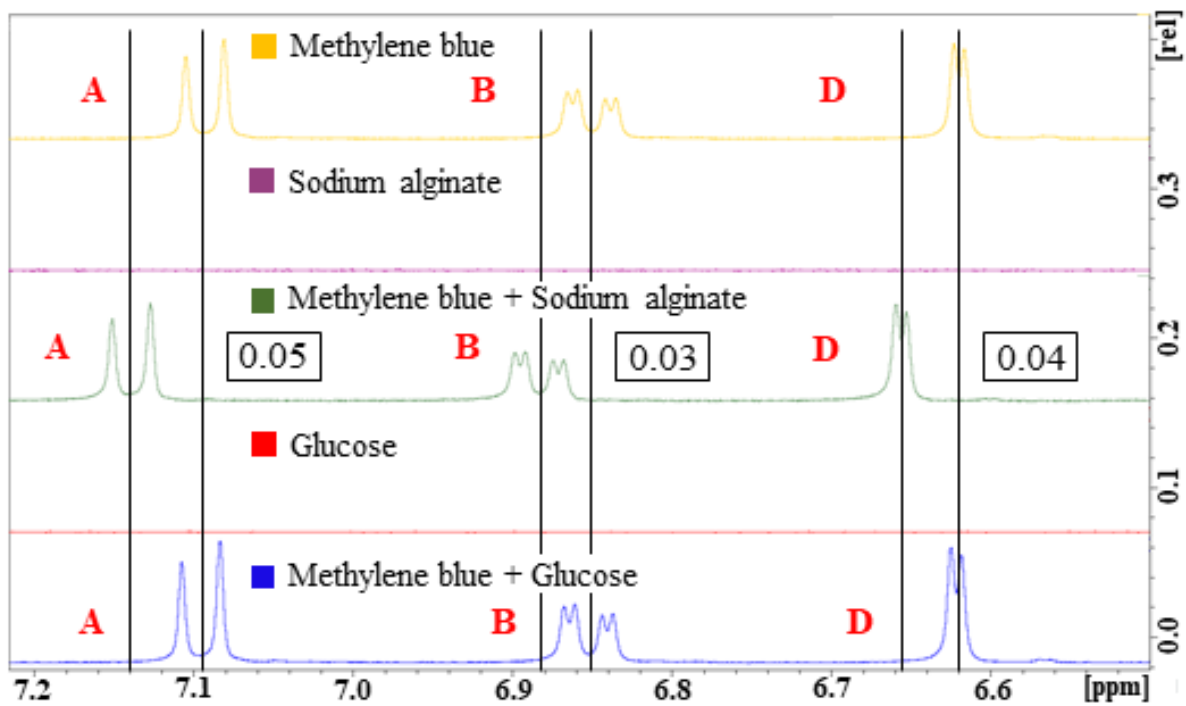


Fig. 4-5. $^1\text{H-NMR}$ spectra of MB, SA, a mixture of MB and SA, glucose, and a mixture of MB and glucose. A, B, and D correspond to the proton positions shown in Fig. 4-1 (a) ⁽⁴⁻⁵⁾.

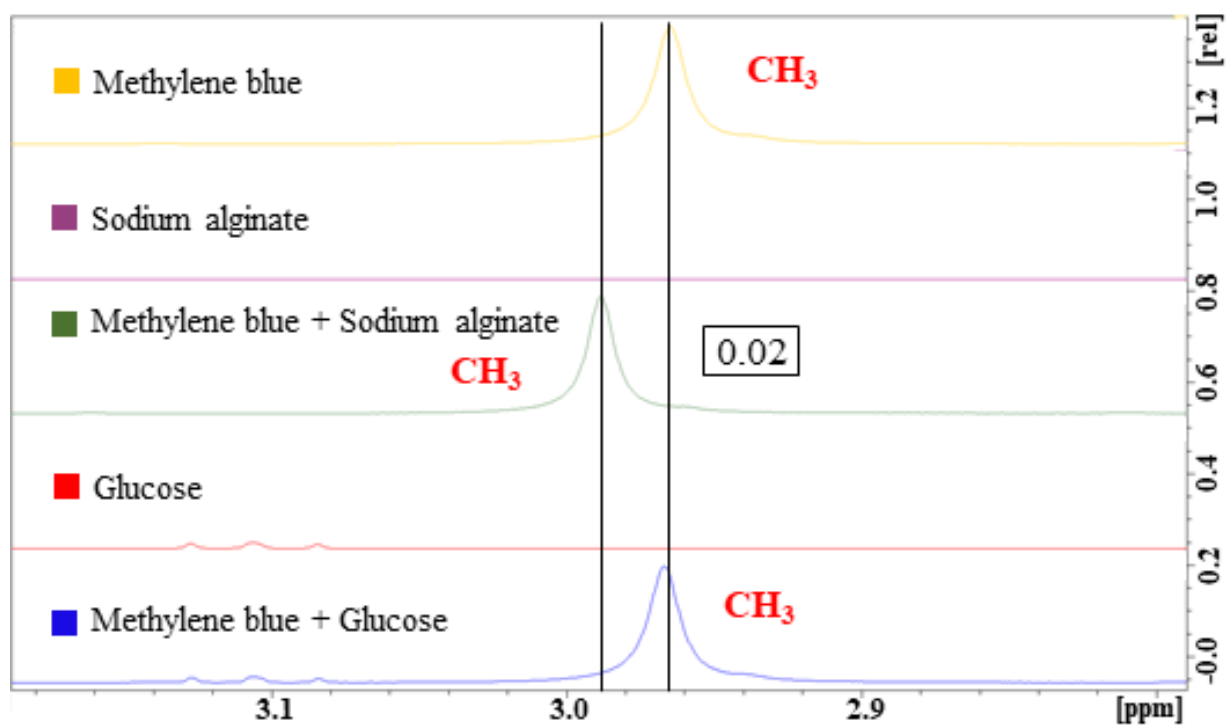


Fig. 4-6. ¹H-NMR spectra of MB, SA, a mixture of MB and SA, glucose, and a mixture of MB and glucose. CH₃ corresponds to the proton positions shown in Fig. 4-1 (a) ⁽⁴⁻⁵⁾.

4-4-5 Results of the ^{13}C -NMR analysis of MB-dyed pullulan thin films upon AOS exposure in high-humidity conditions

Figure 4-7 illustrates the ^{13}C -NMR spectra of the mixtures of MB and pullulan before and after OH^* exposure under high-humidity conditions. This figure shows that the peak corresponding to the $-\text{N}-(\text{CH}_3)_2$ group of MB can be observed at approximately 40 ppm before OH^* exposure. A shifted peak at approximately 34.5 ppm is also present and is suspected to correspond to the original $-\text{N}-(\text{CH}_3)_2$ fragment of the MB molecule after OH^* exposure. It is supposed that it is the remaining residue of MB following the destruction of the benzene ring. In other words, the magnetic field of this fragment probably shifted as a consequence of the lost aromaticity. These results show that only the benzene moiety of MB is targeted upon exposure to AOS ⁽⁴⁻⁶⁾.

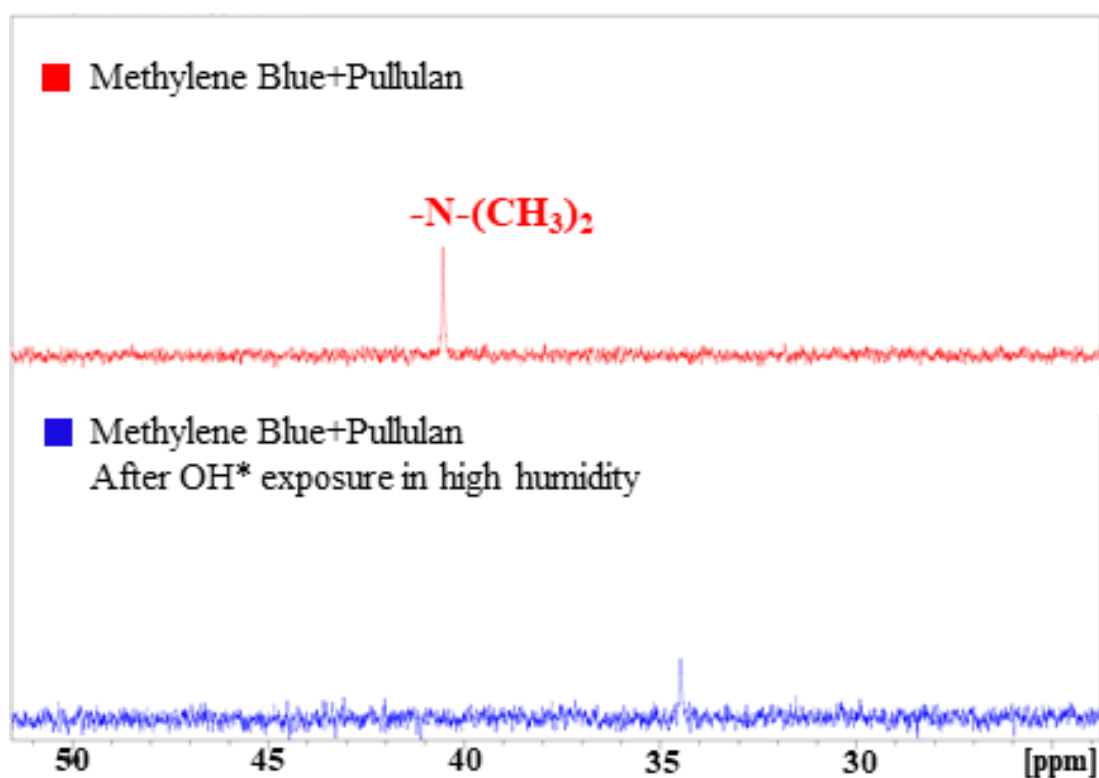


Fig. 4-7. ^{13}C -NMR spectra of mixtures of MB and pullulan before and after OH^* exposure under high-humidity conditions. $-\text{N}-(\text{CH}_3)_2$ corresponds to the carbon positions of the methyl group of MB shown in Fig. 3-1 (a) ⁽⁴⁻⁶⁾.

4-4-6 Determination of the affinity between MB and pullulan for OH* indicator by microplate reader analysis

Figure 4-8 (a) shows the absorbance of the microplate reader spectrum of pullulan, and Fig. 4-8 (b) shows the absorbance of the microplate reader spectrum of glucose. These figures suggest that no reaction was observed. Considering that there was no peak shift that could be confirmed, this indicated that no interaction or binding had occurred. However, TLC and NMR results suggested that MB and pullulan interact with each other, whereas MB does not interact with glucose. Therefore, it can be said that pullulan is suitable for stabilizing with MB compared with glucose⁽⁴⁻⁶⁾.

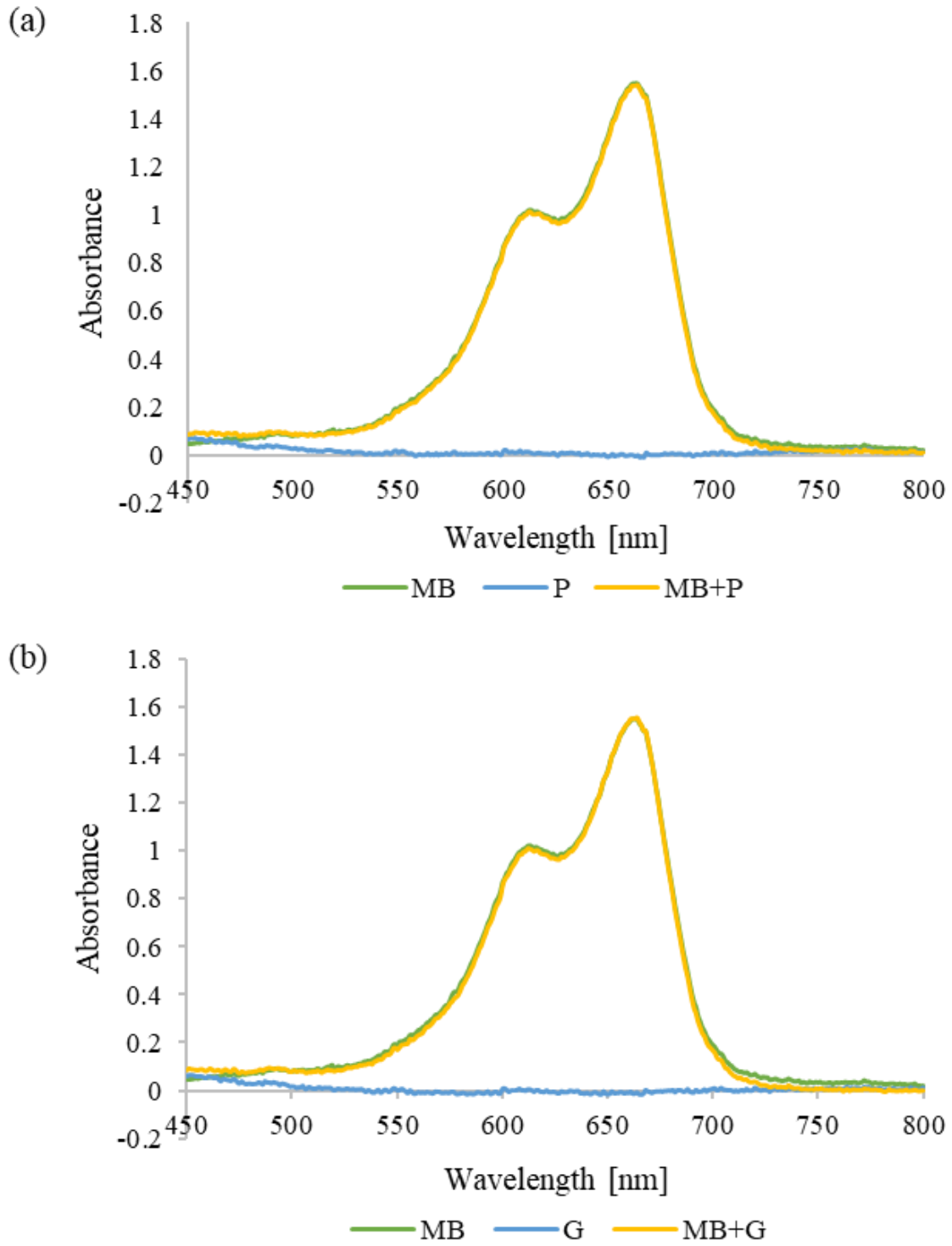


Fig. 4-8. The absorbance microplate reader spectra of (a) MB, pullulan (P), and a mixture of MB and pullulan (MB + P) at a 1:1 ratio and (b) MB, glucose (G), and a mixture of MB and glucose (MB + G) at a 1:1 ratio.

4-4-7 Determination of the affinity between MB and SA for OH* indicator by microplate reader analysis

Figure 4-9 (a) shows the absorbance from the microplate reader spectra of MB, SA, and mixture of MB and SA at a 1:1 ratio. Figure 4-9 (b) shows the absorbance of the microplate reader spectra for MB, glucose, and mixture of MB and glucose at a 1:1 ratio. The peak at 577 nm in the mixture of MB and SA spectrum shifted to 620 nm in the MB spectrum (Fig. 4-9 [a]). Moreover, the absorbances of the peaks between the microplate reader spectra of (i) 577 and 660 nm of the mixture of MB and SA spectrum and (ii) 620 and 670 nm of the MB spectrum (Fig. 4-9 [a]) also show differences. These results indicate that an intermolecular force (interaction between molecules) occurred, thus suggesting that SA and MB undergo intermolecular interaction with one another at the $-\text{COO}^-$ (carboxylate salt) of SA and the N⁺ (nitrogen) or S⁺ (sulfur) position of MB. However, the peaks shift at approximately 613 nm in the microplate reader spectra of the mixture of MB and glucose. The MB spectrum could not be confirmed in Fig. 4-9 (b). Moreover, the absorbances of all of the peaks at approximately 613 and 664 nm in the microplate reader spectra of the mixture of MB and glucose and only MB (Fig. 4-9 [b]) are the same. These results indicate that there is no interaction between glucose and MB ⁽⁴⁻⁵⁾.

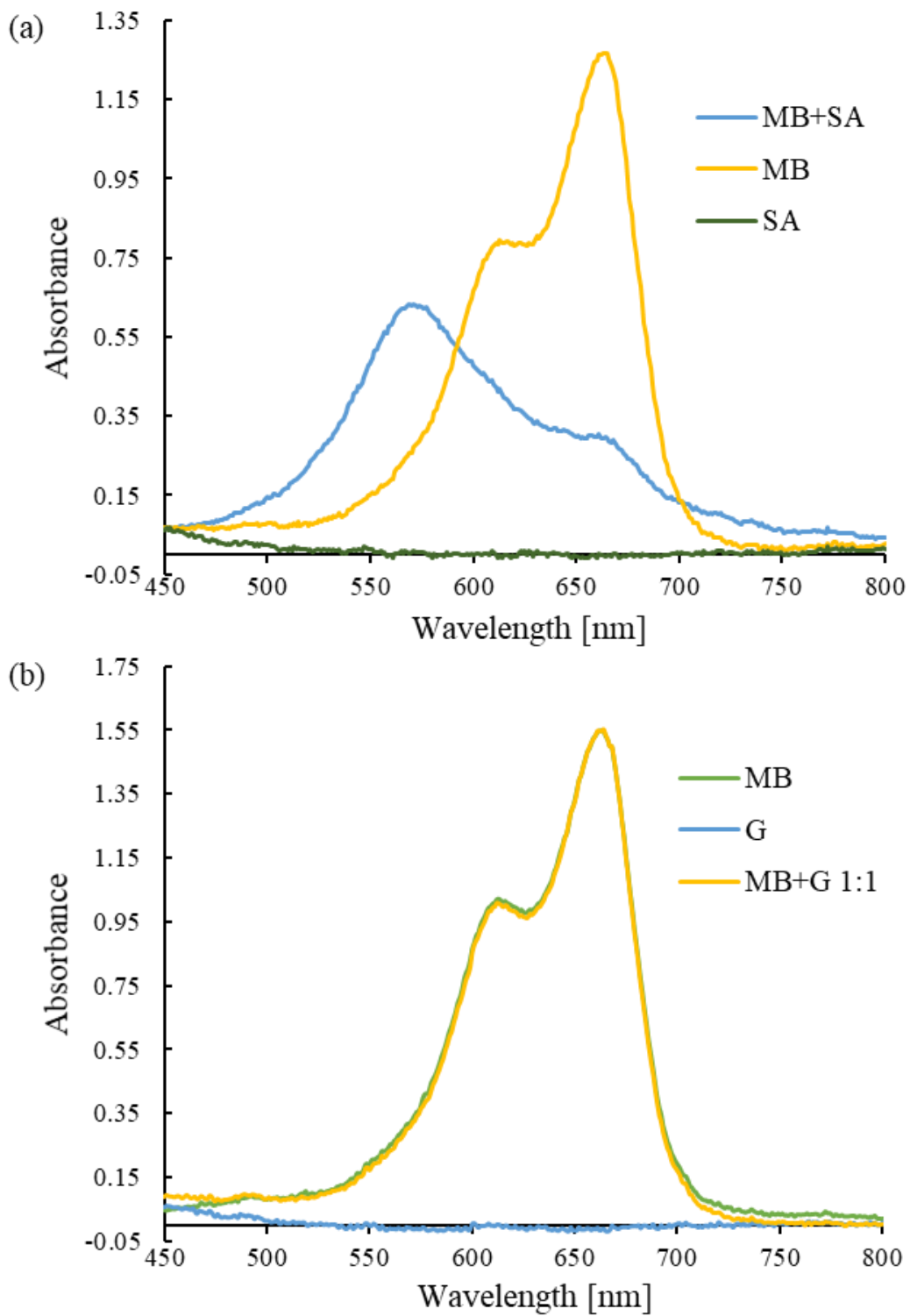


Fig. 4-9. Absorbance microplate reader spectra of (a) MB, SA, and a mixture of MB and SA (MB + SA) at a 1:1 ratio and (b) MB, glucose (G), and a mixture of MB and glucose (MB + G) at a 1:1 ratio

(4-5).

4-4-8 Determination of the affinity between MB and pullulan for OH* indicator by FT-IR analysis

Figure 4-10 shows the FT-IR spectra of MB, pullulan, and a mixture of MB and pullulan and suggests the presence of bonds representing the pullulan structure at 3650–3600 cm^{-1} (OH; hydroxide), 1950–1600 cm^{-1} (C=O; carbonyl group), and 930 cm^{-1} . Pristine MB bonds can be observed at 3100–3000 cm^{-1} (C_6H_6 ; benzene ring), 1380–1355 cm^{-1} , and 1470–1400 cm^{-1} ($-\text{CH}_3$; methyl group). My colleagues and I focused on the bond position of MB and pullulan. The bond position between MB and pullulan will be a N (nitrogen of MB) bond to O (oxygen of pullulan) and a S (sulfur of MB) bond to O (oxygen of pullulan). My colleagues and I cannot confirm the binding signal of the MB to the pullulan in the original position, but my colleagues and I can confirm a new signal in the spectrum of MB mixed with pullulan that appeared at 1670 cm^{-1} in Figs. 4-10 and 4-11. Moreover, my colleagues and I found a small difference in the FT-IR spectra, namely, the width of the $-\text{OH}$ signal of MB mixed with pullulan. It became narrower than that of the $-\text{OH}$ signal of pullulan in Fig. 4-12. My colleagues and I concluded that this new signal indicates the interaction between MB and pullulan.

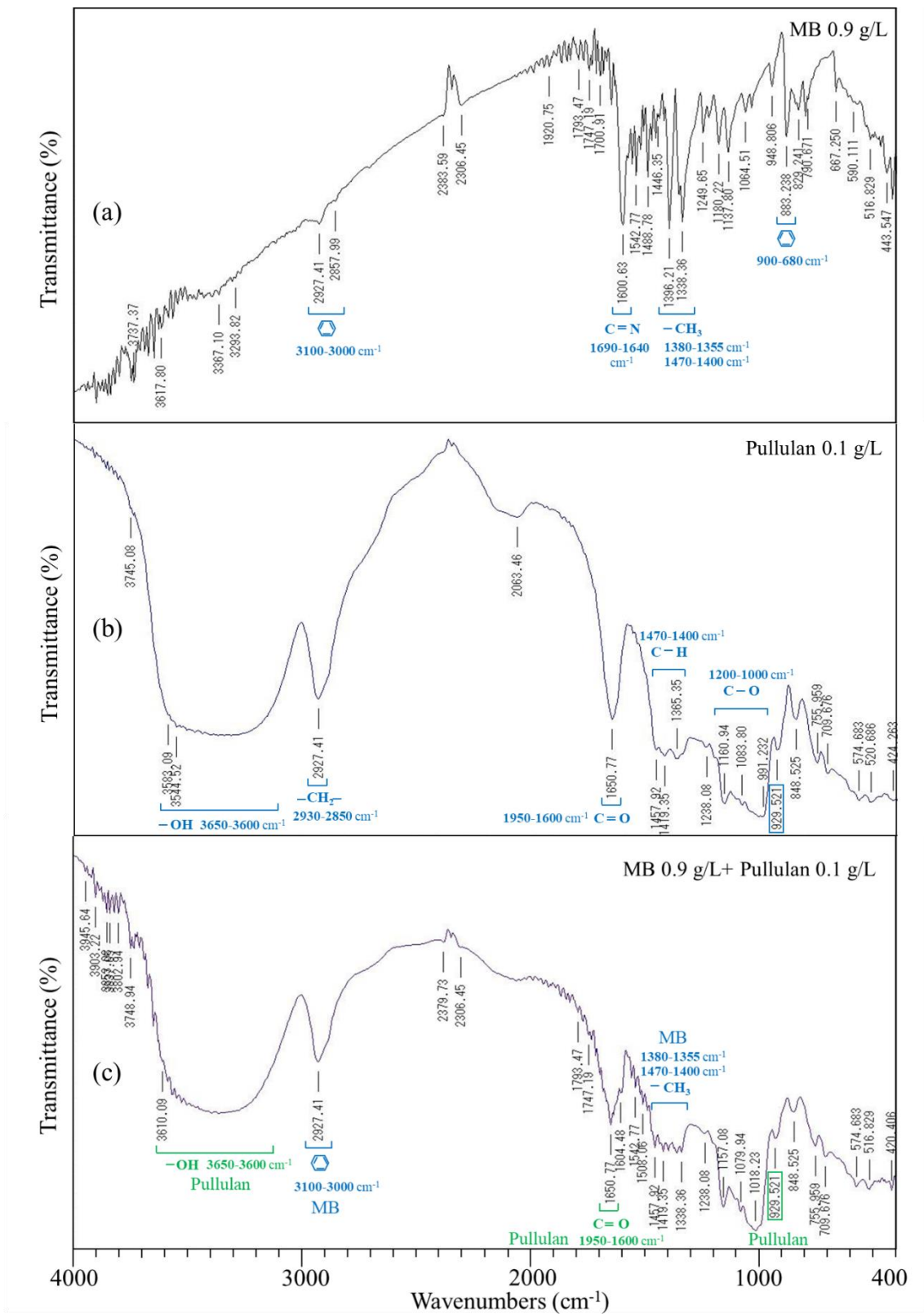


Fig. 4-10. FT-IR spectra of (a) MB, (b) pullulan, and (c) a mixture of MB and pullulan. C#N, -CH3, -OH, -CH2-, and C=O correspond to the molecular structures shown in Fig. 3-1 (a).

MB 0.9 g/L		Pullulan 0.1 g/L		MB + Pullulan	
001	2927.41	001	2927.41	001	2927.41
002	2495.44	002	2348.87	002	2503.15
003	2379.73	003	2063.46	003	2379.73
004	2348.87	004	1990.18	004	2348.87
005	2063.46	005	1967.04	005	2306.45
006	2044.17	006	1940.04	006	2063.46
007	2017.18	007	1920.75	007	2044.17
008	1990.18	008	1909.18	008	2017.18
009	1967.04	009	1866.76	009	1990.18
010	1943.89	010	1843.61	010	1967.04
011	1920.75	011	1824.33	011	1943.89
012	1909.18	012	1770.33	012	1920.75
013	1889.90	013	1650.77	013	1909.18
014	1866.76	014	1558.20	014	1889.90
015	1843.61	015	1538.92	015	1866.76
016	1828.19	016	1457.92	016	1843.61
017	1793.47	017	1419.35	017	1828.19
018	1770.33	018	1396.21	018	1793.47
019	1747.19	019	1365.35	019	1770.33
020	1731.76	020	1342.21	020	1747.19
021	1716.34	021	1238.08	021	1731.76
022	1697.05	022	1199.51	022	1716.34
023	1681.62	023	1160.94	023	1697.05
024	1650.77	024	1106.94	024	1681.62
025	1635.34	025	1083.80	025	1670.05
026	1558.20	026	1010.52	026	1650.77
027	1538.92			027	1635.34
028	1519.63			028	1604.48
029	1508.06			029	1573.63
030	1457.92			030	1558.20
031	1434.78			031	1542.77

Fig. 4-11. The FT-IR spectra between 3000 and 1000 cm^{-1} of MB, pullulan, and a mixture of MB and pullulan. C=N corresponds to the molecular structures shown in Fig. 3-1 (a), and the number corresponds to the wavenumber (cm^{-1}) shown in Fig. 3-8.

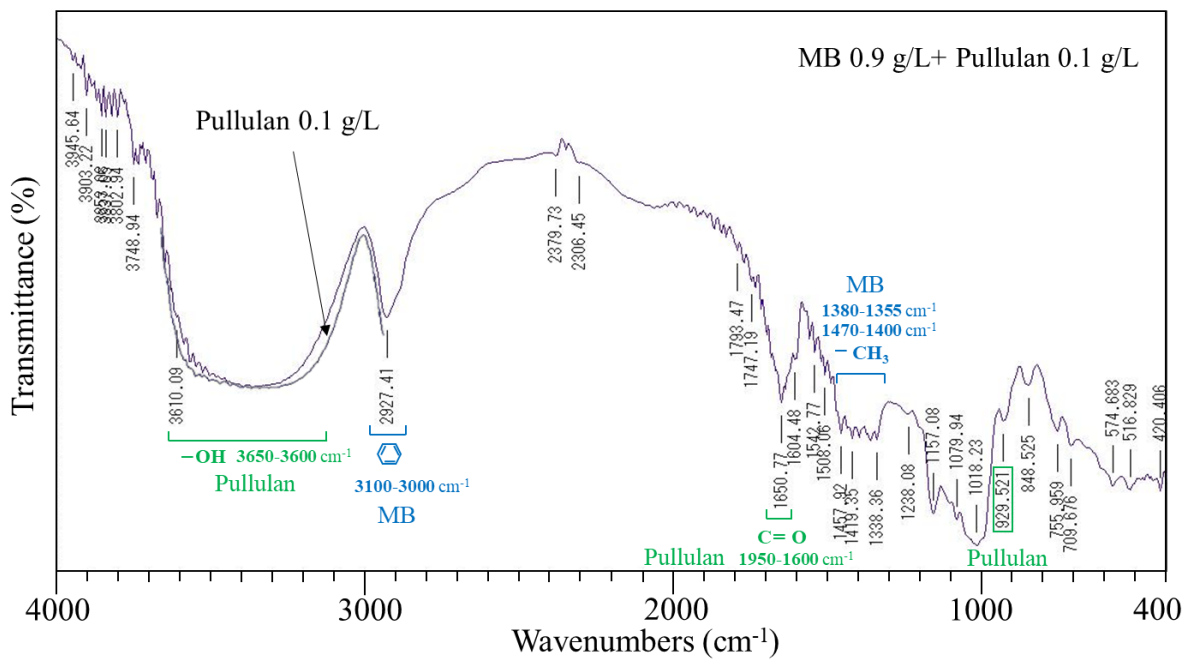


Fig. 4-12. The FT-IR spectra of a mixture of MB and pullulan and only pullulan.

-OH, C1OCOC1, C=O, and -CH₃ correspond to the molecular structures shown in Fig. 3-1 (a).

4-4-9 Determination of the affinity between MB and SA of OH* indicator by FT-IR analysis

Figures 4-13 and 4-14 show the FT-IR spectra of MB, SA, and a mixture of MB and SA and suggest the presence of bonds representing the SA structure that exhibited its asymmetric stretching vibration of carboxylate O–C–O at 1608 cm^{-1} , the C–OH deformation vibration with the contribution of O–C–O symmetric stretching vibration of carboxylate group at 1416 cm^{-1} , and the C–O stretching vibration of pyranose rings at 1031 cm^{-1} , respectively ^{(4-23)- (4-25)}. Pristine MB bonds can be observed at $3100\text{--}3000\text{ cm}^{-1}$ (C₆H₆; benzene ring), $1380\text{--}1355\text{ cm}^{-1}$, and $1470\text{--}1400\text{ cm}^{-1}$ (-CH₃; methyl group). My colleagues and I focused on the bond position of MB and SA. The bond position between MB and SA will be a S (sulfur of MB) bond to O (oxygen of SA), and the S–O and S–Na peaks appeared in the spectrum of the mixture. The detection range of the S–O peak is $1060\text{--}1040\text{ cm}^{-1}$ ⁽⁴⁻²⁶⁾.

Figures 4-13 (a) and (b) show the FT-IR spectra of MB, SA, and 1:1 and 1:10 mixtures of MB and SA and suggest that no significant change occurred in the spectra and that no S–O peak could be detected. In Fig. 4-13 (a), the S–C peak (1040 and 1060 cm^{-1} ⁽⁴⁻²⁶⁾) present in MB is near the S–O peak, and a 1:1 mixture has a spectrum with a high proportion of MB and is considered to be difficult to detect owing to the influence of the S–C peak. In Fig. 4-13 (b), the C–O peak present in SA is near the S–O peak, and it is probable that the 1:10 mixture had a higher proportion of SA than MB and was difficult to detect owing to the influence of the C–O peak.

Figures 4-14 (a) and (b) show the FT-IR spectra of MB, SA, and 1:2 and 1:0.2 mixtures of MB and SA, respectively, which suggests that no significant change was observed in the spectra, and no S–O peak could be detected. In Fig. 4-14 (a), the C–O peak present in SA is near the S–O peak, and the 1:2 mixture had a higher proportion of SA than MB and was considered difficult to detect owing to the influence of the C–O peak. In Fig. 4-14 (b), the S–C peak present in MB is near the S–O peak, and a 1:0.2 mixture contained less SA than MB and was difficult to detect owing to the influence of the S–C peak.

In both Figures 4-13 and 4-14, the S–Na peak represents an ionic bond, which is difficult to detect by FT-IR because of the weakness of this bond. An ionic bond is a bond between a nonmetallic element with high electronegativity and a metal element with low electronegativity. Originally, FT-IR

could not confirm the binding state of the metal element and could not detect the S–Na peak. Therefore, my colleagues and I concluded that it is possible that S–O and S–Na bonds may form between MB and SA.

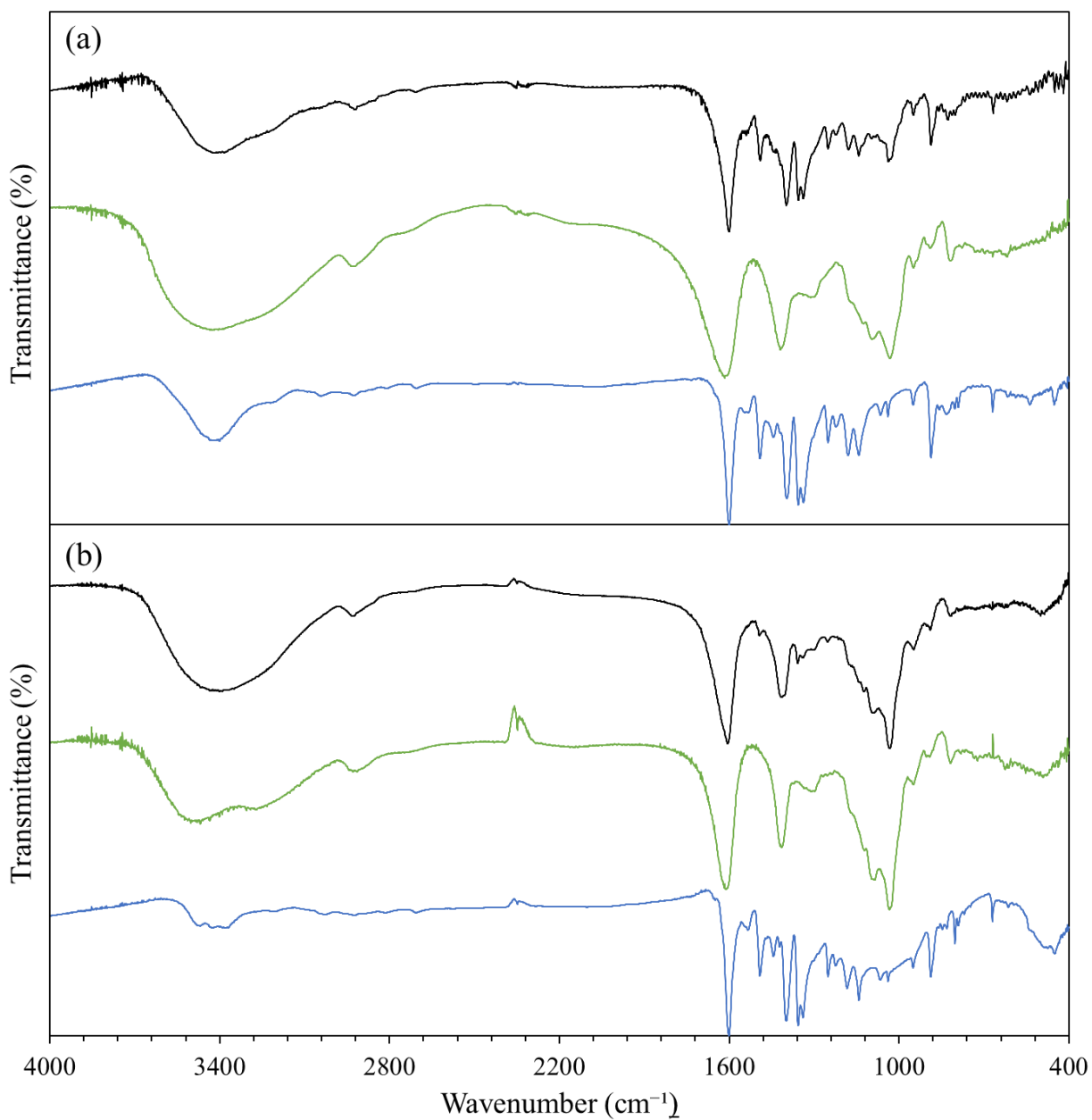


Fig. 4-13. The FT-IR spectra of (black line) of an MB and SA mixture, (green line) SA, and (blue line) MB at ratios of (a) 1:1 and (b) 1:10.

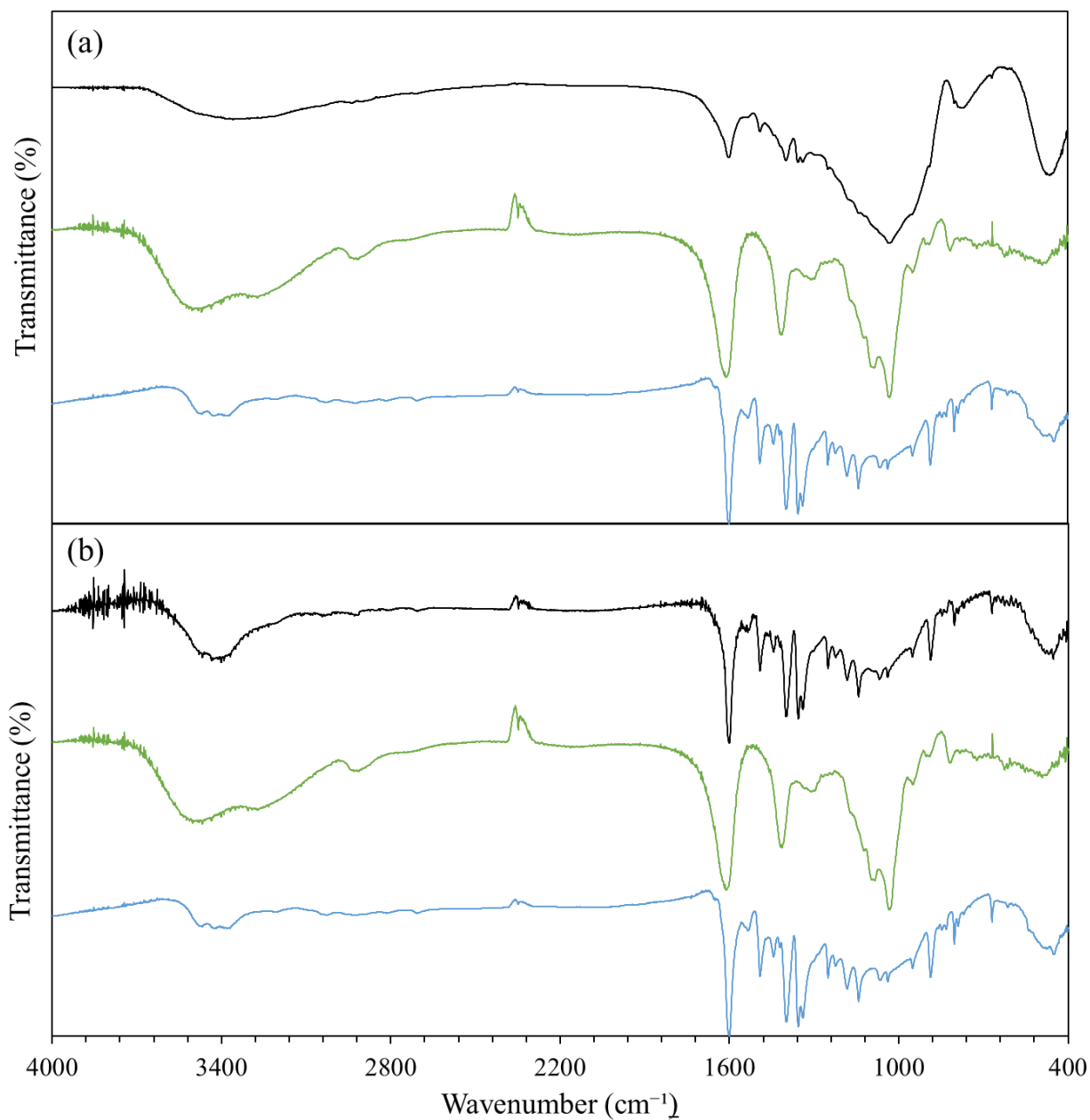


Fig. 4-14. The FT-IR spectra of (black line) an MB and SA mixture, (green line) SA, and (blue line) MB at ratios of (a) 1:2 and (b) 1:0.2.

4-4-10 Determination of the molecular structure of MB, pullulan, and SA of OH* indicator by Raman spectroscopy

Figure 4-15 shows the Raman spectrum of MB, and Table 4-5 shows the Raman shift peak of MB^{(4-22), (4-27)}. Figure 4-16 shows the Raman spectrum of pullulan, and Table 4-6 shows the Raman shift peak of pullulan. Figure 4-17 shows the Raman spectrum of SA, and Table 4-7 shows the Raman shift peak of SA⁽⁴⁻²⁸⁾.

Figures 4-18 and 4-19 show a comparison of the Raman spectra of MB and 1:10 ratio mixtures of MB/pullulan and MB/SA and suggest that the changes of the peaks at 900 and 1170 cm⁻¹ were confirmed. The peak at 900 cm⁻¹ disappeared and that at 1170 cm⁻¹ shifted. From this Raman spectrum, it is possible that the reaction occurs in the C–H (C [carbon of MB] bond to H [hydrogen of SA]). It is possible that the reaction sites from the structure of MB are the phenothiazine skeleton (C₁₂H₉NS) or methyl group (–CH₃).

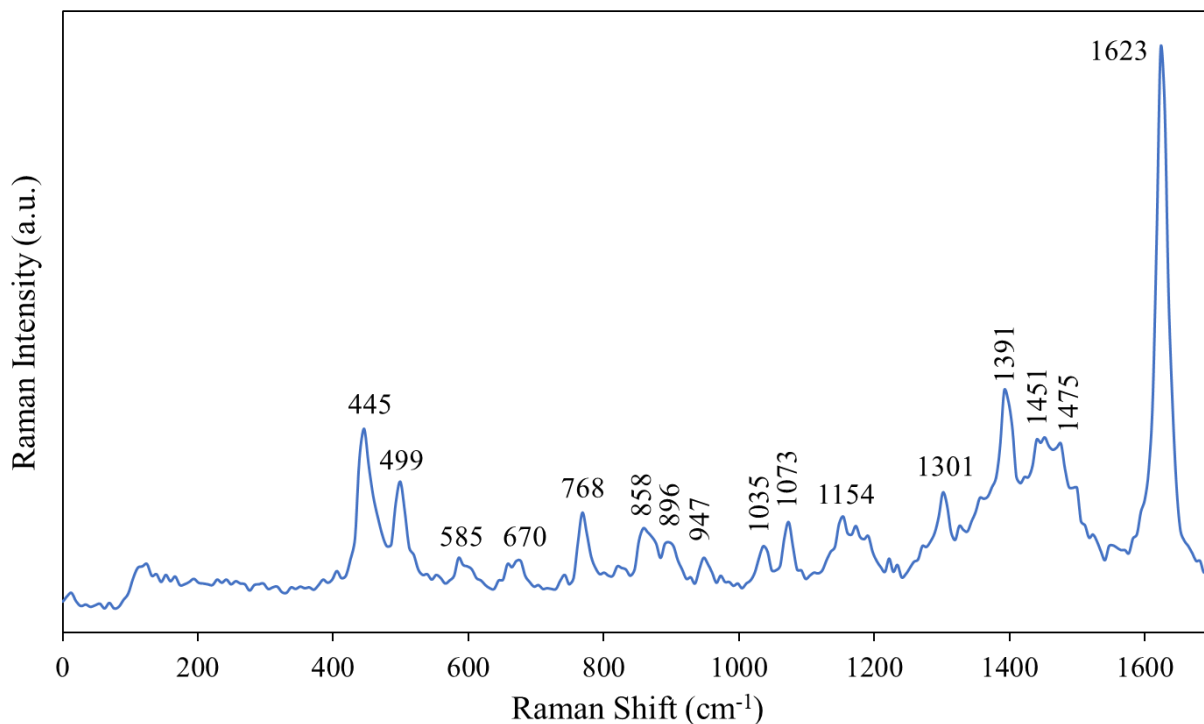


Fig. 4-15. The Raman spectrum of MB.

Number of Raman shifts corresponding to the molecular structures of MB shown in Table 4-4.

Table 4-5. Identification of the Raman shift peaks of MB.

Raman shift (cm ⁻¹)	Band assignments
445 (s), 499 (w)	C–N–C skeletal deformation
585 (w)	C–S–C skeletal deformation
670 (w)	C–H out-of-plane bending
768 (m)	C–S stretch (strong)
858, 896, 947, 1035, 1073, 1154 (m)	C–H in-plane bending
1301 (w)	C–H in-plane ring deformation
1391 (m)	C–N symmetrical stretching
1451, 1475 (w)	C–C asymmetrical stretching
1623 (s)	C–C ring stretching

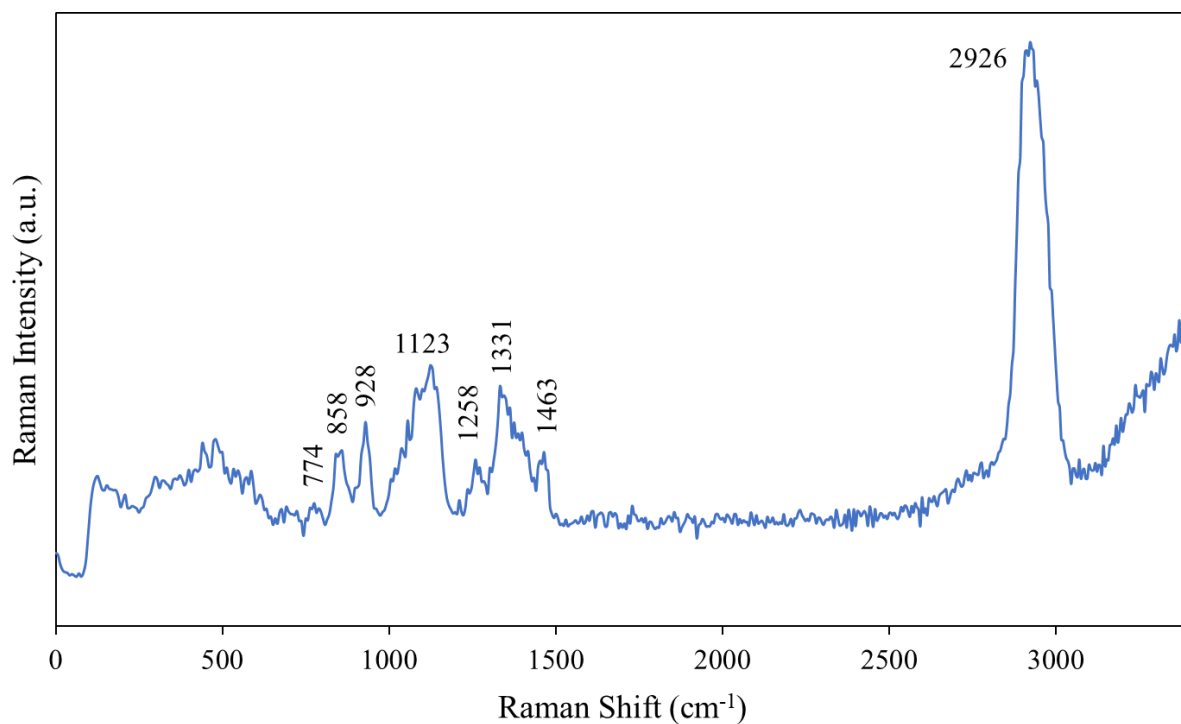


Fig. 4-16. The Raman spectrum of pullulan.

Number of Raman shifts corresponding to the molecular structures of pullulan shown in Table 3-3.

Table 4-6. The identification of Raman shift peak of pullulan.

Raman shift (cm ⁻¹)	Band assignments
928, 858 (sharp peaks)	C–O–C stretching
1123 (broad band)	C–O–C asymmetric
1331	O–H bending
1463	C–H bending
2926	C–H stretching

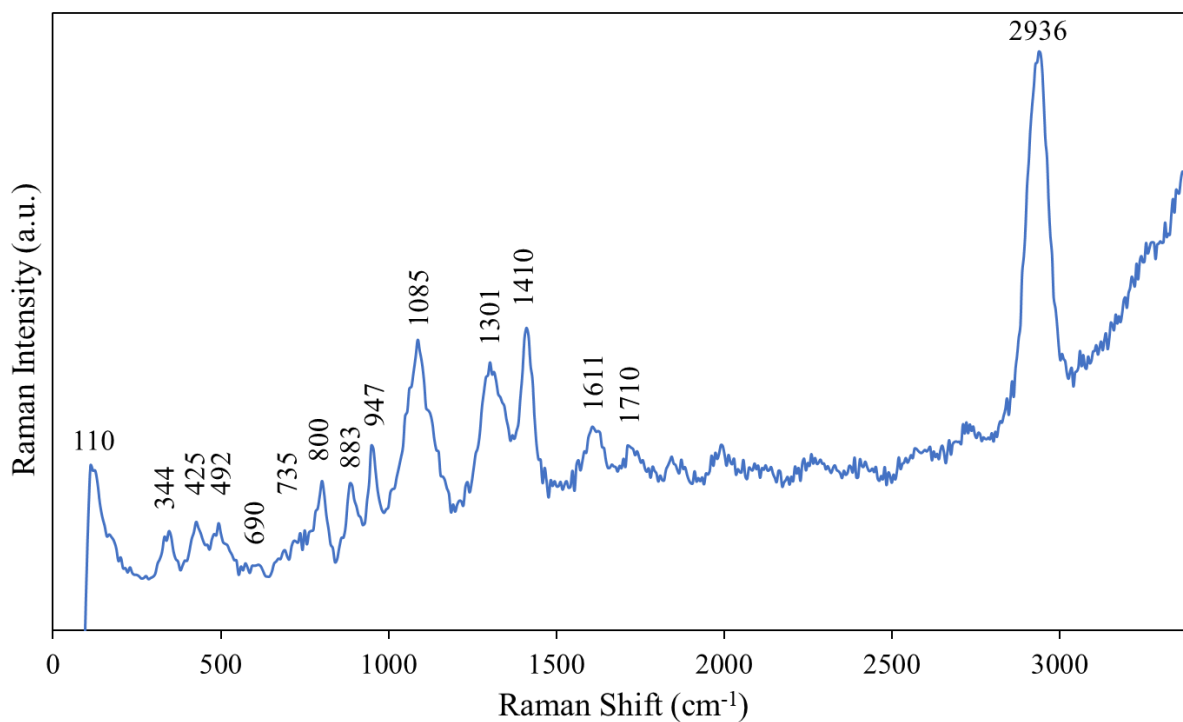


Fig. 4-17. The Raman spectrum of SA.

Number of Raman shifts corresponding to the molecular structures of SA shown in Table 4-5.

Table 4-7. The identification of Raman shift peaks of SA.

Raman shift (cm ⁻¹)	Band assignments
425, 492	C-O-C, C-C-C
690	C-O-C (glycosidic link)
735	Ring breathing
800	C-O-H, C-C skeletal, C-O, C-C-H, C-C-O
883	C-C-H, C-O-H, C-O-C symmetric
947	C-O stretching, C-C-H, and C-O-H deformation
1301	C-H deformation
1410	COO- (strong)
2936	C-H stretching

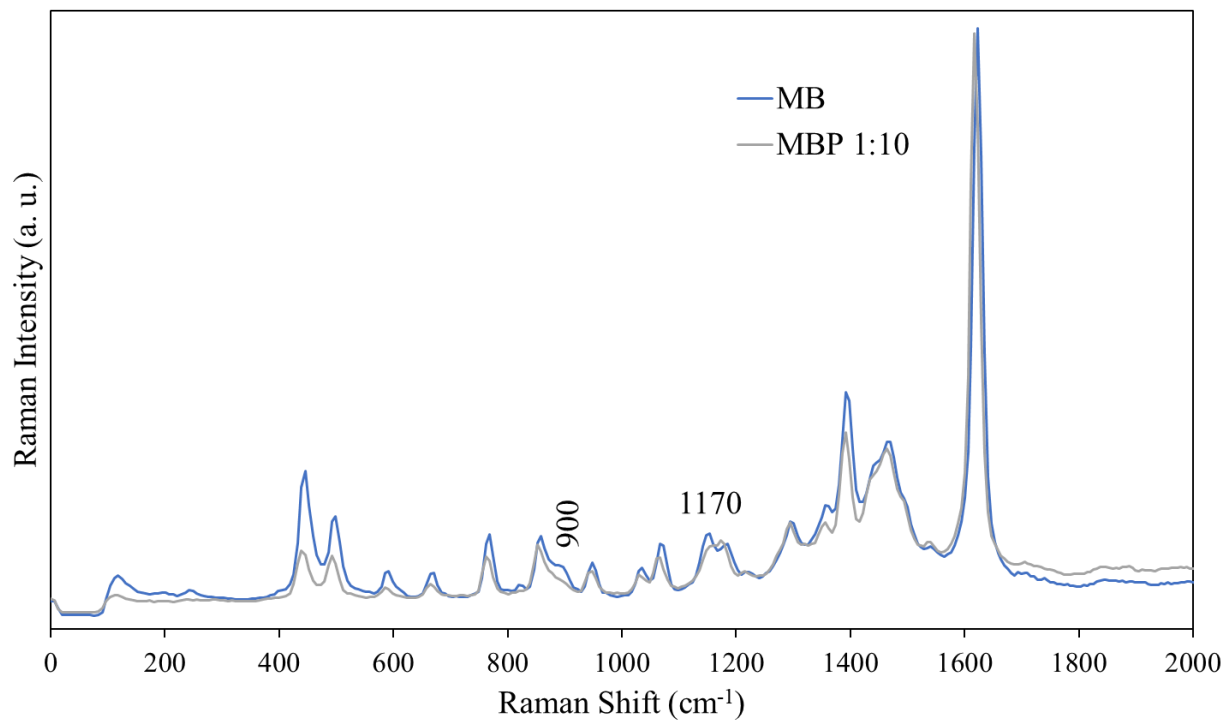


Fig. 4-18. The Raman spectra of MB and a 1:10 ratio mixture of MB and pullulan.

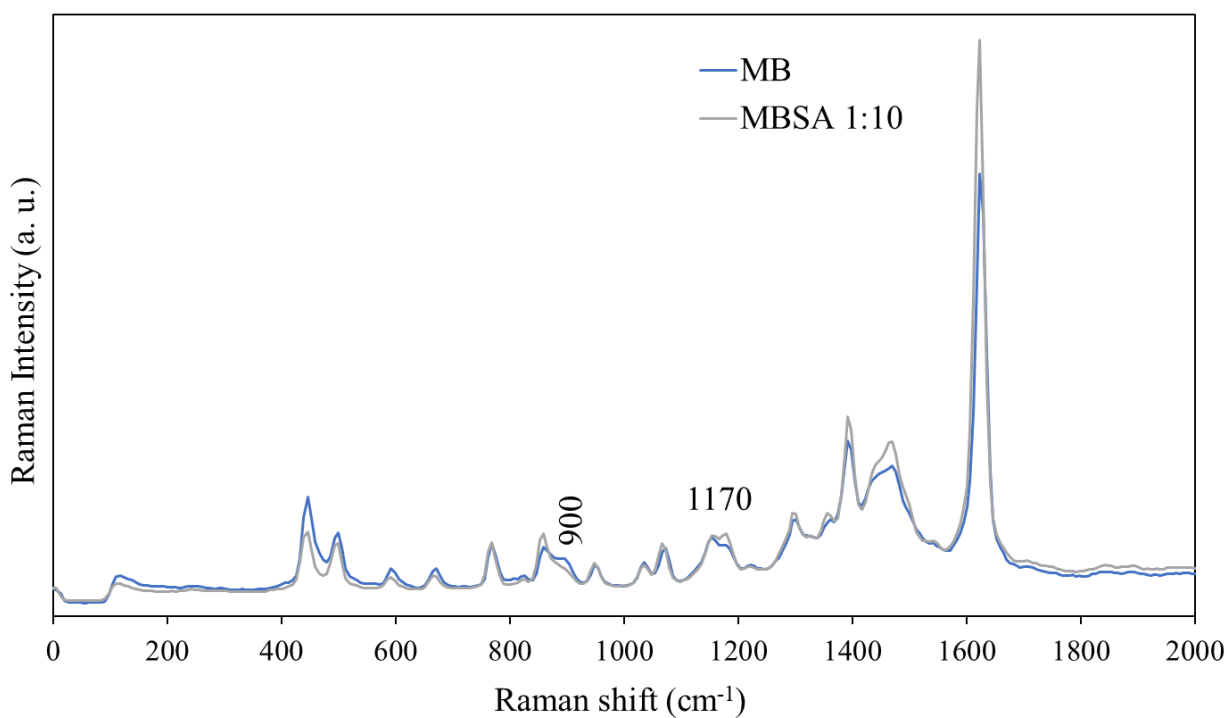


Fig. 4-19. The Raman spectra of MB and a 1:10 ratio mixture of MB and SA.

4-5 Discussion

The molecular structure of pullulan is helical, and this compound is considered a macromolecule. The MB stabilization that is achieved by mixing the dye with pullulan is necessary for MB decolorization because the macromolecule can effectively shield the molecules of MB from AOS. As shown in Fig. 4-4 and Figs. 4-8 (a) and (b), pullulan is suitable for stabilizing MB; however, glucose is not.

4-6 Summary

My colleagues and I succeeded in preparing uniform MB-dyed pullulan and SA uniform thin films as indicators of OH*. TLC confirmed the weak affinity between MB and pullulan, whereas the results of ¹H-NMR analyses suggested that MB and pullulan interacted with each other, as evidenced by the shift of the peaks corresponding to the benzene ring of MB in the mixture of MB and pullulan. Moreover, the molecular structure of pullulan is helical, and the compound is considered a macromolecule. The MB stabilization that is achieved by mixing the dye with pullulan is necessary for the decolorization of MB because the macromolecule can effectively shield the molecules of MB from AOS. Pullulan is suitable for stabilizing MB; however, glucose is not. Moreover, my colleagues and I suspect that the positions of pullulan and MB following mixing are close and that the molecules of MB are shielded by pullulan. The occurrence of the interaction between MB and pullulan influenced the decolorization process. The ¹H-NMR spectrum of MB-dyed pullulan showed that only three peaks corresponding to the hydrogen atoms of the benzene ring disappeared upon AOS exposure under high-humidity conditions. However, the three peaks remained following AOS exposure under low-humidity conditions. Therefore, it is considered that the OH* species attacks the benzene ring of MB in the mixture of MB and pullulan, whereas the typical AOS cannot attack this moiety. Considering that AOS other than OH* cannot be used to analyze MB, MB stabilization by mixing MB with pullulan is necessary for the decolorization of MB because MB molecules are protected by pullulan.

The results of TLC, ¹H-NMR, and microplate reader analyses suggested that MB and SA share an ionic bond, as evidenced by the shifts in the peaks corresponding to the benzene ring of MB in the mixture of MB and SA. It is considered that MB and SA intermolecularly interact with one another.

Therefore, SA is suitable for stabilizing MB. MB stabilization by mixing MB with SA is also necessary for the decolorization of MB because the binding between MB and SA may contribute to the stability of AOS excluding OH*.

References

- (4-1) K. Yoshino, H. Matsumoto, T. Iwasaki, S. Kinoshita, K. Noda, K. Oya, and S. Iwamori, Investigation of a Sterilization System Using Active Oxygen Species Generated by Ultraviolet Irradiation, *Biocontrol Science*, Vol. 20, No.1 (2015), pp. 11-18.
- (4-2) S. Iwamori, N. Nishiyama and K. Oya, A colorimetric indicator for detection of hydroxyl radicals in atmosphere using a methylene blue dye based on nafion film, *Polymer Degradation and Stability*, Vol. 123 (2016), pp. 131-136.
- (4-3) H. Sugimitsu, *Application and Foundation of Ozone* (Korin, Tokyo, 1996), p. 20 [in Japanese].
- (4-4) K. Oya, R. Watanabe, Y. Soga, Y. Ikeda, T. Nakamura and S. Iwamori, Effect of humidity conditions on active oxygen species generated under ultraviolet light irradiation and etching characteristics of fluorocarbon polymer, *Journal of Photochemistry and Photobiology A: Chemistry*, Vol.298 (2015), pp. 33-39.
- (4-5) S. Yenchit, H. Yamanaka, P. Temeprasertkij, Y. Oda, O. Kanie, Y. Okamura, T. Inazu and S. Iwamori, Chemical stability of a colorimetric indicator based on sodium alginate thin film and methylene blue dye upon active oxygen species exposure, *Japanese Journal of Applied Physics*, Vol. 59, No. SD (2020), SDDF09.
- (4-6) S. Yenchit, H. Yamanaka, P. Temeprasertkij, Y. Oda, Y. Okamura, T. Inazu and S. Iwamori, A Colorimetric Indicator Based on Methylene Blue-Dyed Pullulan Thin Films for the Detection of Hydroxyl Radicals, *材料の科学と工学*, (Accepted).
- (4-7) J. P. Dzoyem, V. Kuete, and J. N. Eloff, *Toxicological Survey of African Medicinal Plants* (Elsevier, Amsterdam, 2014), pp. 659.
- (4-8) H. Okabe, *Photochemistry of Small Molecules* (Wiley, New York, 1978), p. 177.
- (4-9) T. Matsunaga, K. Hieda, and S. Nikaido, Wavelength dependent formation of thymine dimers and (6-4) photoproducts in DNA by monochromatic ultraviolet light ranging from 150 to 365 nm, *Photochemistry and Photobiology*, Vol. 54, No. 3 (1991), pp. 403-410.
- (4-10) D. L. Baulch et al., Evaluated Kinetic Data for Combustion Modeling: Supplement II, *Journal of Physical and Chemical Reference Data* 34 (2005), pp. 757-1397.

- (4-11) R. Atkinson, D. L. Baulch, R. A. Cox, J. N. Crowley, R. F. Hampson, R. G. Hynes, M. E. Jenkin, M. J. Rossi, and J. Troe, Evaluated kinetic and photochemical data for atmospheric chemistry: Volume I - gas phase reactions of Ox, HOx, NOx and SOx species, Atmospheric chemistry and physics, Vol. 4 (2004), pp. 1461-1738.
- (4-12) L. T. Molina and M. J. Molina, Absolute absorption cross sections of ozone in the 185- to 350-nm wavelength range, Journal of Geophysical Research, Vol. 91 (1986), pp. 14501-14508.
- (4-13) R. Atkinson, D. L. Baulch, R. A. Cox, R. F. Hampson, J. A. Kerr, and J. Troe, Evaluated Kinetic and Photochemical Data for Atmospheric Chemistry: Supplement IV. IUPAC Subcommittee on Gas Kinetic Data Evaluation for Atmospheric Chemistry, Journal of Physical and Chemical Reference Data, Vol. 21 (1992), pp. 1125-1568.
- (4-14) D. S. Stafford and M. J. Kushner, O₂(1Δ) production in He / O₂ mixtures in flowing low pressure plasmas, Journal of Applied Physics, Vol. 96 (2004), pp. 2451-2465.
- (4-15) J. A. Manion et al., NIST Standard Reference Database 17, Version 7.0 (Web Version), Release 1.6.8, Data version. 2015.09, National Institute of Standards and Technology, Gaithersburg, Maryland, pp. 20899-8320.
- (4-16) J. P. Burrows, R. A. Cox, and R. G. Derwent, Modulated photolysis of the ozone-water vapour system: kinetics of the reaction of OH with HO₂, Journal of Photochemistry, Vol. 16 (1981), pp. 147-168.
- (4-17) M. Salvermoser, D. E. Murnick, and U. Kogelschatz, Influence of Water Vapor on Photochemical Ozone Generation with Efficient 172 nm Xenon Excimer Lamps, Ozone: Science & Engineering, Vol. 30 (2008), pp. 228-237.
- (4-18) K. Yoshihara, Y. Takatori, K. Miyazaki, and Y. Kajii, Ultraviolet light-induced water-droplet formation from wet ambient air, Proceedings of the Japan Academy, Ser. B, Vol. 83 (2007), pp. 320-325.
- (4-19) R. Kiss, Á. Fizil and C. Szántay Jr., What NMR can do in the biopharmaceutical industry, Journal of Pharmaceutical and Biomedical Analysis, Vol. 147 (2018), pp. 367-377.
- (4-20) A. Shahvar, M. Saraji, and D.1 Shamsaei, Smartphone-based chemiluminescence sensing for TLC imaging, Sensors and Actuators B, Vol. 255 (2018), pp. 891-894.

- (4-21) I. R. Lewis and H. Edwards (ed.) Handbook of Raman spectroscopy (the research laboratory to the process line. CRC Press, 2001).
- (4-22) M. D. Moghari (ed.) Optimised methylene-blue detection and quantification utilizing conventional raman spectroscopy (A Master degree research thesis, Macquarie University, 2006).
- (4-23) C. Peniche, W. Arguelles-Monal, N. Davidenko, R. Sastre, A. Gallardo, and J.S. Roman, Self-curing membranes of chitosan/PAA IPNs obtained by radical polymerization: preparation, characterization and interpolymer complexation, *Biomaterials*, Vol. 20 (1999), pp. 1869–1878.
- (4-24) D. Leal, B. Matsuhiro, M. Rossi, and F. Caruso, FT-IR spectra of alginic acid block fractions in three species of brown seaweeds, *Carbohydrate Research*, Vol. 343 (2008), pp. 308–316.
- (4-25) H.Y. Zhaoa, W. Zhenga, Z.X. Menga, H.M. Zhoua, X.X. Xua, Z. Lia, and Y.F. Zhenga, Bioelectrochemistry of hemoglobin immobilized on a sodium alginate-multiwall carbon nanotubes composite film, *Biosensors and Bioelectronics*, Vol. 24 (2009), pp. 2352-2357.
- (4-26) H. Horiguchi (ed.) Infrared Absorption Illustrations (Quoted from Sankyo Publishing) (in Japanese).
- (4-27) G. N. Xiao and S. Q. Man, Surface-enhanced Raman scattering of methylene blue adsorbed on cap-shaped silver nanoparticles, *Chemical Physics Letters*, Vol. 447 (2007), pp. 305–309.
- (4-28) M. M. Campos-Vallette, N. P. Chandía, E. Clavijo, D. Leal, B. Matsuhiro, I. O. Osorio-Román, and S. Torres, Characterization of sodium alginate and its block fractions by surface-enhanced Raman spectroscopy, *Journal of raman spectroscopy*, Vol. 41 (2010), pp. 758-763.

Chapter 5

CONCLUSIONS

CONCLUSIONS

In this study, an indicator of active oxygen species (AOS) made from uniform thin films were developed using MB-dyed pullulan and MB-dyed sodium alginate, which can be generated under atmospheric conditions and have high reactivity. The aim was to detect the presence of AOS and establish AOS technology for the sterilization and surface modification of polymer substrates. Furthermore, the mechanism of diffusion of OH^* across nonwoven fabric was investigated.

Chapter 1 presented the introduction, which described the definition and mechanism of AOS generation, and summarized the advantages obtained by applying them to the sterilization process and surface modification technology. The applications of AOS in surface modification technology in an industrial setting were also described. Thereafter, the method of measuring AOS and the purpose of this study were described.

In Chapter 2, the importance of using nonwoven fabric in sterilization with AOS was discussed. However, it was difficult to determine whether the AOS were uniformly sterilized spatially in the nonwoven fabric. A spin-trapping agent for application to the sterilization process using AOS was used to confirm the presence of AOS inside the nonwoven fabric constituting the sterilization bag. Given that it is unlikely that the short-lifetime AOS were generated outside the sterilization bag, it is considered that the AOS cannot reach the long-distance stage into nonwoven fabric. Therefore, evaluation was performed using an aluminum test box with three internal stages, with the upper section of the box sealed with nonwoven fabric. To check whether AOS were present in the test box, the AOS spin-trapping agents were placed in the three stages in the test box, and the AOS diffusion rate, particularly the existence of hydroxyl radicals, was investigated by electron spin resonance (ESR). Each stage in the test box was spread with OH^* . Therefore, spin-trapping agents were placed on these three stages inside the box, and the AOS diffusion and presence of OH^* were investigated by monitoring the intensity of the ESR peak associated with CYPMPO/OH observed in the different stages of the aluminum box. The peaks in the ESR spectrum in the presence of CYPMPO/OH, which is a product of the reaction between CYPMPO and OH^* , in all stages were investigated to probe the mechanism by

which OH* diffuses across the various stages inside the test box. The interior of the test box was sealed to completely block out ultraviolet (UV) light by using a three-layer nonwoven fabric. The OH* existing in the test box sealed with a nonwoven fabric was generated by the ozone generated outside the test box by UV irradiation. Thereafter, it was passed through a nonwoven fabric to react with water in the nonwoven fabric or was generated in the nonwoven fabric. It was assumed that OH* was generated in the test box via the ozonolysis of water molecules.

As described in Chapter 3, new AOS indicators made from uniform thin films were successfully developed using MB-dyed pullulan and MB-dyed sodium alginate, which are both water-soluble polymers with film-forming properties. These indicator thin films can visually determine the presence or absence of AOS on the spot. It was found that these thin films were decolorized upon exposure to OH* generated under high-humidity conditions in AOS. The results showed that the peaks of the ¹³C-NMR spectrum corresponding to the aromatic carbon atoms of MB in the mixture of MB and water-soluble polymers disappeared after exposure to OH* under high-humidity conditions. It was found that MB decomposed only when OH* was irradiated in AOS, and decolorization occurred. Moreover, MB-dyed pullulan thin films were placed on the three stages inside the test box for confirmation using ESR, and the AOS diffusion and OH* presence were investigated by monitoring the degree of thin film decolorization at different stages of the test box. The decolorization of an MB-dyed pullulan thin film caused by exposure to OH* was investigated to ascertain the mechanism by which AOS diffuse across the various stages inside the test box.

In Chapter 4, the decolorization characteristics of the MB-dyed water-soluble polymer (i.e., pullulan and sodium alginate) were examined using uniform thin film detection after exposure to OH*. Glucose, which is a monomer of pullulan, was used as a reference to investigate the stabilization feature of MB and water-soluble polymers of the uniform thin film indicator. The results confirmed the interaction between MB and pullulan and indicated that MB molecules are protected by pullulan. Three peaks of the ¹H-NMR spectrum corresponding to the protons in the benzene ring disappeared upon the exposure to AOS under high-humidity conditions despite the fact that they remained after the exposure to AOS under low-humidity conditions. Therefore, it was considered that the OH* species attacks the

benzene ring of MB in the mixture of MB and pullulan, whereas the typical AOS cannot attack this moiety. Furthermore, a shift in the absorption wavelength in the microplate reader analysis corresponding to the benzene ring of MB in the mixture of MB and sodium alginate suggested that MB and sodium alginate could have formed an ionic bond. Therefore, MB stabilization by mixing MB with water-soluble polymers is necessary for the decolorization of MB. Considering that MB and pullulan interacted with each other and that MB and sodium alginate were bound to each other, both may contribute to the stability to AOS, except OH*.

This study discussed the mechanism behind the generation of OH* in a test box sealed with nonwoven fabric via the ozonolysis of water molecules. Therefore, the entire area inside the sterilization bag was sterilized (even in the deepest area). This proved that sterilization and surface modification using AOS can be effectively applied in industrial processes. Moreover, my colleagues and I successfully developed new indicators for detecting OH* by preparing uniform MB-dyed water-soluble thin films, which can be applied for on-the-spot detection. These indicators were easy to prepare and do not require special equipment. All the merits of these uniform thin films for AOS detection can overcome the disadvantages of the present measurement methods for AOS. Furthermore, the chemical bonding of the MB-dyed indicator thin films is important for OH* exposure; therefore, my colleagues and I might be able to increase the functionality of the indicator thin films depending on the type of interaction.

ACKNOWLEDGMENT

This thesis is in part based on the work described in the following articles: “Measuring Active Oxygen Species Across a Nonwoven Fabric Using a Pullulan-mixed Methylene Blue Thin Film and Electron Spin Resonance” (S. Yenchit, Y. Tadokoro, and S. Iwamori, *IEEJ Transactions on Sensors and Micromachines*, published in 2019, Vol. 139, No. 3, pp. 54-60, DOI: <https://doi.org/10.1541/ieejsmas.139.54>), “Chemical stability of a colorimetric indicator based on sodium alginate thin film and methylene blue dye upon active oxygen species exposure” (S. Yenchit, H. Yamanaka, P. Temeeprasertkij, Y. Oda, O. Kanie, Y. Okamura, T. Inazu, and S. Iwamori, *Japanese Journal of Applied Physics*, published in 2020, Vol. 59, No. SD, SDDF09, DOI: <https://doi.org/10.7567/1347-4065/ab6340>), and “Colorimetric Indicator Based on Methylene Blue-Dyed Pullulan Thin Films for the Detection of Hydroxyl Radicals” (S. Yenchit, H. Yamanaka, P. Temeeprasertkij, Y. Oda, Y. Okamura, T. Inazu and S. Iwamori, *材料の科学と工学*, Accepted).

Dr. Satoru Iwamori (Department of Mechanical Engineering, Tokai University’s Faculty of Engineering) provided valuable guidance and advice for this research and in writing this dissertation. He always provided support with a smile whenever I asked. For five years from the first year of my master’s studies, I received a great deal of experience as a member of Prof. Iwamori’s laboratory. I am thankful to him for the encouragement he has given me in completing this project.

Dr. Yoshiki Oda and Dr. Yoshimi Kanie (Department of Research Promotion Division), as well as Prof. Osamu Kanie (Department of Applied Biochemistry, Tokai University), provided detailed consultations and substantial advice in carrying out this research. In addition to providing advice and guidance on writing papers and presenting at conferences, I was also strongly supported at times of indecision. I also received guidance on how to use each analyzer and on how to perform the data analysis, for which I am very grateful.

I am also grateful to Prof. Yosuke Okamura, (Department of Applied Chemistry, Prof. Toshiyuki Inazu, Department of Applied Chemistry) and Kazuki Hosoya (Graduate School of Science

and Technology, Tokai University) for providing valuable comments regarding manuscript preparation.

Senior and junior students at Prof. Iwamori's laboratory not only helped with the experiments, but also helped me with many other aspects. In particular, Hiromi Yamanaka (a first year master's student at the Department of Mechanical Engineering, Graduate School of Engineering) and Kazuki Hosoya, Nobuto Nishiyama, Yuta Tadokoro, Yusuke Abe, and Naoya Iwasaki (Graduate School of Engineering, Tokai University) were involved in a number of experiments as members of the same research group for many years. I am grateful for their support. This paper would not have been completed without them.

I would also like to thank the other faculty and staff members of my department for their cooperation and assistance. Finally, I would like to thank my parents for watching over and supporting me.